MODELING AND SIMULATION OF FILM BLOWING PROCESS

A Dissertation

by

RAVISANKAR S. MAYAVARAM

Submitted to the Office of Graduate Studies of
Texas A&M University
in partial fulfillment of the requirements for the degree of

DOCTOR OF PHILOSOPHY

May 2005

Major Subject: Mechanical Engineering

MODELING AND SIMULATION OF FILM BLOWING PROCESS

A Dissertation

by

RAVISANKAR S. MAYAVARAM

Submitted to Texas A&M University
in partial fulfillment of the requirements
for the degree of

DOCTOR OF PHILOSOPHY

Approved as to style and content by:

Junuthula N. Reddy
(Chair of Committee)

Nagamangala K. Anand
(Member)

Hung-Jue Sue
(Member)

Jon T. Pitts
(Member)

Dennis. O'Neal
(Head of Department)

May 2005

Major Subject: Mechanical Engineering

ABSTRACT

Modeling and Simulation of Film Blowing Process. (May 2005)
Ravisankar S. Mayavaram, B.E., Bharathiar University, Coimbatore, India; M.S.,
Indian Institute of Technology, Madras, India.
Chair of Advisory Committee: Dr. Junuthula N. Reddy

Film blowing process is a flexible mass production technology used for manufacturing thin polymeric films. Its flexibility in using an existing die to produce films of different width and thickness, just by controlling process conditions such as, extrudate velocity, excess pressure, and line speed, makes it an attractive process with less capital investment. Controlling the process conditions to obtain a stable bubble, however, is not a trivial task. It is a costly trial and error procedure, which could result is a large wastage of material and other resources. Hence, it is necessary to develop methods to simulate the process and design it using numerical experiments. This important need of the industry defines the objective of this work. In this dissertation, a transient, axisymmetric, nonisothermal, viscoelastic model is developed to simulate the process, and it is solved using finite element method. Material behavior of polymer melt is described using a modified Phan-Thien-Tanner model in the liquid–like region, and anisotropic Kelvin–Voight model in the solid zone, and the transition is modeled using a simple mixture theory. Crystallization kinetics is described using a modified Avrami model with factors to account for the influence of temperature and strain. Results obtained are compared with available experimental results and the model is used to explore stability issues and the role of different parameters. Software developed using this model comes with a GUI based pre- and post-processor, and it can be easily adapted to use other constitutive models.

To my mother

Mātā Amṛtānandamayī

for making this resolve.

ACKNOWLEDGMENTS

I am indebted to Prof. J. N. Reddy, who is the Chair of my committee for his valuable guidance and support. I have learned so many valuable things from Prof. Reddy, not just in the field of our endeavor, but on all aspects of life. His wisdom, patience, and kindness never cease to amaze me.

I thank the members of my committee, Prof. N. K. Anand, Prof. H. -J. Sue, and Prof. Pitts. Their support and guidance was very valuable for this work; and I express my sincere gratitude to them. I would like to specially thank Prof. Sue, his leadership role in PTC was a great motivation for this work. In early stages of this work, Dr. R. W. Flumerfelt and Dr. L. A. Archer served as my committee members. I am grateful to them for their support. I thank Prof. K. R. Rajagopal for educating me on finer aspects of continuum mechanics and Prof. Pitts for creating a deep interest in differential geometry. I took over twelve courses in A&M and I learned immensely from each one of them – I am thankful to all my teachers. I would also like to thank Kim Moses of Department of Mechanical Engineering for helping me with official matters.

I thank my beloved teacher Prof. K. N. Seetharamu (IIT, Madras) for his constant words of encouragement. It will not be an exaggeration if I say that my professional career was shaped by him. I only wish that I had listened to his valuable advice more often than I did. He was deeply upset when I took a full time job and switched my Ph.D to part-time. Now I agree with him, in that decision – I overestimated my capability and underestimated the level of difficulty in handling both.

I thank my colleague Dr. Carlos E. Baumann (Altair Engineering) for his valuable help in designing the user interface for the software FilmLine. I am thankful to Dr. Mahender Reddy and Dr. Woytek Tworzydlo of Altair Engineering for their constant support and encouragement. I would also like to thank all my colleagues at Altair Engineering and the company itself for the all their help and encouragement.

I thank my friends and colleagues, Govind Rengarajan, Grama Praveen, Achuth Rao, Kenneth Chin, John Mitchell, Dakshina Moorthy, and Partha Bose for their friendship and support. I would like to thank my friends Rajesh Devarajan, Srinivas Mirmira, and many other who made my stay in College Station enjoyable.

Finally, I thank my family, especially my wife Saraswathy and my daughter Amritavarshini for their love and support. Coping with 10 hours a day at work and weekends on this dissertation was not an easy thing for any one of us. I hope I will make up for that in the years to come. I would like to thank my mom and dad for their encouragement. I would also like to thank my mother-in-law Mrs. Lakshmi Somabhatta for always keeping me in her prayers.

I thank Sri Paramahansa Yogananda, Sri Ramana Maharishi and Sri Shirdi Sai Baba, for teaching me the value of surrender to God. It is their golden words that kept my sanity in check during the moments of frustration. If I am asked to name one person, whom I utterly relied on to complete this work – it is my spiritual teacher Mātā Amṛtānandamayī. Without her support and resolve, I would not have completed this work. Hence, I have dedicated this work to her.

TABLE OF CONTENTS

LIST OF TABLES

LIST OF FIGURES

FIGURE Page

FIGURE Page

FIGURE Page

FIGURE Page

CHAPTER I

INTRODUCTION

Modeling and simulation of polymeric film blowing process is the subject matter of this doctoral dissertation. Principal objectives of the present work and the organization of the dissertation are presented in this chapter together with the necessary introductory material. In the first section, a brief description of the process and the key issues that concern film manufacturers are presented. These manufacturing concerns define the objectives of this work, which is presented in Section B. In the subsequent sections, the scope of the work and the organization of the dissertation are described.

A. Description of the Process

Polymeric films are used in a wide variety of applications. These films are made of thermoplastic polymers. Some of the important applications are in the packaging industry, and products such as, garbage bags, carry bags, and thin plastic sheets are often manufactured using film blowing process.

Film blowing process is a rapid and an economic method of manufacturing polymeric films. This process produces in polymeric sheets, which are thin and biaxially oriented. The biaxial orientation of the film is one of the desirable features of the process as it can be used to alter the strength characteristics of the film produced. Figure 1 shows the schematic of a typical film blowing process. To achieve biaxial stretching, polymer melt extruded from an annular die is inflated along the azimuthal direction

---

This dissertation follows the style of Journal of Rheology.

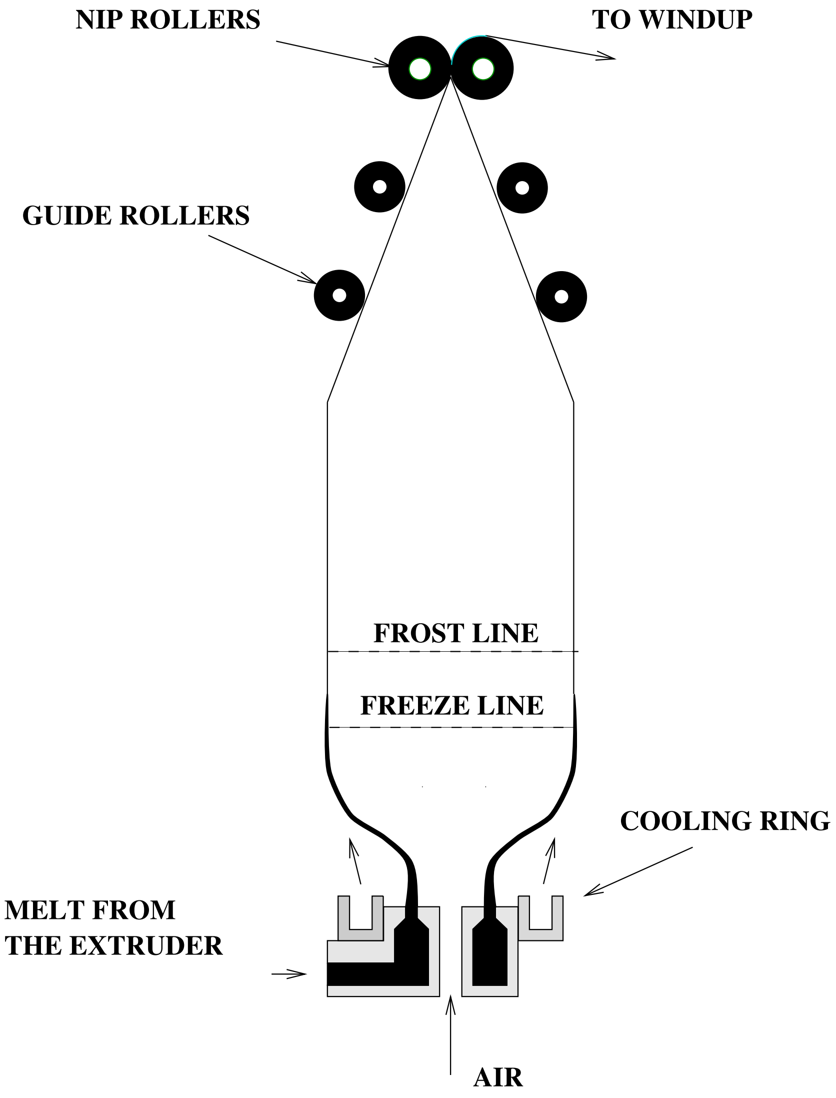

FIG. 1. Schematic of a typical film blowing process.

and simultaneously stretched along the axial direction. The inflation of bubble is actuated by forcing air into the bubble and increasing its volume. The stretching along the axial direction is achieved by controlling the velocity of the nip rollers and the mass flow rate at the die. These two stretchings occur simultaneously resulting in an increase in the bubble radius and a decrease in the film thickness. The cylindrical bubble is flattened using a series of guide rollers before it is drawn out via the nip rollers. The bubble formed between the die and nip rollers is supported by additional structure on which the guide rollers and nip rollers are mounted. This structure in not shown in the figure and it is also used to mount the instrumentation for measuring the film properties.

The complex dynamics of sustaining such a bubble is accomplished by cooling the polymer melt using turbulent air jets. The temperature of the polymer melt is approximately around 475 – 525 K at the die and it drops by 100 K before it reaches the freeze-line. The radius of the bubble remains constant beyond the freeze-line. The temperature of the film further drops by another 100 K before it is wound up as lay-flat tubing.

Stretching of the film stops at the freeze line, where the film is parallel to the centerline of the bubble. Beyond the freeze line no significant deformation is observed. Depending on the nature of the resin and the cooling rate, crystalline structures are formed in the film. This results in the change of refractive index of the film at the frost line and can be observed with unaided eyes. The distinction between the frost line and the freeze line is exaggerated in the figure 1 for the purpose of depiction.

Specification of initial conditions for the transient analysis in this work is based on one of the techniques used to start the process. Figure 2 shows the details of this procedure. From an annular die, a cylindrical tube is first extruded and as the tube comes out, its end is capped and tied to a rope. This tube is then pulled upward

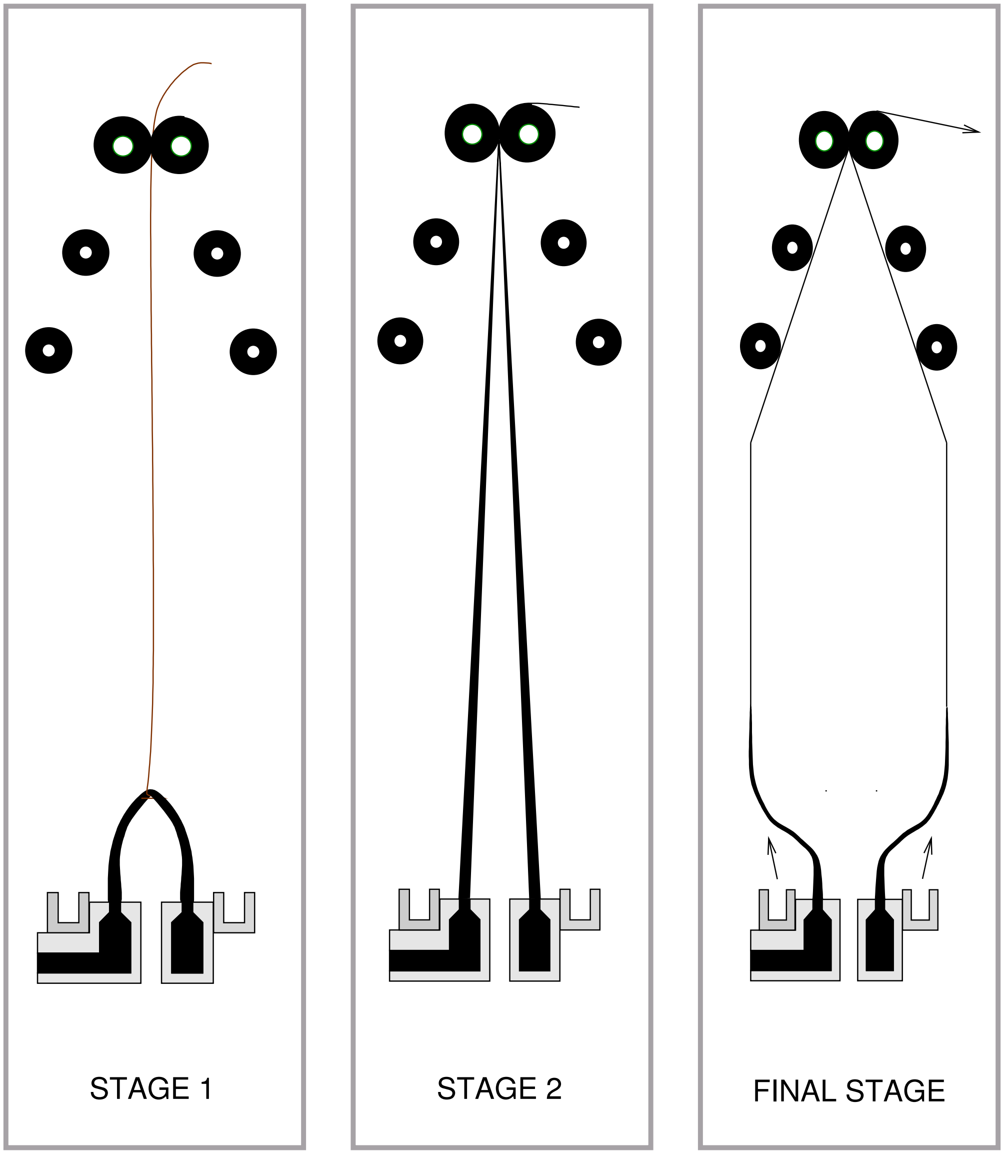

FIG. 2. Procedure used to start the process.

towards the nip rollers carefully without tearing it. This accomplished by balancing the pulling rate with the mass flow rate at the die. Once the tube reaches the nip rollers, it is sealed by the pinching action of the rollers. Then the pressurized air is injected into the tube to inflate into a bubble as shown in the figure. The amount of air injected inside and the nip roller velocity are adjusted together with the other system parameters to achieve a stable process. Hence, the analysis can be started from a cylindrical tube extending from the die to the freeze line.

1. Terminology

Some of the terminology that are part of the film blowing industry's *lingua franca* and used in this dissertation frequently is described in this section:

- Blow–Up Ratio (BUR)

  The BUR is the ratio of radius at the freeze line to the radius at the die. The normal values range from 2–10.

- Draw–down Ratio (DR)

  The DR is the ratio of the velocity at the nip rollers (or freeze line as the velocity remains constant beyond this point) to the velocity at the die. This value determines the stretching along the machine direction. This is also referred to as Take–Up Ratio (TUR), as the speed of nip rollers are known as take-up speed. Its value ranges from 5–20.

- Machine Direction (MD)

  The MD is the tangential direction of the bubble surface (perpendicular to the circumferential plane). This is the direction along which the polymer flows from the die to the nip rollers. Stretching in the MD is primarily due to the DR.

- Mils

  The final film thickness is often expressed in thousandth of an inch or milli inch. In SI units, it is $25.4 \times 10^{-6} m$.

- Thickness Ratio

  The ratio of the final bubble thickness to the thickness at the die. It is equal to the product of BUR and DR. Its values ranges from 10 to 100.

- Transverse Direction (TD)

  Azimuthal direction is referred as TD. It is also known as the Circumferential Direction (CD). The stretching along this direction is primarily due to the excess air pressure and it is quantified by BUR.

2. Key Manufacturing Issues

A stable operation of a film blowing process depends on various process parameters. Some of the important parameters are shown in the figure 3. The ultimate objective of a manufacturer is to produce a film based on the customer's specifications at the maximum possible rate. The speed of the nip rollers directly determine the amount of film produced in a second. Ideally, a manufacturer would like to maximize this value without compromising on the product quality. It has been observed, however, that a stable operation of the film blowing process is not always possible. Often tons of resins are wasted before the parameters are tuned to obtain a stable processing condition.

There are three key players (see Figure 4) the film processing industry. The customer is the first who defines the product specifications based on his needs, the second being the film manufacturer who tries to optimally produce the film with

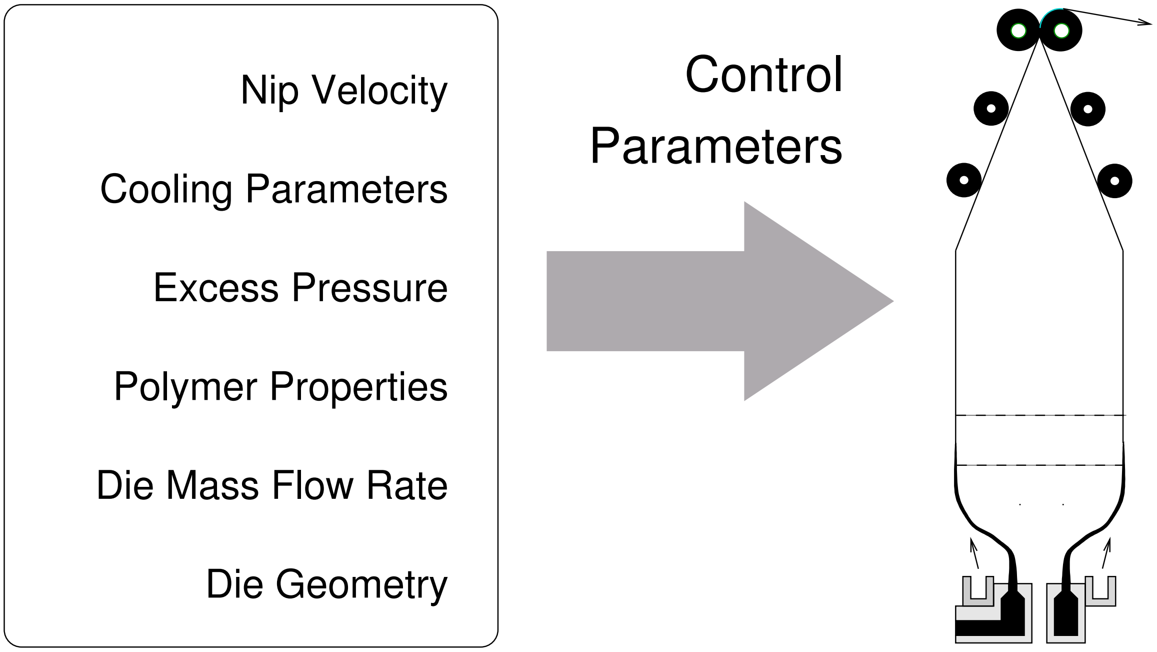

FIG. 3. Some critical process control parameters.

available equipments, and the third is the polymer manufacturer who supplies the material. It should be noted that this work is supported primarily by the polymer manufacturers.

The development of new techniques in polymerization has made available a wide variety of polymeric materials for manufacturing polymeric films. The constitutive behavior of these polymers directly affect many aspects of the process. The melt strength of a polymer determines the range of stable operating conditions for the process, the process becomes more stable as the melt strength increases. In general, the influence flow and strength characteristics of the material used on the process should be quantified to understand and control the process. In addition, this will enable the polymer manufacturers to alter the materials based on the needs of the film manufacturer.

The take-up speed (speed of the nip rollers) defines the productivity of the equip-

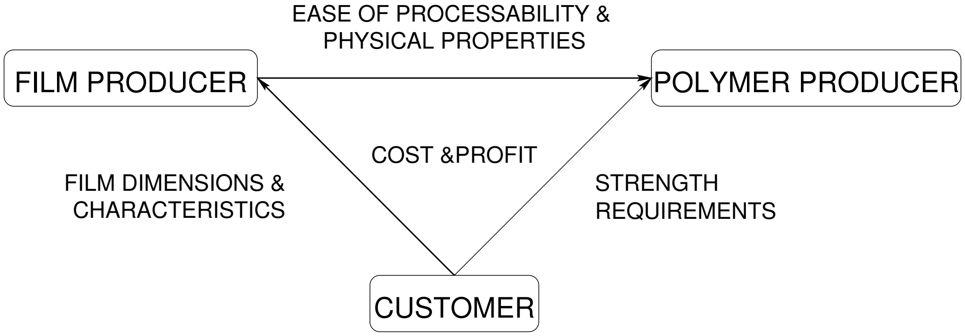

FIG. 4. Key players, who define the film blowing industry.

ment in terms of meters of film produced per second and any film manufacturer would like to maximize it. The mass flow rate at the die, which based on the die geometry determines the velocity at the die (V_{die}). The draw ratio then determines the amount of stretching in the machine direction. Even though the die geometry can be changed, it may be quite economical to use the same die and produce films of different specification by controlling other parameters. Excess pressure inside the bubble is responsible for the stretching in the transverse direction. The type of and nature of cooling used influence the phase change of the polymer, thereby altering its strength characteristics. All these variables are coupled in a nonlinear way and pose a daunting task to the film manufacturer in obtaining a stable operating zone.

The key issue that concerns the film producer is how to effectively control the process and manufacture the film in an optimum manner. In this context, either through experiments, experience, or theoretical investigations he would like arrive the rules which would help him to determine the process parameters that would give a stable operating zone and more importantly on how the process and polymer characteristics affect the ultimate strength and behavior of the film produced.

B. Objectives of the Study

1. To develop an accurate mathematical model of the film blowing process.
2. To develop a numerical algorithm to solve the mathematical model using the finite element method and validate the solutions through comparison with experimental data.
3. To analyze instabilities that affect the process using the model developed.

1. Mathematical Model

The dynamics of film blowing process is transient, nonisothermal and nonlinear. The process and the boundary conditions can be assumed axisymmetric in the region above the die and below the guide-rollers when the process is running in a stable mode. This assumption will be violated sometimes when the process is unstable and always when the bubble collapses. The polymers used for this process are viscoelastic and often they are semi-crystalline. Heat transfer plays a significant role in the process and the material properties are temperature dependent. These aspects of the process to be included in the model in order to study the process accurately. In this work most of these features are included in the model developed. Details of the model developed are presented in the fourth chapter. This model is derived by restricting the generic equations in the curvilinear setting to the bubble surface and it is independently validated using a derivation from control volume approach.

2. Numerical Method

The mathematical model developed is formulated using the finite element method to solve the problem numerically and simulate the process. The model developed is time dependent, hence, the standard practice of using finite element approximation for the space and finite difference approximation for time is used. This scheme results in the so–called α-parameter family. Some of the equations in the model developed are hyperbolic in nature and the Stream-wise Upwinding Petrov Galerkin(SUPG) method is used to overcome the loss of best approximation property of the Galerkin finite element method.

3. Instabilities

Experimental investigations have shown the existence of some instabilities which can be still modeled under axisymmetric assumption. These instabilities will be analyzed using the code developed to quantify the cause–effect relationships between the process parameters and these process instabilities.

C. Significance and Scope of the Study

The motivation and partial support for the present work is from the Polymer Film Center (PFC), which is part of the industry consortium Polymer Technology Center (PTC) of the Texas A&M University. One of the main goals of this consortium is to pursue advanced research and enable the transfer of that technology to the participating industries. It is expected that the present work will enable the industry to do numerical runs on the computer and estimate the important process parameters. These parameters can be further fine tuned using experiments if necessary. This approach will benefit the industry and result in greater productivity.

The accuracy of a numerical simulation directly depends upon the accuracy with which the mathematical model describes physical process. Some of the key issues that affect this process are discussed below:

Constitutive Behavior of the Polymer. Film blowing process uses thermoplastic polymers, which are often semi-crystalline. In addition, the biaxial stretching falls under the category of *strong flows*. Most of the studies in the field of polymeric flows focus on the shearing flows and the models working well in the regime of shearing flow need not perform satisfactorily in the elongational flow. Both uniaxial and biaxial extensional flows are strong as at least one of the eigen values of the velocity gradient tensor is positive. These flows are difficult not only for the theoretical studies but also for the experimental investigations, especially in the case of biaxial extensional flows.

In the present work choice of the model is made based on available literature and no claim will be made that it is the best model. For polymers there is no single model available to describe its behavior in all regimes of motion. In this work for liquid-like zone of the polymer modified Phan-Thien-Tanner model is be used and for the solid zone Kelvin–Voight model is used.

Kinematics. When film blowing process is operating in a stable condition, the region interest for simulation can be classified as axisymmetric (about the z–axis passing through the center of the annular die). This region of interest is the zone above the die and below the guide rollers. This assumption is not valid when the process is unstable or when the bubble is collapsing. To accurately model the problem in all operating regimes it has to be in non-axisymmetric setting. In order to write down the system of equations, the problem requires tools of differential geometry. This becomes slightly complicated as the metric tensor becomes time dependent in transient problems. Most of the published literature deals only with the analysis in steady state and the equations are not rigorously arrived at by restricting the generic equations in curvilinear coordinates to the bubble surface. The equations presented in this dissertation are derived rigorously and cross verified by reducing to simplified setting and also with the equations derived from control volume like approach. To be solved equations written in contravariant, covariant and mixed coordinates, are finally written down in physical coordinates were one can verify equation further for dimensional consistency.

Numerical Method. The system of equations which govern the process do not fall under a single class. For instance, the constitutive model used is hyperbolic in nature and the equation governing the heat transfer is advection dominated. Under these conditions, a simple Galerkin finite element method may have problems obtaining convergence or it will require a very fine mesh. The Galerkin finite element methods approximate the differential operators like central differences. This introduces an error in the way of negative diffusion and often tackled by adding some form of artificial diffusion. These terms added in principle should vanish as the mesh becomes fine. In the present work this problem is handled using a simple version of SUPG and reasonably fine meshes.

Boundary Conditions. Boundary conditions and process parameters are determined using laboratory/field process conditions. But the value of the stresses at the die exit poses a complexity due to the viscoelastic nature of the polymer. It is assumed that the prior shearing history does not influence the behavior of the polymer. Including this is beyond the scope of the current constitutive framework adopted by this work, as strain does not directly play a role in the model for liquid zone.

Validation. Accuracy of the model developed and the numerical technique used is established by comparison with the field data supplied by the members of the Polymer Technology Consortium and published experimental results in the literature.

Instabilities. Experimental studies show that film blowing process can exhibit different kinds of unstable behavior. Of the these instabilities, present work attempts to capture the radius instability and melt–tension instability. Both of these instabilities satisfy the axisymmetry assumption and are simulated using the model developed.

D. Significant Contributions

1. A transient axisymmetric model describing film blowing process is derived from the first principles using the tools of differential geometry.
2. A complete constitutive model for the process is proposed in this work. This model describes the polymer from the die till the nip rollers, and includes a model for the crystallization kinetics.
3. The viscous dissipation terms for the proposed constitutive model are derived rigorously using the principles of thermodynamics.
4. The model developed is validated using experimental data and transient results capturing instabilities are also presented.
5. Theory for a non-axisymmetric model is developed.
6. A software with complete pre– and post–processing tools is developed based on the transient axisymmetric model.

E. Organization of the Dissertation

This dissertation is organized into eight chapters and four appendices. In the next chapter, a detailed survey of the technical literature on the modeling, analysis, and other different aspects of film blowing process is presented. The basis and structure of the constitutive modeling used for the simulation are presented in the third chapter. The development of the mathematical model is described in the fourth chapter with all the required details, and the finite element formulation of the model developed is the topic of the fifth chapter. Validation of the model developed using available experimental data is discussed in sixth chapter and the analysis of instabilities is presented in seventh chapter. Finally, the eight chapter concludes the work with suggestions for the future studies. In appendix A, the details of the differential geometry calculations used in the dissertation are described and appendix B summarizes the transient axisymmetric model. An analysis of film blowing process using shooting method and a critique of that approach is presented in appendix C. The last appendix presents a non-axisymmetric model for film blowing process.

F. Summary

Modeling and analysis of film blowing process is a theoretically challenging problem and very pertinent to the polymer industry. This work attempts to take a step to make the modeling more accurate and validate the work using actual field data.

CHAPTER II
REVIEW OF LITERATURE

A brief review of the literature pertaining to modeling and analysis of film blowing process is presented in this chapter. This review is organized into few sections to address the different issues that arise in this context. The first step in a theoretical study is the development of a mathematical model describing the dynamics of the process and this is discussed in Section A. The momentum equations are incomplete without the understanding of how the stresses are related to the kinematics of the flow. The missing link is the constitutive model of the material and the Section B describes the developments and issues related to constitutive modeling. Film blowing process involves phase change of the polymer from a liquid–like zone to a solid–like zone. This adds complexity to the description of the material behavior. Often, semi–crystalline polymers are used in the manufacture of films and to describe the constitutive behavior of these polymers one has to consider the crystallization kinetics in the analysis. These issues are discussed in the Section C. The model equations describing the process can be solved using various approaches such as, the finite element and the finite difference methods. The advantages and disadvantages associated with these methods and some important questions that arise from the nature of the equations are discussed in Section E.

A. Process Modeling

The dynamics of a process has to be expressed in the language of mathematics before a theoretical solution can be attempted. Even the experimental methods use this theoretical basis for its construction, and thereby the measurement. For instance, when an experiment measures viscosity, it assumes an *apriori* definition of it from the mathematical model of the problem. An incorrect or a simplified model may lead to experimental results which can not be generalized. The first and the most important contribution to modeling film blowing process is by Pearson and Petrie in their work Pearson and Petrie (1970a), (1970b). Till date with few exceptions most of the published works have used their model equations except with changes to the constitutive model [Campbell and Cao (1987)]. Their approach describe the process using a steady state, axisymmetric, and isothermal model. In addition they assume a simple linear constitutive behavior. Even though these assumptions do not hold good in the actual process, they can be easily relaxed. Their work was one of the most important in this field as they give the basic approach and structure of the model to be used. Their first paper [Pearson and Petrie (1970a)] describes the mathematical approach used to derive the model. It is quite relevant to this dissertation as the present work extends that approach to develop a transient model. However, the equations in the Part 1 are not simplified to a point where it can be readily incorporated in a FEM code and solved. They address this issue in their second part [Pearson and Petrie (1970b)], where the equations are derived based on the physical understanding of the process.

Improvements over the Pearson and Petrie's analysis have since been proposed by Petrie(1975) and as well as by several other groups. Typically these extensions include heat transfer analysis and using a viscoelastic or a generalized Newtonian model to describe the polymer. The works by Yeow (1976) and Cain (1988) take a look at the stability problems related to film blowing process. Analysis of Yeow is restricted to linear fluids and the model equations are perturbed to solve a stability problem. Perturbations are assumed to be axisymmetric in order to have a simpler set of equations. Cain in his work besides the steady state analysis, studied the perturbation problem extending it to nonisothermal and nonlinear constitutive behavior (Marucci model). However, these studies do not attempt to capture the actual instabilities that occur in the process. Their work is focused on stability around certain fixed points of the solution using linear stability analysis. Considering the fact these models do not match accurately with experimental results, stability analysis is not so meaningful despite the claim that it will give an qualitative understanding of the process. Besides the use of nonlinear model, considering phase change and crystallization kinetics involve additional model equations, which are essential to model the process accurately.

B. Constitutive Modeling

The model first proposed by Pearson and Petrie (1970b) used a Newtonian model to describe the polymer. This is far from the actual behavior of the model. Following key points should be kept in mind when approaching the constitutive modeling for film blowing process:

- Flow in film blowing process is *elongational* and it is a *strong* flow.
- Polymers used for producing films are *viscoelastic* and *semi–crystalline*.
- The process involves phase change, from a liquid–like state to solid–like state.

These complexities in the flow makes it difficult to describe the constitutive behavior of the polymer accurately. Petrie (1979) provides a very detailed introduction to the previous work done in that field. Film blowing process which is a biaxial stretching is a strong elongational flow problem. Unlike the linear fluids such as, water, which can be modeled easily with a single constitutive model (Newtonian), nonlinear fluids pose an enormous complexity. There is no single model which can handle both shear flows and elongational flows effectively for a particular polymer, let alone generalizing for all polymers.

Various different models were studied in the context of film blowing process. Petrie (1975), for example, assumed that the polymer could be modeled as a purely elastic fluid and that the effect of temperature could be accounted for by assuming Arrhenius-like temperature dependencies for the density and modulus [Petrie (1975)]. He avoided the heat transfer and time-dependent aspects of the problem by assuming that the axial temperature profile (the temperature dependence on z) could be determined apriori, and that the process has attained steady-state. Although the predicted dependence of bubble shape and size on z were not too far from the experimental ones, details such as velocity profiles and material properties, were incorrect. Interestingly, Petrie found that the bubble shape predictions for a simple Newtonian liquid and those for a perfectly elastic fluid bracketed the experimental ones, suggesting that a more realistic polymer model could help close the gap between predicted and actual bubble shapes.

Han and Park (1975) assumed that the polymer could be modeled as a power-law fluid and solved the problem under nonisothermal conditions. Their work includes both radiative and conductive heat transfer from the film to the cooling air and the surroundings. Furthermore, as in the study by Petrie, Han and Park assumed an Arrhenius temperature-dependence for the polymer viscosity. But a power-law fluid used in their work is inadequate to describe a viscoelastic material. In addition, they do not consider the crystallization kinetics in their work. The predicted bubble shape and temperature profiles though close to the measured ones for low-density polyethylene (LDPE) blown films, disagreed considerably with data from high density polyethylene (HDPE) films; presumably because the model failed to account for crystallinity in the films. Many different constitutive models were considered for studies by different research groups, such as, the Marucci model [Cain and Denn (1988)]. Most of this work stop at the freeze–line. And make a tacit assumption that the polymer is liquid–like till the freeze–line.

Cao and Campbell's (1990) work developed a model which extended the analysis beyond the freeze–line. They modeled the melt with a modified contravariant Maxwell model and beyond the freeze–line used a Hookean solid. In their work, the freeze–line is defined based on the yield stress of the material. It is one of the first attempts to extend the analysis beyond the freeze–line. The change from liquid–like zone to solid–like zone is digital in their work and there is no mushy zone in between. They call this transition as plastic–elastic transition. In addition, their work does not include crystallization kinetics, hence, restricted to amorphous polymers. Cao and Campbell's predictions of bubble radius, temperature, and velocity profiles are in reasonably good agreement with Gupta's (1980) experimental measurements using amorphous polystyrene blown films. However, in the critique of shooting method presented in appendix C, reasons behind these agreements are presented.

Among the many models available in the literature, Khan and Larson (1987) point out that PTT model is one good models in predicting elongational flows. PTT model is a variant of the contravariant Maxwell model and it is derived from a network theory.

C. Phase Change and Crystallization Kinetics

Polymers can be either amorphous or semi–crystalline. The polymers used for production of films are often semi–crystalline. Hence it is important to include the crystallization kinetics in the modeling. The crystallization kinetics in film blowing process is nonisothermal. In addition, the strain induced crystallization accelerates the rate of crystallization. A recent study by Rao (1999) has a detailed review of the literature and presents a sophisticated method based on principle of multiple natural configurations. The principle of multiple natural configurations developed by Rajagopal (vide Rao (1999)) is a natural and accurate way to model problems such as this one. Take for instance the issue of reference frame for newly crystallizing material, it can be assumed that it is formed in a stress free state in the absence of gravity [Baldoni and Rajagopal (1997)] and can be used as the reference state for that material, and this approach is used in the present work as it has a strong logical basis. It is not necessary to have stress free state as a reference configuration, in fact any configuration, even the one the body may not occupy, can serve a reference configuration. But to be solvable, however, one chooses a stress free configuration, otherwise the problem (which is already complex enough) will become intractable.

Modeling crystallization kinetics has a rich history and it is very well presented in Eder *et al.* (1990). Most of the models used in the literature have Melvin Avrami's model as the starting point their analysis. This equation is modified to account for nonisothermal effects and strain induced crystallization. A chief exception to this approach is the one adopted by Rao (1999) and the model is derived here purely from thermodynamic considerations.

In the case of film blowing process, Baranov *et al.* (1992) improved analysis by explicitly including the effect of polymer crystallinity. These authors assumed iso-kinetic crystallization and that the degree of crystallinity attained the maximum level possible at the freeze–line. Baranov further assumed that beyond the freeze–line the degree of crystallinity in an "oriented" blown polymer film is independent of the position. Their bubble shapes and temperature profile predictions, though better than Han and Park's, still disagreed with the experimental results of oriented films.

D. Instabilities

The term “instability” is used here to denote the experimentally observed instabilities in film blowing process and not the studies which deal with linear stability theory around certain fixed points in the solution [Cain and Denn (1988)]. It is reasonable to do a stability analysis for problems which are posed accurately such as flow governed by Navier–Stokes equation and draw conclusions from it. In this case, Cain and Denn do not consider even the important aspects of film blowing like phase change and crystallization kinetics, hence, it is not so meaningful do a perturbation analysis and draw conclusions from it.

Kanai and White’s (1985) work on the stability of the film blowing process has valuable experimental data and qualitative understanding of instabilities. They compare the behavior of LDPE, LLDPE, and HDPE polymers. Their work concludes that under similar conditions LDPE is the most stable and HDPE is the least stable for the process. The instabilities observed in their work are non-axisymmetric in nature. The work done by Minoshima and White is of great importance and gives three experimentally observed instabilities. These instabilities are: bubble–radius instability, melt-tension instability, and helical stability. The first two of these can be assumed to maintain axisymmetry, but the helical instability is non-axisymmetric.

Larson (1992) discusses some of the chief instabilities that affect film blowing process. His review mainly covers the work done by Cain and Denn (1988) and Minoshima and White (1986). Other related issues in film blowing process are the scale up problems and draw resonance. Due to draw resonance, variations in the film thickness are observed despite maintaining a constant extruder rate and take–up velocity. This problem has received considerable attention in the field of fiber spinning process [Jinan (1991); Kurtz (1992)]. Scale up problems arise when the results obtained in a experimental set up are translated to actual conditions. Often the performance is not the same. This is essentially due to incorrect scaling parameters. The nonlinear behavior of the polymer and the complexity of the process makes it difficult to identify the scaling parameters, and very few studies have addressed this problem [Simpson and Harrison (1991)]

E. Numerical Techniques

Solution to the model equations are obtained using numerical techniques. The model equations governing film blowing process are nonlinear and coupled, hence an analytical solution to the problem is not possible. Numerical solution is an approximation and its accuracy depends on the many factors. When a real life problem like film blowing process is solved, approximations happen at two levels. The mathematical modeling introduces the first level of approximation. It is practically impossible to translate a real life event accurately into a mathematical statement. In the limit of engineering accuracy, however, one can say the model equations are accurate. In the case of film blowing process, one cannot even say that. The reason being the lack of accurate description of the constitutive behavior. The second level of approximation is introduced while solving the partial/ordinary differential (or integral) equations describing the phenomenon.

Almost all numerical work in film blowing process use what is known as the shooting method, the only exception is Cain and Denn (1988) who solved the problem correctly using a finite difference method as a two point boundary value problem. A description of shooting method can be obtained from many texts on numerical methods [Issacson and Keller (1994); Keller (1976)]. It can accurately solve a two-point boundary value problem like an initial value problem using an iterative approach only in the case of linear problems. The film blowing process is nonlinear and the boundary conditions at both ends (die and nip) control the dynamics of the problem. A delicate balance between the velocity of the nip rollers and the mass flow rate at the die end is required to achieve a stable blowing process. In our previous work [Mayavaram and Reddy (1996)] many of the flaws in using the shooting methods are pointed out. In principle, shooting method is not applicable to this problem. A brief summary of Mayavaram and Reddy (1996) is presented in appendix C.

Among the popular techniques used to solve partial differential equations, finite difference methods and finite element methods are the most important. In the finite element method solution is obtained by approximating the space in which is solution is sought and in the case of finite difference method the differential operator is approximated. It can be shown that the finite difference scheme is a subclass of the finite element method. Reddy (1993) is one of best introduction to the finite element method and the finite element method applied to fluid mechanics problems is well introduced in Reddy and Gartling (1994). The mathematical theory of FEM is well developed for linear elliptic problems [Brenner and Scott (1994); Oden and Reddy (1983)], for such class of problems the even studies in error estimation and adaptivity are well studied [Ainsworth and Oden (2000)].

The equations describing the constitutive behavior are often hyperbolic in nature. Finite element method looses its best approximation property for such equations [Brooks and Hughes (1982)]. In simple words, it is like using a central difference approach to model an advection dominated problem for which it is ill-suited. This is because the central difference schemes are under diffusive and to overcome this, techniques such as, artificial diffusion, and upwinding are used. The ideal solution to such problems in 1-D would be to use forward differences with CFL number 1 [Veque (1992)]. This condition is rarely met in realistic problems. A popular approach in finite element method is the SUPG (streamwise upwind petrov galerkin) developed by Hughes and his coworkers [Brooks and Hughes (1982); Hughes *et al.* (1986); Hughes and Mallet (1986a,b)]. The SUPG technique upwinds the system in the direction of the flow, hence it is called streamwise. The terms added to restore the best approximation property vanish to zero as the mesh size h tends to zero, i.e, that is when the mesh is fine. In other words, when the mesh is very fine (which in turn will demand smaller time step) one need not resort to such techniques. There are many variants of these upwinding methods and SUPG is one of the best. In cases were one tracks a front (like filling or phase change), SUPG smoothes the front. This undesirable effect can be overcome by a method called discontinuity capture (DC) developed by Hughes and Mallet (1986b), however, this will place restrictions on the time step and the mesh size.

F. Other Issues

Heat transfer from the film to the turbulent cooling air from the air rings by convection and surrounding by radiation is influences the dynamics of the process. In laboratory scale experiments [Gupta (1980)] cooling is often achieved via natural convection. Under such conditions radiative heat transfer becomes competitive and comparable to the convection heat transfer. The lack of accurate data for the emissivity of the film is a definite setback for simulating the radiative heat transfer and the variation in emissivity in a numerical experiment [Mayavaram and Reddy (1996)] did affect the solutions significantly. In an industrial setting the heat transfer is achieved by turbulent air jets from the air ring and here the radiation heat transfer can be neglected. The heat transfer due to cooling jets can be estimated by solving the flow around the bubble using a turbulent flow model. Campbell *et al.* (1992) and Rao

(1998) estimate the heat transfer using such an approach. There are many commercial flow solvers like FIDAP [Rao (1998)] which can give an quick estimate of the heat transfer. However these studies do not consider the nonlinear coupling between the flow and the bubble shape. The bubble shape depends on the properties of the polymer which is a strong function of the temperature. The temperature distribution depends on the heat transfer dynamics which is achieved using the turbulent air flow and the flow dynamics depend on the bubble shape. Hence, an accurate analysis should couple these phenomenon and iterate till a convergence is achieved. No such analysis is available in the published literature.

G. Summary

A brief survey of literature pertaining to problem at hand was presented in this chapter. Additional references to relevant works are cited as and when they are required. The principal objectives of this survey is to make sure that the present work is new and an improvement over previous studies, and understand the background and critical issues in the field. There are no studies simulating the problem in transient setting and even in steady state there is no work analysis the problem as a two point boundary value problem considering phase change and crystallization kinetics. Hence, the proposed work is a new and an important contribution. The key issue in film blowing process is not only to predict the bubble shape accurately but also the stresses. An accurate estimate of stresses is required to establish structure–property relationship. A transient study is required to capture the bubble instabilities which are observed in the experimental studies. In order to understand bubble collapse and the unstable behavior the problem should be studied in non-axisymmetric setting. A transient axisymmetric model can capture only the radius and melt–tension instability. There is plenty of scope in film blowing process for further work to increase our understanding of this process and develop better control procedure.

CHAPTER III

CONSTITUTIVE MODELING

Accurate description of the material behavior during film blowing process is one of the chief factors in determining the success of the numerical simulation. Viscoelastic nature of the melt and the phase change/crystallization kinetics during the film blowing process increases the complexity of describing the constitutive behavior of the material. In this chapter, an overview of the constitutive model used for the simulation is described. In the following section, some of the critical issues that should be addressed by a model for this class of problem is discussed and in the subsequent sections, methodology used to resolve these issues are explained. Final section of this chapter summarizes the model equations and the relevant boundary conditions.

A. Modeling Issues

Constitutive model used to describe the polymer used in film blowing process should address the following fundamental questions that are relevant to this process:

- What is the criteria used to determine the transition from liquid–like zone to the solid–like zone?
- What is the best model to describe the material behavior of the liquid–like zone?
- What is the best model to describe the constitutive behavior of the solid–like zone?
- How is crystallization kinetics modeled?

- What is the effect of orientation and alignment on the material behavior?
- How is the mixture of crystalline and amorphous phases modeled?
- What portion of the stress is dissipated?

In the following sections these issues are addressed in detail.

1. Criteria for Phase Change

The question “what is a solid and what is a liquid?” is very fundamental and requires a careful consideration [Dunn and Rajagopal (1995)]. In this dissertation, a simple thermal basis will be used to distinguish the solid and liquid models. Polymers are either semi–crystalline or amorphous. Semi–crystalline polymers are characterized by both glass transition temperature and melting temperature. Unlike metals, polymeric solids are rarely completely crystalline. They exist as a mixture of both amorphous and crystalline zones. Below the glass transition temperature, the amorphous zones in the material are frozen and they behave like a viscoelastic solid. And above the glass transition temperature the amorphous zones behave like a liquid. The crystalline zones in the material remain solid till the melting temperature and above that temperature these zones melt. Hence, the glass transition temperature and the melting temperature of the polymer form the criterion for switching between the liquid–like zone and the solid–like zone.

$$\begin{aligned} T &\leq T_g \quad \text{Solid–like behavior} \\ T &\geq T_m \quad \text{Liquid–like behavior} \\ T_m > T &> T_g \quad \text{Transition zone} \end{aligned}$$

Even though T_g is ideally the temperature at which the amorphous zones of the polymer freeze, from experimental observations, the material ceases to flow at a temperature higher than T_g and it is referred to as "no–flow temperature", T_{nf}. Hence, for computational purposes this T_{nf} will be used instead of T_g.

Solid–like zone in the film–line is characterized as a mixture of amorphous and crystalline phases. The degree of crystallization attained depends on the process dynamics and a nonisothermal model is used to describe the crystallization kinetics (see section E). When the temperature is above the melting point T_m the polymer melt exists as a viscoelastic liquid. The transition zone is modeled as a mixture of viscoelastic liquid and crystalline solid. This framework is general enough to admit different models to be used for the liquid and the solid zones. The choice of actual models used is based on the available literature and the computational convenience.

In this work, Phan-Thien-Tanner (PTT) model is used to describe the viscoelastic melt and a modified Kelvin-Voight (KV) two element solid will be used to describe the solid zone. The basis for this decision is discussed in the subsequent sections.

B. Liquid Zone: Phan-Thien-Tanner Model

The field of rheology is abundant with constitutive models describing the polymer's behavior's under various conditions. Unlike linear fluids which are uniquely described by the Stokes model, nonlinear fluids exhibit a wide range physical dynamics which are quite difficult to capture. As it was mentioned in Chapter II, film blowing process falls under the classification of bi–axial extensional flow which is a strong flow. Many models which predict shear flows (weak flows) satisfactorily, fail to predict the extensional flow accurately. Previous studies [Khan and Larson (1987)] indicate that Phan–Thien–Tanner model predicts the extensional flow problems satisfactorily and hence, it is chosen for this work. In the framework developed it is possible to use a different model instead of Phan–Thien–Tanner model. It should be noted that most of the models used in the literature are minor variants of contravariant Maxwell model (popularly known as Upper Convected Maxwell model), hence implementing these variations is relatively easy once a robust framework is present.

Phan–Thien–Tanner model is a network model which assumes that the polymer molecules form a network due to strong local attractions. In this network the junctions are formed and destroyed continually. And the model ignores the effects due to the stray chains and loose ends in the network. Besides these assumptions, incompressibility is assumed. One of the important feature of PTT model is it allows non-affine motion. In this context, non-affine motion is understood as follows: if the continuum suffers a velocity gradient $\mathbf{L}$ then the individual polymer chains need not strictly adhere to this motion and they can experience a slip. If there is no slip, then the motion is affine, which is the case in most other models. From these assumptions. PTT model is derived using the standard methods, and following equation describes the final form of the model.

$$\lambda \left[\frac{d\boldsymbol{\tau}}{dt} - \boldsymbol{\mathcal{L}}\boldsymbol{\tau} - \boldsymbol{\tau}\boldsymbol{\mathcal{L}}^T \right] + Y\boldsymbol{\tau} + H_T \frac{dT}{dt}\tau = 2\lambda G\mathbf{D} \tag{1}$$

$$\boldsymbol{\mathcal{L}} = \mathbf{L} - c_1\mathbf{D} \tag{2}$$

$$Y = \exp\left[c_2 \mathrm{Trace}(\boldsymbol{\tau})\right] \tag{3}$$

where, $\mathbf{L}$ is the velocity gradient tensor, $\mathbf{D}$ is the rate of deformation tensor (symmetric part of $\mathbf{L}$), λ is the relaxation time, G is the elongational modulus, and c_1 and c_2 are constants. The term $H_T dT/dt\boldsymbol{\tau}$ accounts for the nonisothermal behavior. It is not enough to consider the properties such as, viscosity and modulus as functions of temperature to extend the model to non-isothermal realm, and the additional term involving H_T should also be considered. This accounts for the dependence of the connector force on temperature in the underlying model [Peters and Baajens (1997)] and should be considered in the analysis. This term is often neglected due to the lack of data.

C. Crystalline Solid Model

The polymeric melt begins to crystallize below the melting point of the polymer. The model that describes this crystalline solid should account for the anisotropy resulting from the orientation and reference configuration for the crystallizing material. Often, the stress free configuration is assumed to be the reference configuration for the analysis. Even though this not necessary from a theoretical stand point, it is quite important to simplify the computation. For the present problem, it is assumed that the newly formed crystalline solid is stress free. This assumption is true only in the absence of gravity. The gravity effects in this context are ignored in this analysis. The orientation of the crystalline structures formed is strongly influenced by the flow. It is assumed in this study that the orientation of the crystallizing molecules coincide with the principal axes of the rate of deformation tensor at that point. This greatly simplifies the computational implementation.

In this work, modified Kelvin's model is used to describe the crystalline solid. Figure 5 shows the mechanical description of Kelvin Voight model, which is a spring element is connected in parallel to the dash-pot. The following equation describes the model.

$$\sigma = \mathbf{E}\epsilon + \eta_e \mathbf{D} \tag{4}$$

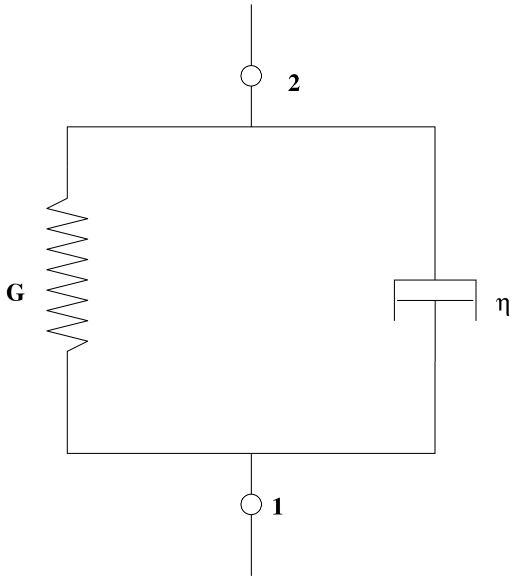

FIG. 5. Kelvin's two element viscoelastic solid is used to model the solid zone.

where E is the elongational modulus tensor and η_e is the elongational viscosity. The modulus tensor brings in the effect of orientation of the crystalline structure. The strain tensor ϵ in the domain is computed from the velocity distribution at every instant, and $\mathbf{D}$ is the rate of deformation tensor. Since the equations are solved in the principal coordinates, matrices arising out of these tensors are diagonal.

This model is sometimes known as the Kelvin-Voight model. The initial response of this model is liquid-like, however, the ultimate response is like a solid [Petrie (1979)]. More details about the strengths and weaknesses of this model is discussed in [Findley *et al.* (1976)]. This model was chosen for the analysis because it is simpler to implement among the available viscoelastic models for solid. In the model equation

4, both E and η_e depend on temperature and the transformation is achieved using Arrhenius function.

Below the T_g the same model is used to describe the amorphous phase, but with an isotropic **E** tensor. This implies that below glass transition temperature, the material is a mixture of isotropic and anisotropic Kelvin-Voight model.

$$\begin{aligned}\mathbf{E} &= \mathbf{E}(T_0)exp\left(\frac{A_E}{T}\right)\\ \eta_e &= \eta_e(T_0)exp\left(\frac{A_\eta}{T}\right)\end{aligned}$$

In the above expressions, A_E and A_η have the units of temperature, and referred to as temperature sensitivity. It is the ratio of activation energy to universal gas constant R.

D. Strain Computation

Using the fundamental relations in continuum mechanics, strain tensor ε is computed. The deformation gradient tensor **F** is given by the equation $\mathbf{F} = \partial\mathbf{x}/\partial\mathbf{X}$, where BX refers to the reference configuration and **x** refers to the current configuration. A strain free configuration is chosen as the reference configuration and it is assumed that the material solidifies in a strain free state.

For the purposes of this analysis Eulerian strain tensor is computed and it is given by $\varepsilon = 1/2(\mathbf{1} - (\mathbf{F}\mathbf{F}^T)^{-1})$. In order to compute **F**, the equation $d\mathbf{F}/dt = \mathbf{L}\mathbf{F}$ is solved. From the deformation gradient tensor, the strain tensor is then easily computed as the tensors are diagonal in the principal coordinate system.

E. Degree of Crystallinity

The equation governing crystallization kinetics should be derived based on a thermodynamic analysis of the system such that it minimizes the dissipation function. But often a simpler empirical approach starting from the Avrami equation is adopted. The form crystallinity equation used for the present analysis is.

$$\frac{d\chi}{dt} = f_1(T)f_2(\chi)f_3(\boldsymbol{\tau})$$

where the degree of crystallinity is expressed as a function of temperature, degree of crystallinity, and the stress tensor. The starting point for the particular form used in this analysis is the Avrami's model [Avrami (1939)] with corrections to the crystallization rate K. The original Avrami's model is given by,

$$\chi(t) = 1 - exp(-Kt^n).$$

This model assumes that the crystalline phase is nucleated by the germ nuclei that already exists in the melt. The density of the germ nuclei diminishes through the activation of some of them to become growth nuclei for grains of the crystalline phase and the ingestion of the others by the growing crystals. The crystals cease to grow when they impinge on each other. In this model, if the rate of crystallization K is written as $\int K(T)dt$ and the equation is rewritten, we get

$$\frac{d\chi}{dt} = nK(T)(1-\chi)\left(-log_e(1-\chi)\right)^{\frac{n-1}{n}}.$$

This equation is further modified by including the effect of flow in the model. Experimental investigations show a dramatic increase in the crystallinity rate due to the flow. This is approximately represented by an exponential term depending on the effective deformation rate of the flow.

$$\frac{d\chi}{dt} = nK(T)(1-\chi)\left(-log_e(1-\chi)\right)^{\frac{n-1}{n}} \exp(c_\chi II_D) \tag{5}$$

In the above equation c_χ is a constant and II_D is the second invariant of the rate of deformation tensor. There are different approaches to specify the FIC [Kulkarni and Beris (1998)]. Since the focus of this dissertation is not on developing a crystallinity model, a simpler model is implemented. It should be noted, however, that the nature of dependence can be modified and implemented in the present framework quite easily. The crystallinity rate K(T) is defined by the following equation based on Lambrigger (1998).

$$K(T) = K(T_0)\exp(-\frac{A_\chi}{T}).$$

Instead of Arrhenius like dependence, one can use alternative specification as in Kulkarni and Beris (1998) which uses a Gaussian function to describe the dependence. The science of modeling crystallization kinetics is still in the state of development, hence a plethora of different models with varying physical justifications exist.

F. Mixture Calculations

Below the melting point temperature, the polymeric material is modeled as a mixture of a amorphous region and semi-crystalline region. Following assumptions are invoked for doing the mixture calculations:

1. The amorphous and the crystalline zones are modeled as a constrained mixture and they move together. This is an reasonable assumption as it is possible for the same polymer molecule to traverse both the crystalline and amorphous zone.

2. A point in the mixture is described in an averaged sense, i.e., it may have n%

crystalline zone and (100-n)% amorphous zone. Hence, the co-occupancy of both the phases are permitted.

3. Locally the mixture is at equilibrium between the two phases. This is enforced for both thermal and momentum dynamics.

The ratio of the mixture is computed using the degree of crystallinity. The effective stress is in this region is computed using the following equation.

$$\boldsymbol{\tau} = (1-\chi)[\boldsymbol{\tau} \text{ Phan–Thien–Tanner model}] + \chi[\boldsymbol{\tau} \text{ Kelvin's Model}]. \tag{6}$$

In the above equation, the degree of crystallinity will never become 1, as the polymer is semi-crystalline. Hence, even beyond the glass transition temperature, the material will be treated as a mixture of anisotropic and isotropic Kelvin's solid with $\chi = \chi_{max}$, as described by the following equation.

$$\boldsymbol{\tau} = (1-\chi_{max})[\boldsymbol{\tau} \text{ isotropic Kelvin's model}] + \chi_{max}[\boldsymbol{\tau} \text{ anisotropic Kelvin's Model}] \tag{7}$$

G. Viscous Dissipation

In the case of viscoelastic fluids not all the stress work, $trace(\boldsymbol{\sigma}\mathbf{D})$ is converted into heat and dissipated in the system. The amount of stress work that is dissipated has to be calculated based on the model equations using the second law of thermodynamics. In this section, details of these calculations are presented. Constitutive model developed in this chapter is a combination of PTT model (for liquid-like behavior) and modified KV model (for crystalline solid).

In the case of the modified KV model it is easy to arrive at the partition. The stress tensor computed using this model is written as $\boldsymbol{\sigma} = \boldsymbol{\sigma}_e + \boldsymbol{\sigma}_v$, and as there is no entropic effect in memory of the material, it is then concluded that only $Trace(\boldsymbol{\sigma}_v\mathbf{D})$ is dissipated. Hence, the viscous dissipation term due to KV model is $\eta_E Trace(\mathbf{DD})$.

For Phan–Thien–Tanner model, the following approach is adopted to compute the viscous dissipation terms. The first step is to identify the possible list of independent variables that affect the constitutive behavior of material. Then the second of law thermodynamics is used to determine those variables which really matter. For instance, Helmholtz free energy f may not depend on $\dot{\nabla T}$ and it is determined using a standard approach which is described in most text books on continuum mechanics [Bowen (1989)]. Using this procedure, the restrictions on the model to satisfy the Clausius-Duhem inequality are identified. Based on this the constitutive form for the internal energy (u) is determined and hence, the amount dissipated is also estimated.

The first law of thermodynamics is written as,

$$\rho\dot{u} = -\nabla \bullet \mathbf{q} + \rho r + Trace(\boldsymbol{\sigma}\mathbf{D}), \tag{8}$$

where u is internal energy, $\mathbf{q}$ is heat flux vector, r is radiation term and the final term is the stress work. And the second law of thermodynamics is written as,

$$\rho T\dot{s} - \rho\dot{u} + Trace(\boldsymbol{\sigma}\mathbf{D}) - \frac{\mathbf{q} \bullet \nabla}{T} \geq 0. \tag{9}$$

Above equation is rewritten in terms of Helmholtz free energy (f) which is given by $f = u - Ts$ and $\dot{f} = \dot{u} - T\dot{s} - \dot{T}s$. Using in the second law of thermodynamics following equation is obtained.

$$-\rho(\dot{f} + s\dot{T}) + Trace(\boldsymbol{\sigma}\mathbf{D}) - \frac{\mathbf{q} \bullet \nabla}{T} \geq 0. \tag{10}$$

The flow is assumed to be isochoric and density is steady. And the following independent variables are probable factors that may influence the constitutive behavior of the material:

- Velocity gradient tensor, $\mathbf{L}$
- Temperature, T
- Temperature gradient, ∇T
- Network strain tensor, $\mathbf{B}$

Phan–Thien–Tanner model is a network model and the network can undergo a non-affine motion. Vector, $\mathbf{R}$ is the connector of two junctions and the network strain tensor is given by $\mathbf{B} =< \mathbf{RR} >$. The model defines $\dot{R} = \mathbf{L} \bullet \mathbf{R} - c_1 \mathbf{D} \bullet \mathbf{R} - \beta \mathbf{1} \bullet \mathbf{R}$ and the last two terms make the motion non–affine. The rate of $\mathbf{B}$ is given by

$$\dot{\mathbf{B}} = (\mathbf{L} - c_1 \mathbf{D} - \beta \mathbf{1}) \bullet \mathbf{B} + \mathbf{B} \bullet (\mathbf{L}^T - c_1 \mathbf{D} - \beta \mathbf{1}).$$

Helmholtz free energy, f is now written as a function of these independent variables, $f = f(\mathbf{L}, \mathbf{B}, T, \nabla T)$. And $\dot{f}$ is expressed as,

$$\dot{f} = Trace(\frac{\partial f}{\partial \mathbf{L}} \bullet \dot{\mathbf{L}}) + Trace(\frac{\partial f}{\partial \mathbf{B}} \bullet \dot{\mathbf{B}}) + \frac{\partial f}{\partial T} \dot{T} + \frac{\partial f}{\partial \nabla T} \bullet \dot{\nabla T}.$$

Substituting the above expression in the second law following equation is obtained.

$$\begin{aligned} &- \rho\, Trace(\frac{\partial f}{\partial \mathbf{L}} \dot{\mathbf{L}}) - \rho(\frac{\partial f}{\partial T} + s)\dot{T} - \rho\, Trace(\frac{\partial f}{\partial \nabla T} \bullet \dot{\nabla T}) \\ &\qquad - \rho\, Trace(\frac{\partial f}{\partial \mathbf{B}} \bullet \big((\mathbf{L} - c_1 \mathbf{D} - \beta \mathbf{1}) \bullet \mathbf{B} + \mathbf{B} \bullet (\mathbf{L}^T - c_1 \mathbf{D} - \beta \mathbf{1})\big) \\ &\qquad\qquad + Trace(\boldsymbol{\sigma} \mathbf{D}) - \frac{\mathbf{q} \bullet \nabla}{T} \geq 0. \end{aligned}$$

From the above equation, using the standard approach, it can be shown that, $\partial f / \partial T = -s$, $(\partial f / \partial \mathbf{L} = 0$, and $\partial f / \partial \nabla T = 0$. The stress, $\boldsymbol{\sigma}$ is written as $\boldsymbol{\sigma} = \boldsymbol{\sigma}_v + \boldsymbol{\sigma}_e$, where

$\boldsymbol{\sigma}_v$ is purely viscous contribution and $\boldsymbol{\sigma}_e$ is the elastic stress of the network.

$$\begin{aligned} Trace\left((-2\rho\mathbf{B}\bullet\frac{\partial f}{\partial\mathbf{B}}+\boldsymbol{\sigma}_e)\bullet\mathbf{D}\right) & \\ +Trace((2\rho\mathbf{B}\bullet\frac{\partial f}{\partial\mathbf{B}})\bullet(c_1\mathbf{D}+\beta\mathbf{1}) & \\ +Trace(\boldsymbol{\sigma}_v\mathbf{D})-\frac{\mathbf{q}\bullet\nabla}{T}\geq 0, & \end{aligned}$$

and $\boldsymbol{\sigma}_e = 2\rho\mathbf{B}\bullet\partial f/\partial\mathbf{B}$. And the final form the inequality is expressed by the following equation.

$$Trace\ (\boldsymbol{\sigma}_v\bullet\mathbf{D})+Trace\ (\boldsymbol{\sigma}_e\bullet\mathbf{A})-\frac{\mathbf{q}\bullet\nabla}{T}\geq 0. \tag{11}$$

The slip tensor $\mathbf{A}$ is given by $\mathbf{A} = c_1\mathbf{D}+\beta\mathbf{1}$. Internal energy u is expressed in terms of $\boldsymbol{\sigma}_e$. Internal energy also depends only on $\mathbf{B}$ and T, hence,

$$\rho\dot{u}=\rho\frac{\partial u}{\partial T}\dot{T}+\rho\ Trace(\frac{\partial u}{\partial\mathbf{B}}\bullet\dot{B}).$$

Using $u = f + Ts$ and $s = -\partial f/\partial T$, it is shown that,

$$\frac{\partial u}{\partial\mathbf{B}}=\frac{\partial f}{\partial\mathbf{B}}+T\frac{\partial^2 f}{\partial T\partial\mathbf{B}}$$

and

$$\rho\dot{u}=\rho\frac{\partial u}{\partial T}\dot{T}+\ Trace\left((\boldsymbol{\sigma}_e-\rho T\frac{\partial\boldsymbol{\sigma}_e/\rho}{\partial T})\bullet(\mathbf{D}-BA)\right).$$

It should be noted that in the standard PTT model $\boldsymbol{\sigma} = \boldsymbol{\sigma}_e$, that is, the network stress is same as the total stress and there is no additional pure viscous stress term. It is shown that $\partial\boldsymbol{\sigma}_e/\partial T = H_T$. The nonisothermal term of Phan–Thien–Tanner model is written as,

$$H_T=\frac{1}{\rho}\frac{\partial\rho}{\partial T}+\frac{\alpha}{T}$$

and using $C_v = \partial u/\partial T$, the final form of the energy equation is obtained.

$$\rho C_v\dot{T}=-\nabla\bullet\mathbf{q}+\alpha\ Trace(\boldsymbol{\sigma}\bullet\mathbf{D})+(1-\alpha)Trace(\boldsymbol{\sigma}\bullet\mathbf{A}). \tag{12}$$

The material function α is obtained from experiments. Depending on the value of α the nature of memory effect is decided. When $\alpha = 1$, the contribution to the internal energy is from the "so-called" energy elasticity and when $\alpha = 0$ it is from the entropic effects. Nature of the partition arrived at depends on the assumptions made in the calculations. It is possible to alter some of the assumptions and come to a different result.

H. Summary

Constitutive model developed in this chapter addresses the key issues that are essential to model a polymer undergoing film blowing process. Material behavior of the polymer in the liquid zone is described using PTT model, in the transition zone as a mixture of PTT and anisotropic Kelvin–Voight model, and in the solid zone as a mixture of isotropic and anisotropic Kelvin–Voight solid model. Degree of crystallinity is estimated using a simple model for crystallization kinetics and the orientation of the crystalline structures is assumed to be aligned with the principal axes. Viscous dissipation calculations starting from laws of thermodynamics, partition the model correctly to account for the dissipation terms in the energy equation.

CHAPTER IV

TRANSIENT AXISYMMETRIC MODEL

Development of a transient, nonlinear, axisymmetric model of film blowing process is presented in this chapter. In Section A, underlying assumptions of the model and its consequences are discussed in detail. In the subsequent section a brief discussion of the coordinate system used and the metric tensor is presented, however, the details of the computations including the derivation of the Christoffel symbols are relegated to Appendix A. In Section C the derivation of rate of deformation tensor is presented. This tensor contains transient terms and is a key entity in the model development. Derivation and significance of the governing equations are presented in Section D. In the final sections of this chapter, boundary and initial conditions obtained from the process conditions are described.

A. Modeling Assumptions

1. Axisymmetry

Domain of analysis and the process conditions are axisymmetric. In order to obtain an uniform film thickness and lay–flats, an operational film blowing process has to maintain axisymmetry from the die exit up to the guide rolls. Beyond the guide rolls the symmetry pattern changes to plane symmetry. Attention of the present simulation is focused on the region between the die exit and the guide rolls. Hence, in principle, the assumption that the process is axisymmetric is valid. The axisymmetric assumption implies that the variables and their derivatives do not change with the azimuthal angle, ϕ, which is expressed by the following equation.

$$\frac{\partial[\cdot]}{\partial\phi} = 0. \tag{13}$$

There are two distinct experimentally observed instabilities [Minoshima and White (1986)] that are axisymmetric. They are the bubble diameter oscillation instability (Figure 6) and the melt tension instability (Figure 7). Both these instabilities can be simulated using the model developed. This approach, however, will not be able to predict the behavior of the process under non-axisymmetric disturbances and bubble collapse. It is important to investigate the causes of these instabilities, whether they arise from the complex constitutive behavior of the polymer or from some external disturbances. In the case of latter, is it reasonable to expect an order like axisymmetry from a disorder? The axisymmetry of the process is often lost due to the unbalanced die exit velocity resulting from the uneven distribution of melt in the die. Design of the film blowing die is crucial in creating an axisymmetric annular extrudate. Often this is not the case and a variation in thickness in the order of 5% to 15% arises out of this error.

2. Thin Membrane Approximation

Variation of properties and process conditions across the thickness of the film is ignored. Since the thickness of the film is small in comparison with the radius of the bubble and both the radii of curvature, thickness averaging can be used to reduce the dimensionality of the problem. This assumption implies that the variables and their derivatives do not vary significantly across the film thickness.

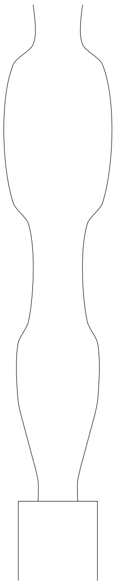

FIG. 6. Periodic fluctuation of bubble diameter.

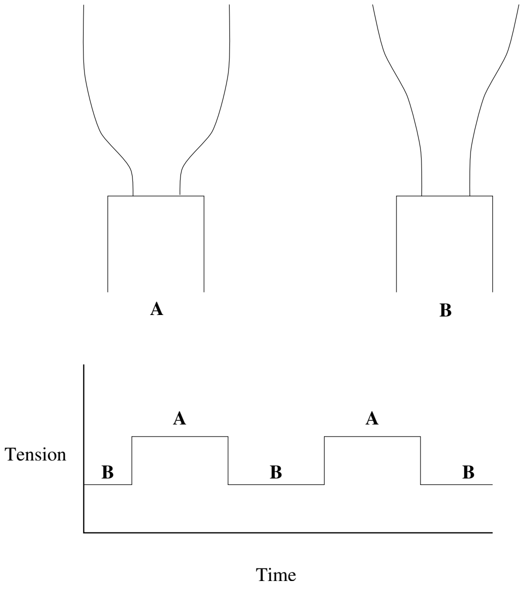

FIG. 7. Melt tension instability.

Thin membrane approximation limits the models ability to include the crystallization kinetics of the process. Under this assumption it is not possible to simulate processes that control crystallization kinetics using variable cooling on internal and external surfaces of the film.

3. Extrudate Swell

Analysis does not include the effect of extrudate swell. Extrudate swell at the die exit is ignored in this analysis. Most polymers exhibit extrudate swell (often incorrectly referred to as die swell) and this is a mark of their viscoelastic nature. Depending on the Deborah and Weissenberg number, it could be due to the memory or the normal stress effects. It is not possible to include this without simulating the flow inside the die.

Issues. Experimental observations stress the importance of the extrudate swell in the film blowing process. The effect of extrudate swell is ignored due to the computational complexity in incorporating it. Even the studies that are specifically devoted to extrudate swell phenomenon indicate the problems in modeling it and the present lack of knowledge. This problem can temporarily overcome by developing thumb rules based on experimental studies on extrudate swell. It is well known that the extrudate swell can be directly correlated to the first normal stress difference (if memory effects are negligible). This can serve as a starting point in the analysis to include the effects of extrudate swell.

4. Transient Behavior

Film blowing modeled as a transient process. Model developed in this study includes the transient terms in the governing equations. In principle, with a transient analysis, it is possible to capture some of the instabilities that are experimentally observed in the film blowing process.

5. Inertia Terms

Inertia terms are included in the model. Inclusion of the inertia terms in the model equations will introduce geometric non–linearity in the problem. Significance of these terms depend on the ratio of inertia to viscous forces in the momentum equation, and the ratio of advection to conduction heat transfer in the energy equation. If

$$\frac{\rho \|v^2\|}{\|\tau\|} \ll 1,$$

then the inertia terms can be neglected in the momentum equations. Similarly if,

$$\frac{\rho C_p v L}{k} \ll 1$$

then the advection terms can be ignored. In the present model the inertia terms are not ignored. Using the above equations, it can be shown that inertia terms are important.

6. Gravity

Gravitational forces are considered in the analysis. The significance of the role of gravity on the process operation has to be investigated. It is reasonable assume that gravitational forces may play a role when the process is unstable, or when the bubble collapse occurs. In the present model, the terms arising due to gravitational forces are included in the momentum equations.

7. Surface Tension

Surface tension forces are not included in the analysis. Importance of surface tension forces is determined by capillary number, which is the ratio of surface tension force to the viscous force. It can be shown that this number is small enough to be neglected. One of the chief problems in including the surface tension effects in the analysis is the lack of availability of the surface tension coefficient data as a function of temperature. In the present model the terms arising due to these forces are not considered.

8. Constitutive Behavior

Constitutive behavior of the polymer is modeled using a combination of Phan–Thien–Tanner (with some modifications) and Kelvin–Voight Model. Success or failure of the analysis depends to a large extent on the appropriate choice of the constitutive model. In the present case, this is further complicated by the phase change phenomena. A single constitutive law cannot accurately model both the liquid–like and solid–like states of the polymer. This can be shown using the symmetry arguments. In the present study Phan–Thien–Tanner model is used for the modeling the liquid like state, anisotropic Kelvin–Voight model is used for modeling the crystalline solid, and amorphous Kelvin–Voight model is used for modeling the amorphous solid. Details of constitutive modeling are described in the previous chapter.

9. Heat Transfer

Radiation heat transfer is included in the analysis. Importance of the radiation heat transfer was clearly shown in the preliminary analysis (see Appendix C). Radiation heat transfer plays a dominant role when forced convection cooling is not used. It is expected to play a minor role if the forced convection cooling at high cooling rates using turbulent air jets are used. The effect of radiation shape factor (whether the surface sees itself or not) is not included in the analysis.

The lack of accurate emissivity data is a major setback in including the contribution of the radiation heat transfer accurately. The radiation shape factor can be included in the analysis by approximating the bubble as a cylinder or sphere. However, the lack of accurate emissivity data is bound to create a greater error and hence the shape factor computations are ignored.

Conduction terms are included in the heat transfer model. The inclusion of axial conduction terms will change the nature of the energy equation from parabolic to elliptic. This will bring in an additional complication of specifying the boundary condition at the nip end.

Viscous dissipation terms are included in the model. Including the viscous dissipation terms is not straight forward as material under consideration is viscoelastic. One has to thermodynamically arrive at the portion of the stress that is recoverable (hence elastic and not dissipated) and that is dissipated. A detailed derivation of this partition is presented in Chapter III.

B. Coordinate System and Metric Calculations

Analysis of film blowing process is carried out in principal coordinates. Cylindrical coordinate system is not a good choice for two reasons: i) it results in a stress tensor with off diagonal terms and ii) the velocity vector has two non–zero components. These disadvantages increases the computational complexity. They not only increase the number equations to be solved, but also make the computation of items such as, the convective derivative more complex.

The above mentioned disadvantages are overcome by using the principal coordinate system. Principal coordinates, ξ_i are defined as follows:

- $\xi_1 \equiv$ Machine Direction (MD),
- $\xi_2 \equiv$ Transverse Direction (TD), and
- $\xi_3 \equiv$ Normal direction (ND).

In an axisymmetric analysis, the azimuthal angle ϕ coincides with ξ_2. The normal and machine directions will depend on the axial location, z of the bubble from the die end and it is characterized by the slope angle, θ. Coordinate system used in the analysis is depicted in Figure 8. This coordinate system under consideration is represented using a simple parametrization $\mathbf{X}(z, \phi, t)$, which is expressed as

$$\mathbf{X}(z, \phi, t) = (r(z,t)\cos\phi, r(z,t)\sin\phi, z).$$

Time dependence of the parametrization increases the complexity of the subsequent calculations. This also leads to a time dependent rate of deformation tensor $\mathbf{D}$.

C. Rate of Deformation Tensor

Derivation of the rate of deformation tensor for the transient axisymmetric model is presented in this section. Overall procedure of deriving $\mathbf{d}$ involves the following steps:

Step 1: Prove that $\mathbf{C} = G_{IJ}\mathbf{U}^I \otimes \mathbf{U}^J$

Step 2: Show that $\mathbf{D} = \frac{1}{2} d\mathbf{C}/dt$

Step 3: Push forward $\mathbf{D}$ to current coordinates

Step 4: Write the details of $\mathbf{d}$

Step 5: Express $\mathbf{d}$ in physical coordinates

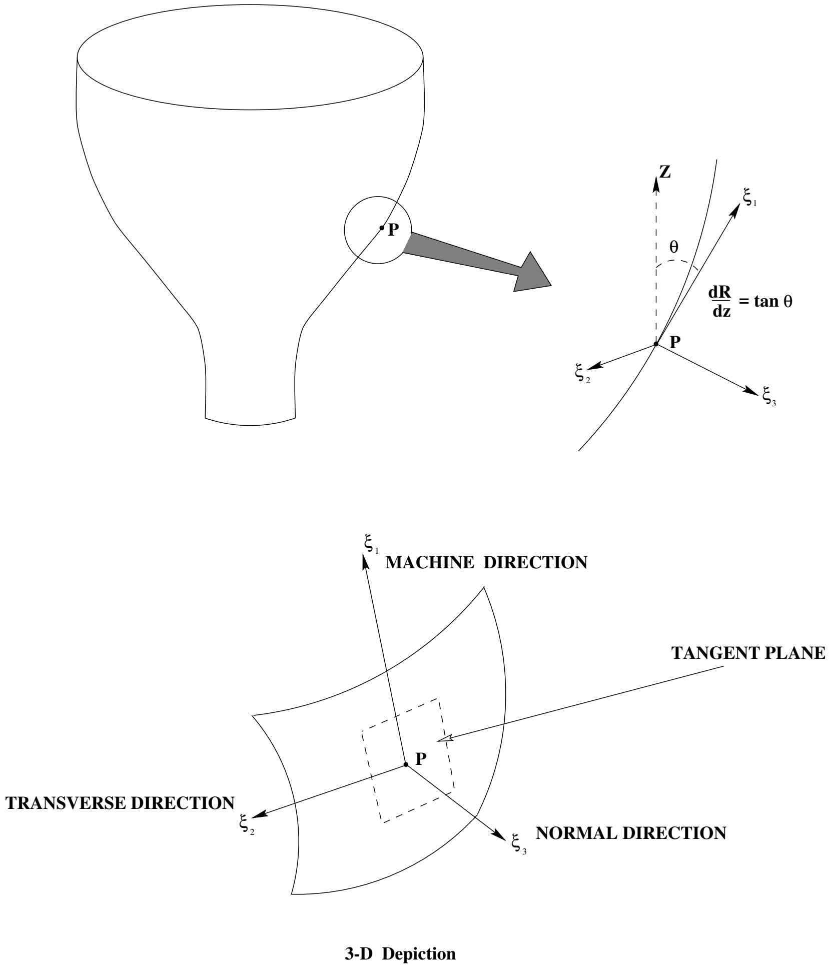

FIG. 8. Coordinate system used for the computation.

Rate of deformation tensor is first derived in a Lagrangian framework and then transformed (pushed forward) to the Eulerian framework. This step involves the definition of "convected derivatives". The subsequent step involves expanding the covariant derivatives and writing the details of rate of deformation tensor. And the final step is the writing out the tensor in physical coordinates for the numerical computation.

1. Lagrangian Framework

Entities in the reference configuration are denoted by uppercase letters. For instance, the metric tensor on the reference surface is denoted by $\mathbf{G}$ and the tangent plane is spanned by the vectors $\mathbf{U}^I$ and $\mathbf{U}^J$. This convention is also followed for the indices of vectors and tensors.

Let $\mathbf{X}$ be the coordinate system on the reference configuration and $\mathbf{x}$ denote the current coordinate system at time t, then the deformation gradient is given by

$$\mathbf{F} = \frac{\partial \mathbf{x}}{\partial \mathbf{X}} = F^i_I \mathbf{u}_i \otimes \mathbf{U}^I = \frac{\partial x^i}{\partial_c X^I} \mathbf{u}_i \otimes \mathbf{U}^I,$$

and the Green deformation tensor, which is also known as the right Cauchy–Green tensor is defined by

$$\mathbf{C} = \mathbf{F}^T \mathbf{F} = F^I_k F^k_J \mathbf{U}_I \otimes \mathbf{U}^J = g_{ab} G^{AC} \frac{\partial x^a}{\partial_c X^C} \frac{\partial x^b}{\partial_c X^B} \mathbf{U}_A \otimes \mathbf{U}^B.$$

This implies that $C^I_J = F^I_k F^k_J$, which is rewritten as $\mathbf{C} = C_{IJ} \mathbf{U}^I \otimes \mathbf{U}^J$. It can also be shown that $C_{IJ} = G_{IJ}$ and details of this derivation is found in Marsden and Hughes (1994). Hence,

$$\mathbf{C} = G_{IJ} \mathbf{U}^I \otimes \mathbf{U}^J$$

and

$$G_{IJ} = \text{Pull back of } (g_{ij}) = g_{ij} \frac{\partial x^i}{\partial_c X^I} \frac{\partial x^j}{\partial_c X^J}.$$

2. D in Lagrangian Framework

Rate of deformation tensor $\mathbf{D}$ in reference coordinates is defined as

$$\mathbf{D} = \frac{1}{2} \frac{d\mathbf{C}}{dt}. \tag{14}$$

Details of this definition are available in Marsden and Hughes (1994), refer to the definition 3.26 (page 61). The factor 2 is introduced for numerical convenience of the linearized theory. This definition is equivalent to the traditional

$$\mathbf{D} = \frac{1}{ds}\frac{d(ds)}{dt}, \tag{15}$$

where ds is the deformation. In current coordinates $ds^2 = d\mathbf{x}.d\mathbf{x}$ and this can be rewritten as $ds = (\mathbf{FX})^T(\mathbf{FX})$. This can be further simplified as $ds = \mathbf{X}.(\mathbf{F}^T\mathbf{F}).\mathbf{X} = \mathbf{X}.C.\mathbf{X}$. Using the standard definition of D, we can show the identity of the above two definitions.

3. Push Forward to Eulerian System

Rate of deformation tensor in Eulerian framework is the push forward of **D**.

$$\mathbf{D} = \frac{1}{2}\frac{d\mathbf{G}}{dt} = \frac{1}{2}\frac{dG_{IJ}}{dt}\mathbf{U}^I \otimes \mathbf{U}^J.$$

Further,

$$\frac{d\mathbf{G}}{dt} = \frac{d}{dt}\left[g_{ij}\frac{\partial x^i}{\partial_c X^I}\frac{\partial x^j}{\partial_c X^J}\right],$$

and

$$\frac{dG_{IJ}}{dt} = \left[\frac{dg_{ij}}{dt}\frac{\partial x^i}{\partial_c X^I}\frac{\partial x^j}{\partial_c X^J} + g_{ij}\frac{\partial v^i}{\partial_c X^I}\frac{\partial x^j}{\partial_c X^J} + g_{ij}\frac{\partial x^i}{\partial_c X^I}\frac{\partial v^j}{\partial_c X^J}\right].$$

Using the relationship,

$$\frac{\partial v^i}{\partial_c X^I} = \frac{\partial v^i}{\partial_c x^l}\frac{\partial x^l}{\partial_c X^I}$$

and rearranging the indices one gets

$$\frac{d\mathbf{G}}{dt} = \left[\frac{dg_{ij}}{dt} + g_{lj}\frac{\partial v^l}{\partial_c x^i} + g_{il}\frac{\partial v^l}{\partial_c x^j}\right]\frac{\partial x^i}{\partial_c X^I}\frac{\partial x^j}{\partial_c X^J}\mathbf{U}^I \otimes \mathbf{U}^J.$$

Hence, rate of deformation tensor in current coordinates is

$$\mathbf{d} = \left[\frac{dg_{ij}}{dt} + g_{lj}\frac{\partial v^l}{\partial_c x^i} + g_{il}\frac{\partial v^l}{\partial_c x^j} \right] \mathbf{u}^i \otimes \mathbf{u}^j, \tag{16}$$

and in other words,

$$d_{ij} = \left[\frac{dg_{ij}}{dt} + g_{lj}\frac{\partial v^l}{\partial_c x^i} + g_{il}\frac{\partial v^l}{\partial_c x^j} . \right] \tag{17}$$

4. Details of d

Components of $\mathbf{d}$: d_{11}, d_{22}, and d_{33} are written in detail expanding the convected derivatives. The expressions resulting from this are not very complex as many of the Christoffel symbols vanish. Components of $\mathbf{d}$ are,

$$d_{ij} = \frac{\partial g_{ij}}{\partial t} + g_{lj}\left[\frac{\partial v_l}{\partial x_i} + v^m \Gamma^l_{mi} \right] g_{ik} \left[\frac{\partial v_k}{\partial x_j} + v^n \Gamma^k_{nj} \right].$$

The metric tensor $\mathbf{g}$ is diagonal, hence, the above equation simplifies to,

$$\begin{aligned}
d_{11} &= \frac{\partial g_{11}}{\partial t} + 2g_{11}\left[\frac{\partial v_1}{\partial x_1} + v^1\Gamma^1_{11} + v^2\Gamma^1_{21} + v^3\Gamma^1_{31} \right] \\
d_{22} &= \frac{\partial g_{22}}{\partial t} + 2g_{22}\left[\frac{\partial v_2}{\partial x_2} + v^1\Gamma^2_{12} + v^2\Gamma^2_{22} + v^3\Gamma^2_{32} \right] \\
d_{33} &= \frac{\partial g_{33}}{\partial t} + 2g_{33}\left[\frac{\partial v_3}{\partial x_3} + v^1\Gamma^3_{13} + v^2\Gamma^l_{23} + v^3\Gamma^l_{33} \right]
\end{aligned}$$

and this can be further simplified by substituting for Christoffel symbols. The final form of rate of deformation tensor $\mathbf{d}$ in covariant representation ($\mathbf{d} = d_{ij}u^i \otimes u^j$) is given by the following equation.

$$\begin{aligned} d_{11} &= \frac{\partial^2 R}{\partial z^2}\frac{\partial R}{\partial t} + \frac{\partial V^1}{\partial z}(1 + \frac{\partial R}{\partial z}^2) + V^1 \frac{\partial^2 R}{\partial z^2}\frac{\partial R}{\partial z} + V^3 H \frac{\partial^2 R}{\partial z^2}\cos\theta \\ d_{22} &= R\frac{\partial R}{\partial t} + RV^1\frac{\partial R}{\partial z} - V^3 RH\cos\theta \\ d_{33} &= H\left(\frac{\partial H}{\partial t} + V^1\frac{\partial H}{\partial z}\right). \end{aligned}$$

It can be shown that the terms associated with V^3 are much smaller than the other terms, hence they are ignored.

5. Tensor d in Physical Coordinates

Numerical computation has to be done only in the physical coordinates and there are standard approaches to convert the tensors and vectors in contravariant or covariant settings to the physical coordinates. Using these methods [Aris (1962)] the final equations for rate of deformation tensor are written below.

$$D_{\underline{11}} = \frac{\frac{\partial^2 R}{\partial z^2}}{1 + \frac{\partial R}{\partial z}^2}\frac{\partial R}{\partial t} + \cos\theta\frac{\partial V_{\underline{1}}}{\partial z} \tag{18}$$

$$D_{\underline{22}} = \frac{1}{R}\left(\frac{\partial R}{\partial t} + V_{\underline{1}}\cos\theta\frac{\partial R}{\partial z}\right) \tag{19}$$

$$D_{\underline{33}} = \frac{1}{H}\left(\frac{\partial H}{\partial t} + V_{\underline{1}}\cos\theta\frac{\partial H}{\partial z}\right) \tag{20}$$

These results agree with the results presented in Yeow (1976), and here it has been derived rigorously using the standard continuum mechanics approach.

D. Governing Equations

Equations governing the dynamics of the film blowing process are presented in this section. Derivation of these equations is described in detail and the approximations made are highlighted. These model equations can be developed either using a control volume approach or it can be arrived at by restricting the equations of motion in a general curvilinear coordinates to the bubble surface. Former approach is error prone, however, it is useful in verifying the terms in the equation and understand their physical significance, especially when used together with the latter. Following is the list of variables that are of interest to a designer and they are computed by the developed mathematical model.

1. Variables of Interest

- Radius of the bubble, R
- Velocity of the film in the machine direction, $V_{\underline{1}}$
- Thickness of the bubble, H
- Pressure, P
- Principal stresses, $\tau_{\underline{11}},\ \tau_{\underline{22}},\ \tau_{\underline{33}}$
- Temperature, T
- Degree of crystallinity, χ

Of these variables, the kinematic quantities R, H, and V, and the thermal variable T are easily measurable using experimental techniques and hence, can be used to validate the model. The stresses are required to correlate the structure–property relationship.

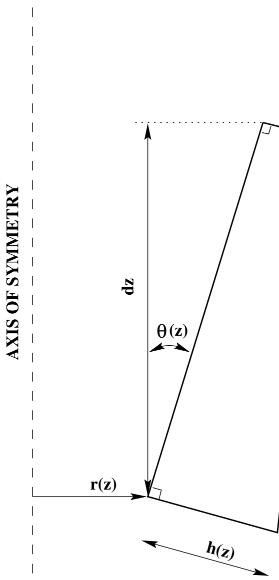

FIG. 9. Control volume used for the analysis.

2. Control Volume

Figure 9 shows the the control volume over which the mass, momentum and energy balances are carried out. Unlike the standard control volume whose dimensions are independent of the spatial coordinates, control volume used for deriving the equations for the film blowing process depends on the spatial coordinate z.

$$\begin{aligned} R &= R(z,t) \\ H &= H(z,t) \\ \theta &= \theta(z,t) \end{aligned}$$

The thin membrane approximation ignores the explicit dependence of the system variables on the thickness of the film. However, while deriving the system of equations, dependence on thickness comes into play. In the subsequent discussions it should be borne in mind that the R describes the radius of the inner surface of the film and the thickness, H is measured in the normal direction from this surface. The *slope angle*,

θ is angle made by the tangent to the inner surface with the z axis. This definition of θ can be written as,

$$\tan\theta = \frac{\partial R}{\partial z}$$

In the present problem, $H << R$ and it is much smaller than the both the radii of curvature. Hence, it is reasonable to conclude that $\frac{\partial H}{\partial z}\Delta z$ is smaller in comparison with the thickness H. These assumptions will simplify the calculation of the area of faces at $z + \Delta z$. For instance,

$$\text{Area of base at } z = (A_1)_z = 2\pi RH$$

and

$$\text{Area of base at } z + \Delta z = (A_1)_{z+\Delta z} = 2\pi RH(1 + \frac{\frac{\partial H}{\partial z}\Delta z}{H} + \frac{\frac{\partial R}{\partial z}\Delta z}{R} + \frac{\frac{\partial R}{\partial z}\frac{\partial H}{\partial z}\Delta z^2}{RH})$$

above equation can be simplified using the above assumptions and rewritten as,

$$(A_1)_{z+\Delta z} = 2\pi RH(1 + \frac{1}{R}\frac{\partial R}{\partial z}\Delta z)$$

In reference to this control volume, the coordinate, ξ_3 is in the thickness direction, ξ_2 is the azimuthal angle, and the coordinate, ξ_1 is along (tangential) the inner surface. The surface area of the control volume normal to the direction i is referred as A_i.

$$\begin{aligned} A_1 &= 2\pi RH \\ A_2 &= h\Delta\xi_1 = H\sec\theta\Delta z \\ A_3 &= 2\pi R\Delta\xi_1 = 2\pi R\sec\theta\Delta z \end{aligned}$$

and the volume, V of the control volume is given by

$$V = 2\pi RH\delta\xi_1 = 2\pi RH\sec\theta\delta z$$

In the above calculation some simplifying assumptions are imposed, such as, the variation in R along the inner surface is small over the $\Delta\xi_1$, etc. The control volume approach was primarily used to verify the terms in the equations and understand their significance.

3. Conservation of Mass

The law of conservation of mass is one of the fundamental laws of physics. Mass is neither created nor destroyed is the basis (ignoring the relativistic $E = mc^2$!) of this equation. In the present work, the polymer melt is treated as an incompressible fluid and the variations in mass density of the polymer due to the changes in temperature are ignored in the context of the conservation law. The general form the equation of conservation of mass in curvilinear coordinates is given below [Aris (1962)].

$$\frac{d\rho}{dt} + \rho\nabla.\mathbf{v} + \frac{\rho}{2g}\frac{\partial g}{\partial t} = 0. \tag{21}$$

In the above equation, $g = g_{11}g_{22}g_{33}$, substituting the appropriate expressions for g (see appendix A) it can be shown that,

$$\frac{\rho}{2g}\frac{\partial g}{\partial t} = \rho\left(\frac{1}{\sec\theta}\frac{\partial \sec\theta}{\partial t} + \frac{1}{R}\frac{\partial R}{\partial t} + \frac{1}{H}\frac{\partial H}{\partial t}\right).$$

Since the polymer mass density is assumed to be a constant, the term $d\rho/dt$ vanishes. The remaining term $\rho\nabla.\mathbf{v}$ is expanded as follows.

$$\nabla.\mathbf{v} = \frac{1}{\sqrt{g}}\left(\frac{\partial(\sqrt{g}v^1)}{\partial z}\right)$$

The other two velocity components in the equation vanish. For computational purpose it is important to express the final equation in physical coordinates. For instance, in physical coordinates, velocity in the MD $V_{\underline{1}} = v^1/h_1$. The final form of the equation of conservation of mass in physical coordinates is given by the following equation.

$$\frac{1}{\sec^2\theta}\frac{\partial \sec\theta}{\partial t}+\frac{1}{R}\frac{\partial R}{\partial t}+\frac{1}{H}\frac{\partial H}{\partial t}+\frac{1}{RH\sec\theta}\frac{\partial(RHV_{\underline{1}})}{\partial z}=0. \tag{22}$$

The above equation is verified using a control volume approach.

$$\begin{aligned}&\text{Rate of change of mass inside the control volume} =\\ &\qquad\qquad\text{Rate at which mass enters the control volume}-\\ &\qquad\qquad\qquad\qquad\text{Rate at which mass leaves the control volume}\end{aligned} \tag{23}$$

For instance the mass entering the control volume through face 1 at z is given by $\rho A_1 v_1$ and the leaving the control volume through face 1 at $z+\Delta z$ is give by $\rho A_1 v_1 + \frac{\partial \rho A_1 v_1}{\partial \xi_1}$. Hence the net mass entering in the direction 1 is $-\frac{\partial \rho A_1 v_1}{\partial \xi_1}$. Using similar approach for other directions we can write the following terms

Rate of change of mass in the volume:

$$\frac{\partial(\rho\delta V)}{\partial t}=\rho 2\pi\delta z\frac{\partial RHsec\theta}{\partial t},$$

along ξ_1:

$$[\rho A_1 V_{\underline{1}}]-[\rho A_1 V_{\underline{1}}+\frac{\partial(\rho A_1 V_{\underline{1}})}{\partial \xi_1}\Delta\xi_1]=-[\frac{\partial(\rho A_1 V_{\underline{1}})}{\partial \xi_1}\Delta\xi_1],$$

along the ξ_2:

$$[\rho A_2 V_{\underline{2}}]-[\rho A_2 V_{\underline{2}}+\frac{\partial(\rho A_2 V_{\underline{2}})}{\partial \xi_2}\Delta\xi_2]=-[\frac{\partial(\rho A_2 V_{\underline{2}})}{\partial \xi_2}\Delta\xi_2],$$

and along the ξ_3:

$$[\rho A_3 V_{\underline{3}}]-[\rho A_3 V_{\underline{3}}+\frac{\partial(\rho A_3 V_{\underline{3}})}{\partial \xi_3}\Delta\xi_3]=-[\frac{\partial(\rho A_3 V_{\underline{3}})}{\partial \xi_3}\Delta\xi_3].$$

Due to axisymmetry and thin membrane approximation the terms representing the variation along directions 2 and 3 will vanish. Hence the balance of mass equation can be written as

$$\frac{\partial(\delta V)}{\partial t}+\frac{\partial 2\pi RHV_{\underline{1}}}{\partial\xi_1}\Delta\xi_1=0. \tag{24}$$

Above equation can be rewritten after expanding all the terms as,

$$\frac{1}{R}\frac{\partial R}{\partial t}+\frac{1}{H}\frac{\partial R}{\partial t}+\frac{1}{\sec^2\theta}\frac{\partial\sec\theta}{\partial t}+ \\ V_{\underline{1}}\cos\theta R\frac{\partial H}{\partial z}+V_{\underline{1}}\cos\theta VH\frac{\partial R}{\partial z}+HR\cos\theta\frac{\partial V_{\underline{1}}}{\partial z}=0. \tag{25}$$

4. Conservation of Momentum

Momentum is a vector quantity and it has three components. In this subsection, equations of momentum is derived in the principal coordinate system. The three equations derived in this section will be used calculate $V_{\underline{1}}$, P and R. The Momentum equation in vector form general curvilinear coordinates can be written as follows.

$$\rho a^i\mathbf{u}_i=f^i\mathbf{u}_i+\nabla\bullet\left(\sigma^{ij}\mathbf{u}_i\otimes\mathbf{u}_j\right) \tag{26}$$

In the above equation $f^i\mathbf{u}_i$ is the body force term and the gravitational force is incorporated through it. The covariant derivative is clearly represented by including the basis vectors in the equation. Starting from the equation 26, momentum equations in physical coordinates are derived. Let us first consider the left hand side term, acceleration. This term can be written as,

$$\mathbf{a}=a^iu_i=\left(\frac{\partial v^i}{\partial t}+v^j\frac{\partial v^i}{\partial\beta^j}+v^lv^k\Gamma^i_{lk}\right)$$

and Γ^i_{lk} are the Christoffel symbols which are derived in detail in Appendix A. Right hand side of the above equation can be written in physical coordinates using the standard approach [Aris (1962)].

$$a(i) = \frac{\partial V(i)}{\partial t} + \frac{V(j)h_i}{h_j}\frac{\partial}{\partial \beta^j}\left(\frac{v^i}{h_i}\right) + \frac{V(l)V(k)}{h_l h_k}\Gamma^i_{lk} \tag{27}$$

Physical components of the acceleration is computed by direct substitution into the above equation.

The total stress tensor $\boldsymbol{\sigma}$ is decomposed into the deviatoric component $\boldsymbol{\tau}$ and the spherical component p and it is written as,

$$\boldsymbol{\sigma} = \sigma^{ij}\mathbf{u}_i \otimes \mathbf{u}_j = \left(-pg^{ij} + \tau^{ij}\right)\mathbf{u}_i \otimes \mathbf{u}_j$$

and the same equation in physical coordinates will translate to,

$$\sigma(ij) = -p + \tau(ij).$$

Hence, the right hand side of the equation can be written as (excluding the body force term),

$$\nabla \bullet \left(\sigma^{ij}\mathbf{u}_i \otimes \mathbf{u}_j\right) = \left(\frac{\partial \sigma^{ij}}{\partial \beta^j} + \Gamma^i_{jk}\sigma^{ij}\right)\mathbf{u}_i$$

and in physical coordinates as,

$$\frac{\partial \sigma(ij)}{\partial \beta^j} = \frac{h_i}{g}\frac{\partial}{\partial \beta^j}\left(\frac{g}{h_i h_j}\sigma(ij)\right) + \frac{h_i}{h_j h_k}\Gamma^i_{jk}\sigma(jk) \tag{28}$$

Combining the right hand side and left hand side the final form of momentum equation can be written as,

$$\rho\left[\frac{\partial V(i)}{\partial t} + \frac{V(j)h_i}{h_j}\frac{\partial}{\partial \beta^j}\left(\frac{v^i}{h_i}\right) + \frac{V(l)V(k)}{h_l h_k}\Gamma^i_{lk}\right] = \frac{h_i}{g}\frac{\partial}{\partial \beta^j}\left(\frac{g}{h_i h_j}\sigma(ij)\right) + \frac{h_i}{h_j h_k}\Gamma^i_{jk}\sigma(jk) \tag{29}$$

It is important to note that the equations are represented in principal coordinates, hence all the cross terms like $\sigma(ij)$ will vanish when $i \neq j$. By substituting for the Christoffel symbols (many of them vanish due to the orthogonal parametrization), this equation can be further simplified. In the subsequent paragraphs the momentum equations in the three principal directions will be presented in a simplified form.

ξ_1**: Machine Direction**. Momentum equation in the machine direction is used to solve for $V_{\underline{1}}$

$$\rho\left[\frac{\partial V_{\underline{1}}}{\partial t} + V_{\underline{1}}\cos\theta\frac{\partial V_{\underline{1}}}{\partial z} + V_{\underline{1}}V_{\underline{3}}\cos\theta\frac{\partial \theta}{\partial z}\right] = -rhogcos\theta + \frac{1}{RH}\frac{\partial}{\partial z}\left(RH\cos\theta\sigma_{\underline{11}}\right) + \sin\theta\frac{\partial \theta}{\partial z}\sigma_{\underline{11}} \tag{30}$$

ξ_2**: Transverse Direction**. As a consequence of the axisymmetry assumption, the equation of motion along the azimuthal direction degenerates to the following form. This equation is used to solve for the pressure.

$$p = \tau_{\underline{22}} \tag{31}$$

ξ_3**: Thickness Direction**. In the case of thickness equation, instead of the following equation, the equation arising out the bubble equation is used for the analysis. This bubble equation (33) is derived by integrating the momentum equation.

$$\rho\left[\frac{\partial V_{\underline{3}}}{\partial t} - V_{\underline{3}}\frac{\partial H}{\partial t} + \frac{V_{\underline{1}}V_{\underline{3}}}{H\sec\theta}\frac{\partial V_{\underline{3}}H}{\partial z} + V_{\underline{1}}^{2}\cos\theta\frac{\partial\theta}{\partial z}\right]$$
$$= -\rho g sin\theta - \cos\theta\frac{\partial\theta}{\partial z}\sigma_{\underline{11}} + \frac{\cos\theta}{R}\sigma_{\underline{22}} \quad (32)$$

$$\Delta pr\sec\theta + \rho grh\tan\theta + (\gamma + h\sigma_{11})\frac{\partial}{\partial z}\left[\frac{\partial r}{\partial z}\right] - (\gamma + h\sigma_{33}) \quad (33)$$

5. Conservation of Energy

The equation of conservation of energy is used to compute the temperature distribution. Polymer melt comes out of the die at a high temperature (500–550 K) and it is cooled rapidly by the turbulent air jets from the cooling ring. In an industrial scale process most of the cooling is achieved by the turbulent cooling air. On the other hand, laboratory scale experiments use natural convection heat transfer aided by radiation heat transfer. Hence it is important to include both modes of heat transfer in the equation. Polymers under consideration for the film blowing process have a low thermal conductivity ($\sim 10^{-}1$) hence, conduction is not bound to play a dominant role. The terms arising out of conduction heat transfer are included for the sake of completeness. Following equation describes the heat transfer in the medium in a generic form.

$$\rho C_p\frac{dT}{dt} + \text{source/sink terms} = -\nabla \bullet \mathbf{q} + \text{viscous dissipation terms.} \quad (34)$$

Including viscous dissipation in the analysis is a tricky issue. In the case of viscoelastic liquids, not all the stress is dissipated into heat. Elastic part of the stress is recoverable and not dissipated. If this is not accounted the model will not truly reflect the reality. One can estimate the amount of stress that is dissipated using the thermodynamic analysis of the constitutive model. The heat flux $\mathbf{q}$ is given by $-k\nabla T$. This term can be further expanded as,

$$\mathbf{q} = q^i\mathbf{u}_i = -k\frac{\partial T}{\partial \beta^i}\mathbf{u}^i = -k\frac{\partial T}{\partial \beta^j}g^{ij}\mathbf{u}_i.$$

in other words, $q^i = -k\frac{\partial T}{\partial \beta^j}g^{ij}$. In this particular case, $g^{ij} = 0$ if $i \neq j$. This further simplifies the expression, for instance, $q^1 = -k\frac{\partial T}{\partial z}g^{11}$. The term $\nabla \bullet \mathbf{q}$ in equation 34 can be expanded as follows,

$$\begin{aligned}
\nabla \bullet \mathbf{q} &= \frac{\partial q^i}{\partial \beta^i} + \Gamma^k_{ki}q^i \\
&= \frac{\partial q^i}{\partial \beta^i} + \frac{1}{\sqrt{g}}q^i\frac{\partial \sqrt{g}}{\partial \beta^i} \\
&= \frac{1}{\sqrt{g}}\frac{\partial}{\partial \beta^i}\left(q^i\sqrt{g}\right) \\
&= \frac{g^{ij}}{\sqrt{g}}\frac{\partial}{\partial \beta^i}\left(\frac{\sqrt{g}}{h_i}\frac{\partial T}{\partial beta^j}\right)
\end{aligned}$$

It can be easily shown that $\Gamma^k_{ki} = \frac{1}{\sqrt{g}}\frac{\partial \sqrt{g}}{\partial \beta^i}$ and in this case g is given by $g = \sqrt{g_{11}g_{22}g_{33}}$. In physical coordinates $q(i) = q^i/h_i$, using this and invoking other conditions (axisymmetry and thin membrane approximation) the right hand side of the equation can be rewritten as,

$$\nabla \bullet \mathbf{q} = \frac{\cos\theta}{RH\sec\theta}\frac{\partial}{\partial z}\left(RH\frac{\partial T}{\partial z}\right)$$

The left hand side of the energy equation 34 can be rewritten as,

$$\rho C_p\frac{dT}{dt} = \rho C_p\frac{\partial T}{\partial t} + \rho C_p\mathbf{v}.\nabla T = \rho C_p\frac{\partial T}{\partial t} + \rho C_p v^i\frac{\partial T}{\partial \beta^i} = \rho C_p\frac{\partial T}{\partial t} + \rho C_p v^1\frac{\partial T}{\partial z}$$

and the source terms arise from the heat transfer between the film surface and the surroundings. Contribution to this heat transfer by radiation and convection are considered. Heat convected away by the cooling air is given by $h_c(T - T_c)$, where h_c is the heat transfer coefficient and T_c is the temperature of the cooling air. Heat radiated to the surroundings is given by $C_{SB}\epsilon(T^4 - T_w^4)$, where C_{SB} is Stefan-Boltzmann constant, ϵ is the emissivity of the bubble surface, and T_w is the surrounding wall temperature. Heat generation during crystallization due to the latent heat is given by $\rho L_h \frac{d\chi}{dt}$. Including these terms, the equation of conservation of energy can be written as follows.

$$\rho C_p \frac{\partial T}{\partial t} + \rho C_p v^1 \frac{\partial T}{\partial z} + \frac{h_c}{H}(T - T_c) + \frac{C_{SB}\epsilon}{H}(T^4 - T_w^4) = - \frac{1}{\sqrt{g}} \frac{\partial}{\partial z}\left(q^i \sqrt{g}\right) \tag{35}$$

This equation has to be written in physical coordinates in order to be solved. Using $q(i) = -kh_i \frac{\partial T}{\partial \beta^j} g^i j$, final form of the equation is obtained.

$$\rho C_p \frac{\partial T}{\partial t} + \rho C_p V_{\underline{1}} \cos\theta \frac{\partial T}{\partial z} + \frac{h_c}{H}(T - T_c) + \frac{C_{SB}\epsilon}{H}(T^4 - T_w^4) = \frac{\cos\theta}{RH} \frac{\partial}{\partial z}\left(kRH \frac{\partial T}{\partial z}\right) \tag{36}$$

6. Constitutive Modeling

Constitutive model used is described in detail in the previous chapter. In this section those equations are presented in physical coordinates with some additional details which enable the numerical calculation. The following set of equations define the Phan-Thien-Tanner model in physical coordinates. The second time dependent term on the left hand side will vanish when the motion is affine.

$$\frac{\partial \tau_{\underline{11}}}{\partial t} + V_{\underline{1}} \cos\theta \frac{\partial \tau_{\underline{11}}}{\partial z} + 2\mathcal{L}_{\underline{11}}\tau_{\underline{11}} - 2\tau_{\underline{11}} \cos\theta \sin\theta \frac{\partial \theta}{\partial t} + \frac{Y}{\lambda}\tau_{\underline{11}} = 2GD_{\underline{11}} \tag{37}$$

$$\frac{\partial \tau_{\underline{22}}}{\partial t} + V_{\underline{1}} \cos\theta \frac{\partial \tau_{\underline{22}}}{\partial z} + 2\mathcal{L}_{\underline{22}}\tau_{\underline{22}} - 2\frac{\tau_{\underline{22}}}{R}\frac{\partial R}{\partial t} + \frac{Y}{\lambda}\tau_{\underline{22}} = 2GD_{\underline{22}} \tag{38}$$

$$\frac{\partial \tau_{\underline{33}}}{\partial t} + V_{\underline{1}} \cos\theta \frac{\partial \tau_{\underline{33}}}{\partial z} + 2\mathcal{L}_{\underline{33}}\tau_{\underline{33}} - 2\frac{\tau_{\underline{33}}}{H}\frac{\partial H}{\partial t} + \frac{Y}{\lambda}\tau_{\underline{33}} = 2GD_{\underline{33}} \tag{39}$$

E. Process Conditions

1. Initial Conditions

Initial conditions for the analysis is specified based on one of the actual procedures used for starting the film line. This procedure is discussed in detail in Chapter I. Typically a film line is started by extruding the polymer melt through the die in the form of a hollow tube. The tip of this tube is then tied to a rope and pulled to nip rollers and passed via the roller drums. In this position, the set up looks as if the cylinder is being pulled uniaxially. Then the pressurized air is blown in the tube to inflate it (see Figure 2).

Based on this understanding, initial conditions are specified using uniaxial extension approximation as shown in Figure 10 and specified by the following equations.

$$R = R_{die} \tag{40}$$

$$V_{\underline{1}} = V_{die} + z\frac{v_{nip} - v_{die}}{L} \tag{41}$$

$$H = H_{die} + z\frac{h_{nip} - h_{die}}{L} \tag{42}$$

$$T = \text{Distribution based on simple convection analysis} \tag{43}$$

$$\chi = \text{Based on temperature profile} \tag{44}$$

Initial condition for the stresses are computed using a steady state solver using the above conditions to specify the kinematics. Variants of this initial condition are used to study the sensitivity of the model to initial conditions.

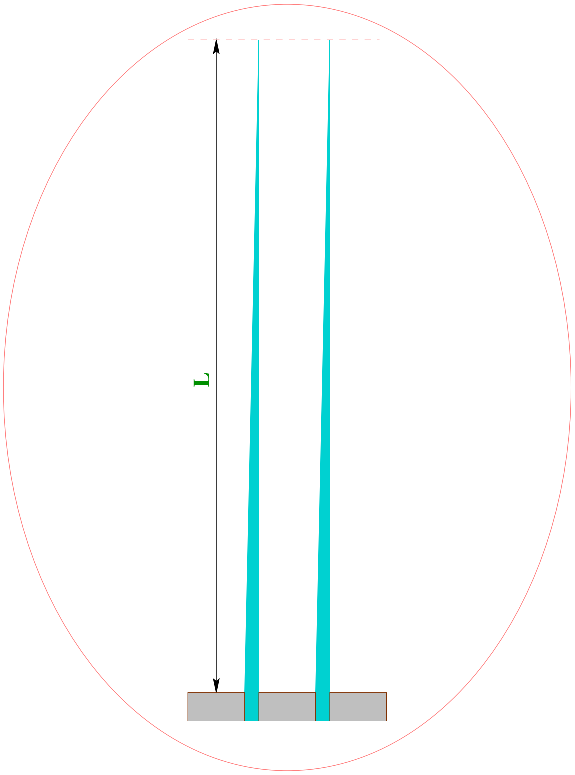

FIG. 10. Initial Condition used in the analysis.

2. Boundary Conditions

In this section a brief discussion on boundary conditions is presented. This is based on the physical understanding of the process and the results of variational formulation presented in chapter V. Boundary conditions specified at the die end is shown in figure 11. This figure is not drawn to scale and it is exaggerated to show the effect of extrudate swell. This effect is neglected in this study (see section A), however, if necessary, it can be included in an approximate way using the available experimental investigations. Following conditions are unambiguously at the die end:

- Radius of the die, R_{die} is determined from the die geometry. Depending on the convention used (see Appendix A) either the inner or outer radius of the annulus is used. In this analysis, outer radius of the die gap opening is taken

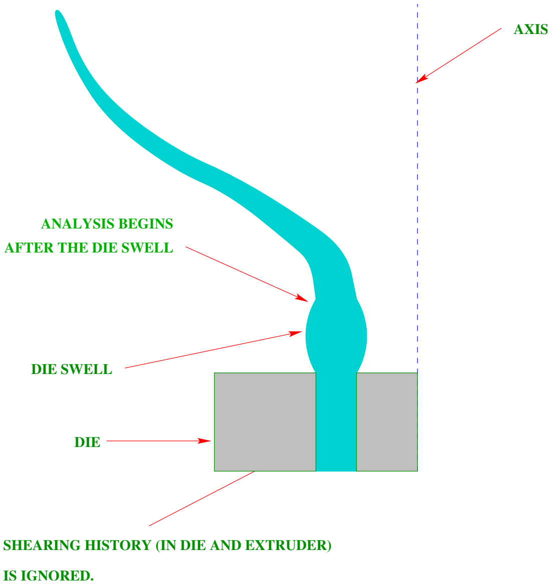

FIG. 11. Boundary conditions at the die end.

as R_{die}.

- Velocity at the die, $V_{\underline{1}}$ is computed directly from the mass flow rate of the polymer. This value is one of the user controlled parameters.

- Thickness of the film at the die end, H_{die} is determined from the die gap.

- Temperature of polymer at the die end, T_{die} is determined experimentally. Other alternative is to numerically determine by simulating the polymer flow in the die.

- Degree of crystallinity, χ is specified as 0 as the die end. This is based on the fact the polymer comes out as a melt from the die.

Stresses are not specified at the die end and it is automatically determined from the kinematics. If the strain history at the die end is known through prior simulation, then it can be included to determine the stresses accurately at the die end.

Boundary conditions at nip end is not as unambiguous as the die end. Chiefly the radius equation offers two alternatives: either to specify Dirichlet or Neumann boundary condition. The actual condition used depends on the nature of the study, whether it an analysis of an existing process or a new design. Boundary conditions specified at the nip end is shown in figure 12.

Following conditions are specified at the nip end:

- Velocity at the nip end is a user specified parameter, it directly determines the production of the film line. Hence, this condition is imposed as Dirichlet boundary condition.
- Either the radius or its derivative can be specified at the nip. If the study is an analysis of an existing and operating film line, radius can be specified. On the other hand, for the given process conditions if one wishes to determine the final diameter then the Neumann condition, $\frac{\partial r}{\partial z} = 0$ can be imposed.
- Inclusion of conduction terms in the energy equation creates the difficult necessity of specifying a boundary condition at the nip end. Since the thermal conductivity of the polymer is low, one would except the sensitivity of the result to this boundary condition will be small. Numerical experiments performed in the study show that the condition specified at the nip end for temperature has no influence on the results. Thus provides the satisfactory reason for not including these terms in the analysis.

F. Closure

Detailed derivation of a transient, axisymmetric, nonisothermal model to simulate film blowing process is presented in this chapter. In the next chapter finite element

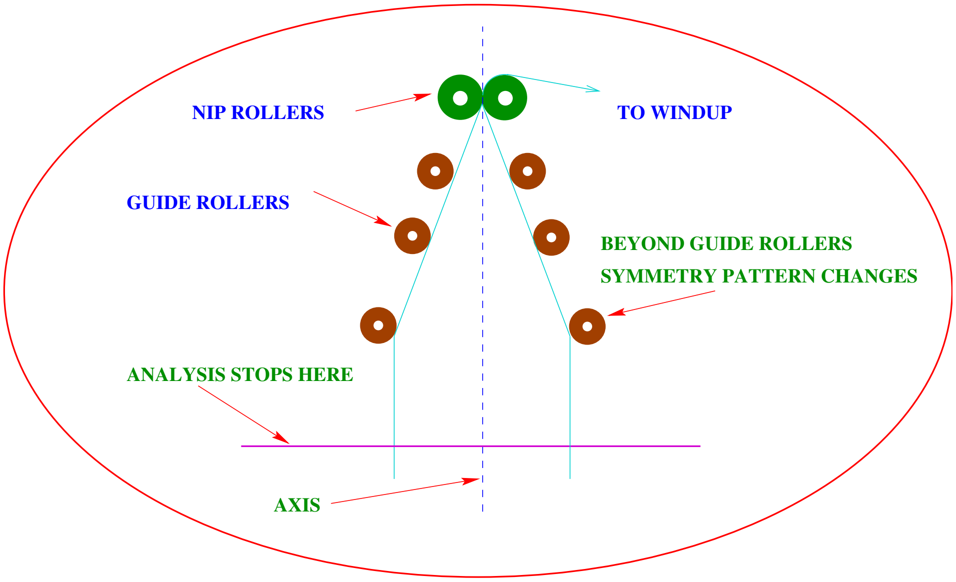

FIG. 12. Boundary condition at the nip end.

formulation of these equations and the methodology used to obtain the solution are explained.

CHAPTER V

NUMERICAL FORMULATION

A. Introduction

Model equations developed in the previous chapter are solved numerically using the finite element method. This chapter describes the finite element formulation of these partial differential equations and the solution algorithm used to solve the resulting algebraic system of equations. In the following section, formulation of each of the model equations is presented. In the subsequent section, special techniques such as SUPG smoothing and the strain computation are described in detail. In Section D, the approach adopted to compute the transient terms is discussed. In Section E, solution algorithm used solve the system of nonlinear algebraic equations is presented. The final section presents the summary and some relevant issues pertaining to the convergence and robustness of the solution procedure.

B. Finite Element Formulation

Finite element method is a powerful numerical technique for solving partial differential equations and one of the elegant features of this method is the natural way in which the boundary conditions are implemented. An introduction to the finite element method can be found in Reddy (1993) and the mathematical aspects of the method relevant to this work can be found in Brenner and Scott (1994). In this dissertation, film blowing process is described using a transient axisymmetric model. Hence, the problem at hand is one-dimensional in space and time dependent. The space dimension is approximated using quadratic finite elements. Figure 13 shows

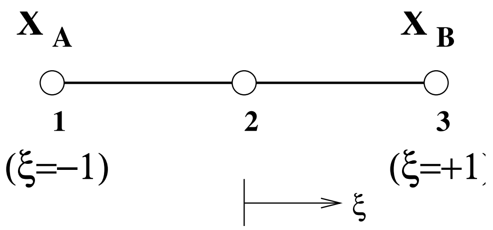

FIG. 13. Depiction of a 1–D, 3-noded quadratic finite element.

this finite element and the shape functions associated with is element are given by following equation.

$$\psi_1 = \frac{\xi(\xi-1)}{2} \quad ; \psi_2 = \xi^2 - 1; \quad \psi_1 = \frac{\xi(\xi+1)}{2} \tag{45}$$

Using these functions, for example, temperature distribution in an element is described as $T = \sum_{i=1}^{3} \psi_i T_i$.

1. Film Thickness

The equation of conservation of mass is used to compute the thickness of the film. This equation is hyperbolic in nature and the information of propagation is along the z direction and the time axis. In a steady state process, the z direction will have a time like nature and can be mapped to the time axis, however, this does not hold true for a transient problem. The initial formulation using the traditional Galerkin approach for this equation resulted in loss of numerical stability and produced a highly oscillatory solution. Hence, it was modified using the Stream–wise Upwind Petrov Galerkin (SUPG) method to smooth the solution. The difference between the above two schemes lies in the choice of the test function, ϕ_i. For Galerkin method, test function is same as the trial function i.e., $\phi_i = \psi_i$. The specific form of ϕ_i used for SUPG method is described in Section E.

The thickness of the film, H is approximated in an element using the trial functions as expressed by $H = \sum_{i=1}^{3} \psi_i H_i$. The equation describing the thickness of the film can be written as follows.

$$\begin{aligned}\mathcal{L}_H(z,t) = \frac{\partial H}{\partial t} + V_{\underline{1}} \cos\theta \frac{\partial H}{\partial z} + \\ H\left(\frac{1}{\sec\theta}\frac{\partial \sec\theta}{\partial t} + \frac{1}{R}\frac{\partial R}{\partial t} + \cos\theta\frac{\partial V_{\underline{1}}}{\partial z} + \frac{V_{\underline{1}}\cos\theta}{R}\frac{\partial R}{\partial z}\right) = 0\end{aligned} \tag{46}$$

The above equation is solved to determine the film thickness, H such that $H \in \mathbb{H}^1(\Omega)$; and $H = H_{die}$ on Γ_{die}. With this requirement, the thickness equation is formulated in the master coordinates using the test function, ϕ_i.

$$\int_{-1}^{+1} \mathcal{L}_H(\xi,t)\phi_i \mathcal{J} d\xi = 0 \tag{47}$$

The test function used in the formulation is modified to account for upwinding.

$$\phi_i = \psi_i + \frac{C_{up} e_h}{2}\frac{\partial \psi_i}{\partial \xi}\frac{1}{\mathcal{J}}$$

This results in,

$$\begin{aligned}M_{ij}^e &= \int_{-1}^{+1} \phi_i \psi_j \mathcal{J} d\xi \\ K_{ij}^e &= \int_{-1}^{+1} V_{\underline{1}} \cos\theta \phi_i \frac{\partial \psi_j}{\partial \xi} d\xi \\ &+ \int_{-1}^{+1} \left(\frac{1}{\sec\theta}\frac{\partial \sec\theta}{\partial t} + \frac{1}{R}\frac{\partial R}{\partial t} + \frac{V_{\underline{1}}\cos\theta}{R}\frac{\partial R}{\partial z} + \cos\theta\frac{\partial V_{\underline{1}}}{\partial z}\right)\phi_i\psi_j\mathcal{J} d\xi \\ f_i^e &= 0\end{aligned}$$

Some of the issues in solving the above equation is the estimation of the time derivatives. The term involving "$\sec\theta$" can be expanded using the relationship $\tan\theta = \partial R/\partial z$, however, that will lead to second derivative of R. The value of C_{up} is decided based on the severity of the problem and it lies in the range of 0 and 2.

2. Velocity Vector

In the principal coordinate system velocity vector has only one non-zero component which is along the machine direction. The equation of momentum along the direction ξ_1 (MD) is used to compute this velocity, $V_{\underline{1}}$. The initial formulation of this equation had no viscous terms as the stress terms is solved separately of the constitutive model (PTT) and this led to the loss of numerical stability. In order to improve the stability of the problem, a viscous term was added to this equation, and this equivalent to solving the problem with a Oldroyd-B like model. In essence, the extra stress term is split into a purely viscous part and its viscoelastic complement, and the viscous part of the extra stress is written out explicitly in the momentum equation.

$$\mathbb{S} = -p\mathbf{1} + \boldsymbol{\tau}_{VE} + \boldsymbol{\tau}_{viscous} = \boldsymbol{\sigma} + \boldsymbol{\tau}_{viscous} \tag{48}$$

The traditional Galerkin weighted residual scheme is used to formulate the problem, that is, $\phi_i = \psi_i$. The equation governing the machine direction velocity is written as,

$$\begin{aligned}\mathcal{L}_V(z,t) = {} & \frac{\partial V_{\underline{1}}}{\partial t} + V_{\underline{1}} \cos\theta \frac{\partial V_{\underline{1}}}{\partial z} + gcos\theta \\ & - \frac{1}{\rho R H} \frac{\partial}{\partial z}\left(RH\mu_2 \cos^2\theta \frac{\partial V_{\underline{1}}}{\partial z}\right) - \frac{1}{\rho}\sin\theta\cos\theta \frac{\partial \theta}{\partial z}\mu_2 \frac{\partial V_{\underline{1}}}{\partial z} \\ & - \frac{1}{\rho R H}\frac{\partial}{\partial z}\left(RH\cos\theta\sigma_{\underline{11}}\right) - \frac{1}{\rho}\sin\theta\frac{\partial\theta}{\partial z}\sigma_{\underline{11}} = 0.\end{aligned} \tag{49}$$

Above equation is solved to find $V_{\underline{1}} \in \mathbb{H}^1$; $V_{\underline{1}} = V^{die}$ at $z = 0$ and $V_{\underline{1}} = V^{nip}$ at $z = L$. The standard Galerkin FEM formulation of the above equation results in,

$$
\begin{aligned}
M_{ij}^{e} &= \int_{-1}^{+1} \psi_i \psi_j \mathcal{J} d\xi & (50)\\
K_{ij}^{e} &= \int_{-1}^{+1} \psi_i \frac{\partial \psi_j}{\partial \xi} V_{\underline{1}} \cos\theta d\xi & (51)\\
&+ \int_{-1}^{+1} \frac{\cos^2\theta \mu_2}{\rho} \frac{\partial \psi_i}{\partial \xi} \frac{\partial \psi_j}{\partial \xi} \frac{1}{\mathcal{J}} d\xi &\\
&- \int_{-1}^{+1} \frac{\sin\theta \cos\theta \mu_2}{\rho} \psi_i \frac{\partial \psi_j}{\partial \xi} d\xi &\\
f_i^{e} &= \int_{-1}^{+1} -g\cos\theta \psi_i \mathcal{J} d\xi & (52)\\
&- \int_{-1}^{+1} \frac{\cos\theta}{\rho} \sigma_{\underline{11}} \frac{\partial \psi_i}{\partial \xi} d\xi &\\
&+ \int_{-1}^{+1} \frac{\sin\theta}{\rho} \frac{\partial \theta}{\partial z} \sigma_{\underline{11}} \psi_i \mathcal{J} d\xi &\\
&+ \left. \frac{1}{\rho} \cos\theta \psi_i \mathcal{S}_{\underline{11}} \right|_{-1}^{+1} &
\end{aligned}
$$

The boundary conditions for the equations naturally arise out of the diffusion terms while applying differentiation by parts to those terms. In the case of film blowing, values of the velocity at the nip and the die ends are known unambiguously from the process data. Hence, the primary variable is specified on both the boundaries.

$$
\begin{aligned}
V_{\underline{1}} &= V^{die} \text{ at z = 0}\\
V_{\underline{1}} &= V^{nip} \text{ at z = L}
\end{aligned}
$$

3. Bubble Radius

The equation governing the radius of the film is derived from the momentum equation along the normal direction. This equation can be expressed in more than one way for the purpose of FEM formulation. This is based on how the $\tan\theta = \partial R/\partial z$ is expressed. In order to extract more information from the formulation the term $\tan^2\theta$ is expressed as $\partial R/\partial z \tan\theta$, so that its contribution will go to the operator matrix. Hence, the equation of R is written as,

$$\begin{aligned}\mathcal{L}_R(z,t) = \frac{\partial^2 R}{\partial z^2}(\sigma_{\underline{11}} - \rho V_{\underline{1}}^2)\cos\theta + \frac{\partial R}{\partial z}\tan\theta\left(\frac{\Delta P}{H} - \frac{\sigma_{\underline{\underline{22}}}}{R} + \rho g \sin\theta\right) \\ + \left(\frac{\Delta P}{H} - \frac{\sigma_{\underline{\underline{22}}}}{R} + \rho g \sin\theta\right) = 0. \quad (53)\end{aligned}$$

Subjecting the above equation to standard FEM formulation the operator matrix and the load vector are obtained.

$$\begin{aligned}K_{ij}^e &= \int_{-1}^{+1}(\sigma_{\underline{11}} - \rho V_{\underline{1}}^2)\frac{\partial\psi_i}{\partial\xi}\frac{\partial\psi_i}{\partial\xi}\frac{1}{\mathcal{J}}d\xi \\ &- \int_{-1}^{+1}\left(\frac{\Delta P}{H} - \frac{\sigma_{\underline{\underline{22}}}}{R} + \rho g \sin\theta\right)\tan\theta\psi_i\frac{\partial\psi_j}{\partial\xi}d\xi \text{ and} \\ f_i^e &= \int_{-1}^{+1}\psi_i\left(\frac{\Delta P}{H} - \frac{\sigma_{\underline{\underline{22}}}}{R} + \rho g \sin\theta\right)\mathcal{J}d\xi + \psi_i(\sigma_{\underline{11}} - \rho V_{\underline{1}}^2)\frac{\partial R}{\partial z}\bigg|_{-1}^{+1}.\end{aligned}$$

This equation is elliptic and requires boundary condition for radius on both the die and the nip end. The boundary term arises from differentiation by parts of the second order term. There are two possible choices for the boundary conditions. Radius of the bubble at the die end is known without any ambiguity. Hence, Dirichlet boundary condition is applied at the die end. On the other hand the nip end condition can be Dirichlet or Neumann. If the film radius is specified at the nip end as shown in the following equation, then the kinematic conditions are fixed on both the ends and this is the preferred boundary condition.

$$\begin{aligned} R &= R_{die} \text{ at z} = 0 \ \text{ and} \\ R &= R_{nip} \text{ at z} = \text{L} \ . \end{aligned}$$

If the radius at the nip end is not known then the logical alternative is to specify the Neumann condition as shown in the following equation. In this case the final radius is predicted by the code.

$$\begin{aligned} R &= R_{die} \text{ at z} = 0 \text{ and} \\ \frac{\partial R}{\partial z} &= 0 \text{ at z} = \text{L}. \end{aligned}$$

4. Constitutive Model

Total Stress. Stresses are computed using mixture theory as a combination of stresses computed by the PTT model describing the liquid–like region and Kelvin-Voight model describing the solid-like zone. Of these, only the computation of the PTT model requires FEM formulation and the rest are algebraic equations.

PTT Model - $\tau_{\underline{11}}$. The model is solved in principal coordinates, it reduces the number of equations for stresses from 6 to 3. Since the formulation of these equations are identical, only the equation for the component along machine direction is presented here. The equation describing the viscoelastic stress in the MD based on the PTT model can be written as,

$$\mathfrak{L}\tau_{\underline{11}}(z,t) = \frac{\partial \tau_{\underline{11}}}{\partial t} + V_{\underline{1}} \cos\theta \frac{\partial \tau_{\underline{11}}}{\partial z} - 2\mathfrak{L}_{\underline{11}}\tau_{\underline{11}} - 2\tau_{\underline{11}} \cos\theta \sin\theta \frac{\partial \theta}{\partial t} + \frac{Y}{\lambda}\tau_{\underline{11}} - 2GD_{\underline{11}} = 0.$$

The equation for stresses also require SUPG smoothing, hence the test function is not same as the trial function. The FEM formulation of the above equation can be written as:

$$
\begin{aligned}
M_{ij}^{e} &= \int_{-1}^{+1} \phi_i \psi_j \mathcal{J} d\xi \\
K_{ij}^{e} &= \int_{-1}^{+1} \phi_i \frac{\partial \psi_j}{\partial \xi} V_{\underline{1}} \cos\theta d\xi \\
&- \int_{-1}^{+1} 2\cos\theta \sin\theta \frac{\partial \theta}{\partial t} \phi_i \psi_j \mathcal{J} d\xi \\
&+ (\frac{Y}{\lambda} - 2\mathcal{L}_{\underline{11}} \phi_i \psi_j \mathcal{J} d\xi \\
f_i^{e} &= \int_{-1}^{+1} 2GD_{\underline{11}} \phi_i d\xi
\end{aligned}
$$

Equation for the stresses require only the initial condition. Since velocities are specified at both the nip and the die end, there is no need for specifying the stresses. Even the initial condition for stresses can be computed based on the initial velocity field. This approach, however, would not account for the stress history prior to the film blowing process.

5. Temperature

Heat transfer in the film blowing process is dominated by advection. In a typical problem Pe number is in the order of 10^6 or more. Also there is a distinct direction, along machine direction, of information propagation. Hence, the role of conduction is limited. The formulation, however, considers the conduction term for the sake of completeness. Numerical experiments show that there is no effect on the solution by the condition imposed on the nip end. This is another reason, why the energy equation requires some kind of upwinding scheme to add numerical dissipation. The specific form of upwinding used here is the SUPG technique. The equation describing the heat transfer in the film blowing process is written as,

$$\begin{aligned}\mathfrak{L}_T(z,t) = \frac{\partial T}{\partial t} + V_{\underline{1}} \cos\theta \frac{\partial T}{\partial z} + \frac{h_c}{\rho C_p H}(T - T_c) + \frac{C_{SB}\epsilon}{\rho C_p H}(T^4 - T_w^4) \\ - \frac{\cos\theta}{\rho C_p R H} \frac{\partial}{\partial z}\left(kRH\frac{\partial T}{\partial z}\right) = 0. \quad (54)\end{aligned}$$

Finite element formulation of the above equation results using the test function ϕ_i results in the following element matrices.

$$\begin{aligned}
M_{ij}^e &= \int_{-1}^{+1} \phi_i \psi_j \mathcal{J} d\xi, \\
K_{ij}^e &= \int_{-1}^{+1} \phi_i \frac{\partial \psi_j}{\partial \xi} V_{\underline{1}} \cos\theta d\xi \\
&+ \int_{-1}^{+1} \phi_i \psi_j \frac{h_c}{H\rho C_p} \mathcal{J} d\xi \\
&+ \int_{-1}^{+1} \frac{\partial \phi_i}{\partial \xi} \frac{\partial \psi_j}{\partial \xi} \frac{k\cos\theta}{\rho C_p \mathcal{J}} d\xi, \text{ and} \\
f_i^e &= \int_{-1}^{+1} \frac{C_{SB}\epsilon}{H\rho C_p}(T^4 - T_w^4)\phi_i \mathcal{J} d\xi \\
&+ \int_{-1}^{+1} \phi_i \frac{h_c}{H\rho C_p} T_c \mathcal{J} d\xi \\
&+ \int_{-1}^{+1} \phi_i \frac{L_\chi}{C_p} \frac{\partial \chi}{\partial t} \mathcal{J} d\xi \\
&+ \left. \frac{k\cos\theta}{\rho C_p} \phi_i \frac{\partial T}{\partial z} \right|_{-1}^{+1}.
\end{aligned}$$

The equation for temperature can take Dirichlet or Neumann conditions. At the die temperature of the melt is known and hence, it is specified (Dirichlet). At the nip end, some approximation has to be made. Either the temperature based on the data or the flux condition can be specified. Considering the fact $k \leq \rho C_p$ the boundary term is very very small, even if it is included its effect on the solution will negligibly small.

6. Degree of Crystallinity

The equation describing the crystallization kinetics is written as follows,

$$\mathcal{L}_{\chi}(z,t) = \frac{\partial \chi}{\partial t} + V_{\underline{1}} \cos\theta \frac{\partial \chi}{\partial z} - nK(T)(1-\chi)\left(-log_e(1-\chi)\right)^{\frac{n-1}{n}} \exp(c_{\chi} II_D) = 0. \quad (55)$$

Above equation is advection dominated and requires some kind of upwinding technique to overcome the loss of best approximation property of the Galerkin method. Hence, the test function is based on the SUPG method and it is not same as the trial function. Finite element formulation of the above equation results in the following element matrices.

$$\begin{aligned}
M^e_{ij} &= \int_{-1}^{+1} \phi_i \psi_j \mathcal{J} d\xi, \\
K^e_{ij} &= \int_{-1}^{+1} \phi_i \frac{\partial \psi_j}{\partial \xi} V_{\underline{1}} \cos\theta d\xi \\
&+ \int_{-1}^{+1} \phi_i \psi_j \; nK(T)\left(-log_e(1-\chi)\right)^{\frac{n-1}{n}} \exp(c_{\chi} II_D) \mathcal{J} d\xi, \text{ and} \\
f^e_i &= \int_{-1}^{+1} nK(T)\left(-log_e(1-\chi)\right)^{\frac{n-1}{n}} \exp(c_{\chi} II_D) \phi_i \mathcal{J} d\xi.
\end{aligned}$$

The model used for predicting the crystallization kinetics does not naturally include the maximum crystallinity limit. This limit is forced on the solution, i.e., if $\chi > \chi_{max}$ then $\chi = \chi_{max}$. One of the associated quantity of degree of crystallization is the orientation of the crystalline structures formed. Typically, this orientation tensor is computed using additional equations which describe the evolution of this tensor. Without this tensor, the degree of crystallinity will be degenerate to the degree of solidification. Here, additional equations are not solved for computing the orientation of this tensor. Instead, it is assumed that the crystalline structures formed assume the orientation along the principal directions at that point. This orientation is retained and it is convected away. To illustrate this consider the following situation. Let the degree of crystallinity be 0.2 at $z = z_1$, and next node be situated at $z_1 + \Delta z$. Let χ increase by 0.01 in this element. This new material, which has crystallized in this element, assumes the orientation of the element's principal directions. And this % of the material retains this orientation as it is advected along the machine direction. This particular approach does increase the computationally complexity of the algorithm. This is accomplished by using an integral (or summation) approach from the die to the point of interest, and this is done in an incremental manner.

C. Special Techniques

1. SUPG Smoothing

For certain classes of problems, Galerkin finite element method loses its best approximation property, hence the resulting solutions have spurious modes and unacceptable wiggles. This typically happens when the flow is advection dominated or if the equation under consideration is hyperbolic. Such instances often manifest through the loss of symmetry in the stiffness matrix. A simple but a computationally intensive way to overcome this problems is to use a very fine mesh, where such effects would not play an important role at an element level. This approach, however, is not always feasible. Hence, techniques such as SUPG method is used compensate for the loss of best approximation property of the traditional Galerkin method. In this work the technique used is based on the SUPG method, which is described in detail in Brooks and Hughes (1982).

$$\phi_i = \psi_i + \frac{C_{up} e_h}{2} \frac{\mathbf{v} \bullet \nabla \psi_i}{\|\mathbf{v}\|} \tag{56}$$

where e_h is the characteristic element size, α is a parameter taking a value between 0 and 2, and $\mathbf{v}$ is the velocity vector. The extra term added to ψ_i is a function of the element size and will vanish when $e_h \to 0$. Since the problem is one dimensional and the velocity is always +ve in the machine direction, the above equation can be written as:

$$\phi_i = \psi_i + \frac{C_{up}}{2} \frac{\partial \psi_i}{\partial \xi} \tag{57}$$

Element size is taken as the determinant of the Jacobian of the element and it is canceled by the $\mathcal{J}$ in the denominator of the derivative of the trial function. There are other classes of upwind methods, which use a similar idea. For instance, some techniques apply this Petrov–Galerkin test function only to the advection terms and use the standard Galerkin test function for other terms. The differences, however, become significant only in multi–dimensional setting.

2. Strain Computation

Computation of strain requires an integral approach starting from the die end to the nip end. The procedure to compute the strain tensor is described below:

1. First, the rate of deformation tensor, $\mathbf{D}$ is computed at all nodes. Since the computation is done in principal coordinate system this is same as the velocity gradient tensor, $\mathbf{L}$.

2. From the velocity gradient tensor, deformation gradient is computed by integrating $\dot{\mathbf{F}} = \mathbf{L}\mathbf{F}$.

3. Using the deformation gradient tensor, **F** the Eulerian strain tensor ε is computed.

These computations are simple in a principal coordinate system, which otherwise could be more difficult to implement. Besides the use in the Kelvin–Voight model, it can be used along with the stresses to determine structure–property relationship.

D. Time Formulation

The α parameter approximation is used to model the transient behavior. The choice of α will determine the accuracy of the solution (first or second order) and its stability. For the studies presented in this work, $\alpha = 0.5$ is used. Consider the element equation for bubble thickness, H which is written as,

$$[M_H]\{\dot{H}\} + [K_H]\{H\} - \{f_H\} = 0. \tag{58}$$

Using the above mentioned approach, following equation is obtained.

$$\begin{aligned}\left([M_H] + \alpha\Delta t\left[K_H^{n+1}\right]\right)\{H^{n+1}\} &= \\ &\left([M_H] - (1-\alpha)\Delta t\left[K_H^{n+1}\right]\right)\{h^n\} + \Delta t\left(\alpha\{f_H^{n+1}\} + (1-\alpha)\{f_H^n\}\right).\end{aligned} \tag{59}$$

Above equation is rewritten as,

$$\left[\hat{K_H}\right]\{h^{n+1}\} = \{\hat{f_H}\}, \tag{60}$$

where,

$$\left[\hat{K_H}\right] = \left([M_H] + \alpha\Delta t\left[K_H^{n+1}\right]\right) \tag{61}$$

and

$$\{\hat{f_H}\} = \left([M_H] - (1-\alpha)\Delta t\left[K_H^{n+1}\right]\right)\{h^n\} + \Delta t\left(\alpha\{f^{n+1}\} + (1-\alpha)\{f^n\}\right). \tag{62}$$

E. Solution Algorithm

The algorithm used for solving the algebraic equations resulting from the finite element formulation has a time loop which drives the transient algorithm (see figure 14), and within this time loop a nonlinear loop (see figure 15) is used the solve the equations using an segregated algorithm.

This transient driver is implemented with the capability to control the time step automatically based on the convergence of nonlinear iterations and revert back to the previous step if the nonlinear iterations did not converge to accepted tolerance. This step is attempted thrice with the time step reduced by a factor each time and if the solution is still unacceptable, then solution procedure stops.

One of the issue associated with the nonlinear loop is the segregated algorithm which is known for its lack of convergence in severe nonlinear problems. This can be controlled by using smaller value for the time step or through relaxation of solution between the nonlinear iterations. It should be noted that the some of the equations (such as, the equation for bubble thickness) has time derivative occurring in the load term. This is computed accurately using solution at two previous time steps, that is, using a quadratic fit between values at t_{n+1}, t_n, and t_{n-1}. At the beginning of each nonlinear iteration, solution at $n+1^th$ step is assumed to be same as the n^th step, hence time derivative is computed for this iteration is extrapolated from the solution at n^th and $n-1^th$ steps. This is error is automatically corrected after the first nonlinear iteration.

The actual sequence of operations in each nonlinear iteration is listed below:

1. Compute strain.

2. Solve for temperature.

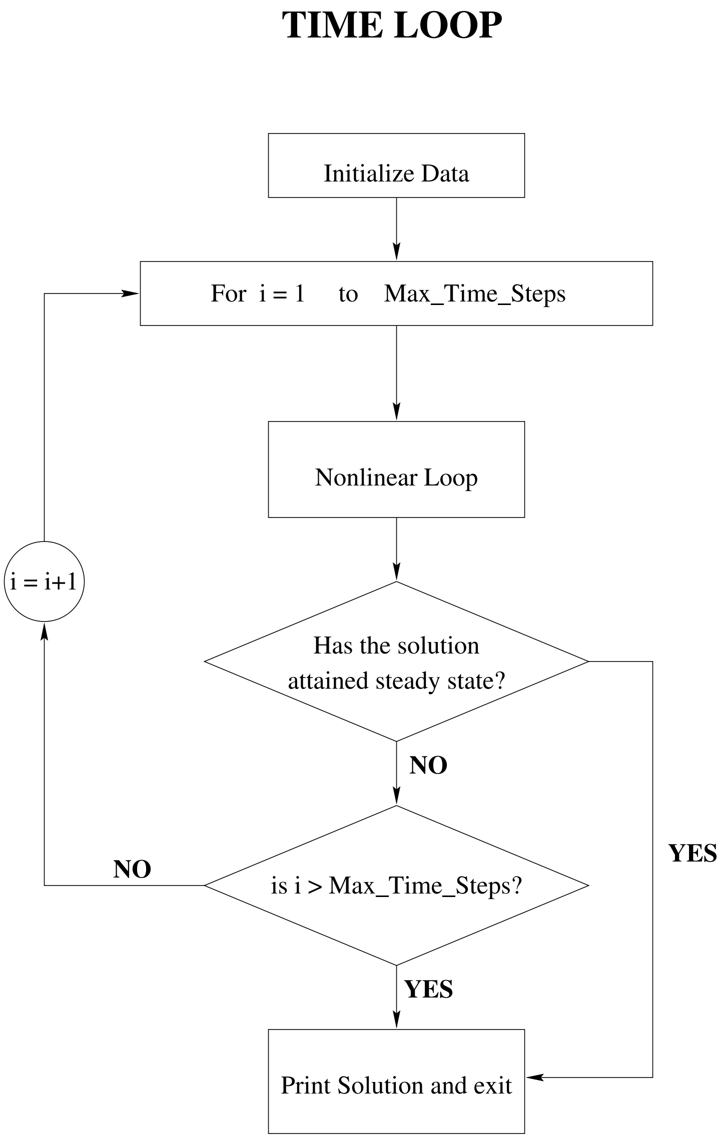

FIG. 14. Transient driver used for the analysis.

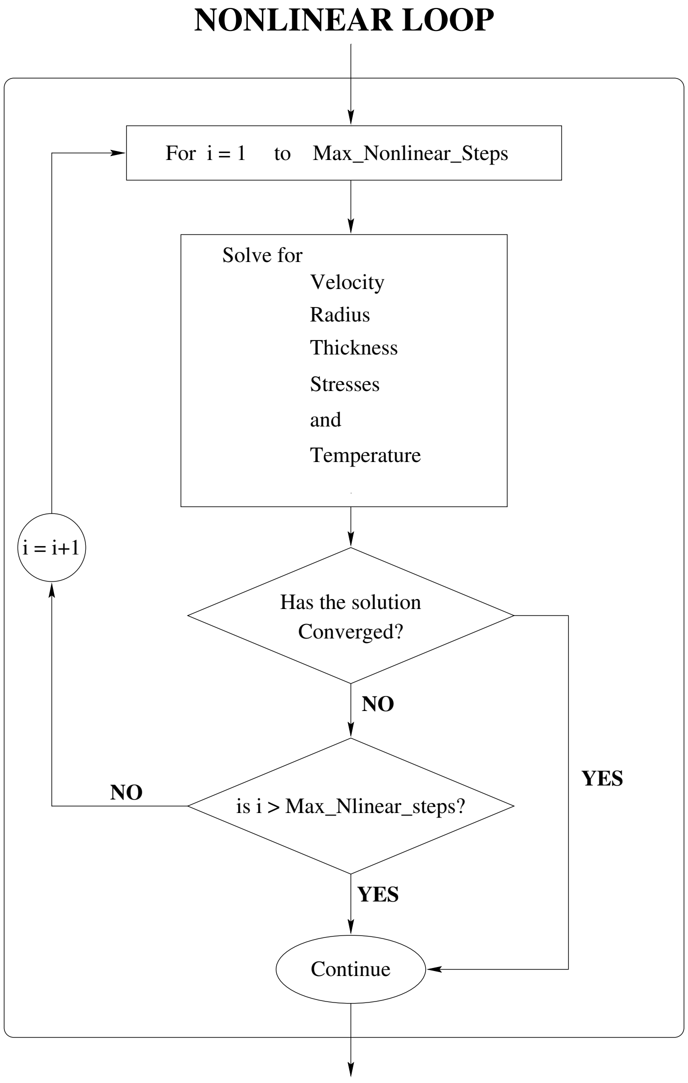

FIG. 15. Algorithm for nonlinear iterations.

3. Solve for viscoelastic stresses.
4. Compute total stress using mixture theory.
5. Solve for bubble radius.
6. Solve for the velocity in machine direction.
7. Solve for bubble thickness.

A fixed sequence may introduce a bias in the solution scheme, however, this can be overcome by altering this sequence after each nonlinear iteration.

F. Closure

Finite formulation of the model equations is presented in this chapter. This numerical formulation is implemented in the software in an object–oriented approach using the language *C++*. This implementation is supported with a user interface for pre and post–processing and this interface is written using a combination of Tcl/Tk and C language.

CHAPTER VI

STEADY STATE RESULTS

A. Introduction

Experimental validation of the model developed and additional parametric studies of the process are presented in this chapter. Experimental validation is accomplished using two sets of data: i) Gupta's laboratory scale experimental data [Gupta (1980)] and ii) Exxon's experimental data. Latter was provided to the Polymer Technology Consortium of Texas A&M University. One of the significant differences between these two sets is the cooling mechanism used. Exxon's process uses forced convection cooling with turbulent air jets. On the other hand, Gupta's experiments rely on natural convection heat transfer, hence, the heat loss through radiation becomes a significant mechanism of heat transfer in his experiments. Parametric studies presented in this chapter investigate the role of different process conditions and their relevance to process stability.

B. Comparison with Gupta's Experimental Data

1. Background

Gupta performed his experiments using "Styron666", which is the commercial name for Polystyrene made by Dow Chemical company. Data presented by Gupta included the results from both isothermal and nonisothermal experiments. In this chapter, only the nonisothermal data is used for comparison. The experimental setup used consisted of an one inch (0.0254m) mandrel die with an annular gap of 0.04 inches (0.001016m $\approx$ 1mm). Of the 20 different sets of experimental data presented in Gupta's work,

TABLE I. Process conditions used in Gupta's experiments.

Data	Value
Mass flow rate	2.90×10^{-4} kg/s
Diameter of the die	2.54×10^{-2} m
Annular die gap	1.016×10^{-3} m
Velocity at the die exit	3.577×10^{-3} m/s
Temperature at the die exit	458.15 K
Freeze line height	0.12 m
Axial force at the nip	0.217 kg
Excess pressure inside the bubble	196.2 Pa

the run #20 (see table I) is used in this chapter for comparison. Reasons for choosing this data set are: i) experiment was performed under nonisothermal conditions, ii) blow up ratio, $BUR > 1$, and iii) results for comparison were available for radius of the bubble, temperature, velocity, and shear rate.

Material data of Styron666 is presented in table II. Density of the polymer does not change significantly in the temperature range of interest. Its value at the base temperature 298.15 K (25 deg C) is 1050 kg/m^3. Below the glass transition temperature, density decreases at the rate 2.65×10^{-4} $kg/m^3/K$ and above this temperature at the rate of 6.05×10^{-4} $kg/m^3/K$. This variation is not significant enough make a difference in the solution, hence the density is set to a constant value of $1000 kg/m^3$. Variation in thermal conductivity and specific heat with temperature of Styron 666 is ignored as they are insignificant.

The two viscosity parameters μ_1 and μ_2 are related by the constraint $\mu_2(T) > \mu_1/8$. Former is associated with the relaxation time and the latter with the re-

TABLE II. Material data of Polystyrene (Styron666) used in the analysis.

Data	Value
Density at 298.15 K	1050 kg/m^3
Specific heat	2100 $J/kg/K$
Thermal conductivity	0.123 $W/m/K$
Viscosity	see the discussion
Modulus	see the discussion
Melting point temperature	373 K
Glass transition temperature	373 K
No flow temperature	393 K

tardation time. Based on the data in Gupta's work, $\mu_1(T)$ is specified as $8.8 \times 10^4 \exp\left[18904(1/T - 1/443)\right]$ (which is internally specified as $2.582 \times 10^{-14} \exp(18904/T)$) as shown in figure 16. This curve fit to Arrhenius model is obtained from Cao and Campbell (1990). The second or retardation viscosity, μ_2 is assumed to have an identical behavior except with a modifying factor. Influence of this factor is described in the section on parametric studies. Further these two are shear viscosities, hence, they can be corrected by an internal factor of 3.4, which is a modified version of Trouton ratio based on molecular arguments [Doi and Edwards (1988)].

Figure 17 shows the variation of modulus as a function of temperature. Experimental data is fitted using an exponential model. As in the case of viscosity, one should use elongational modulus instead of the shear modulus.

$$G(T) = 217369 \exp\left(-0.04(T - 393.15)\right) \tag{63}$$

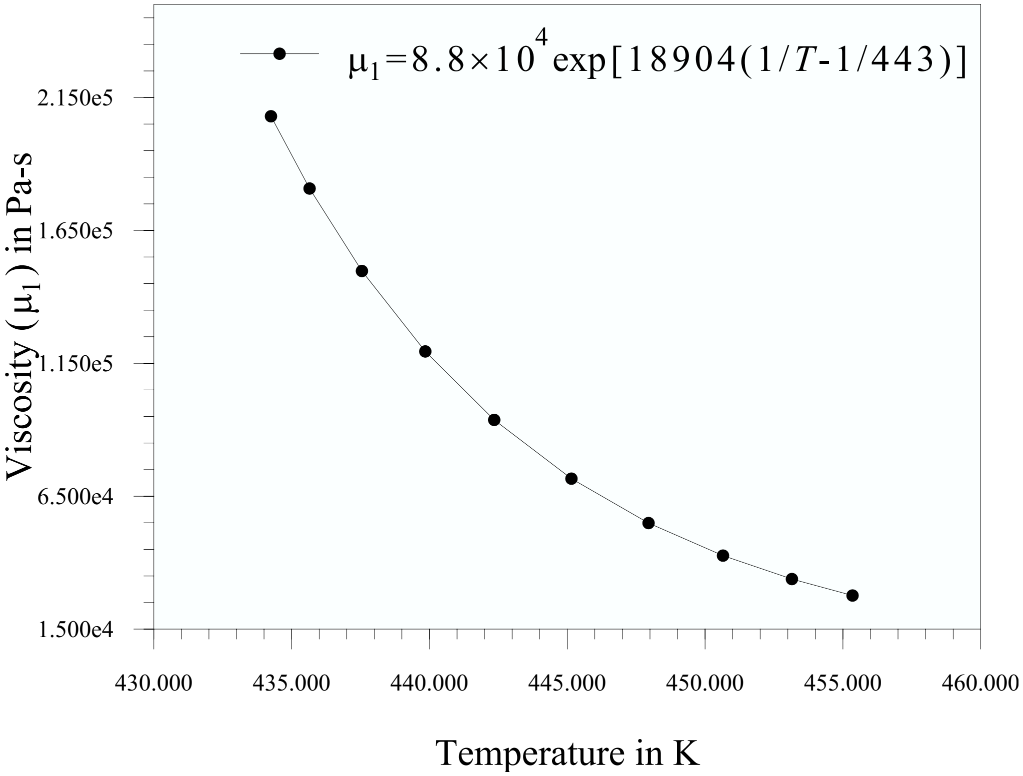

FIG. 16. Viscosity as a function of temperature. Experimental data is fitted using Arrhenius model.

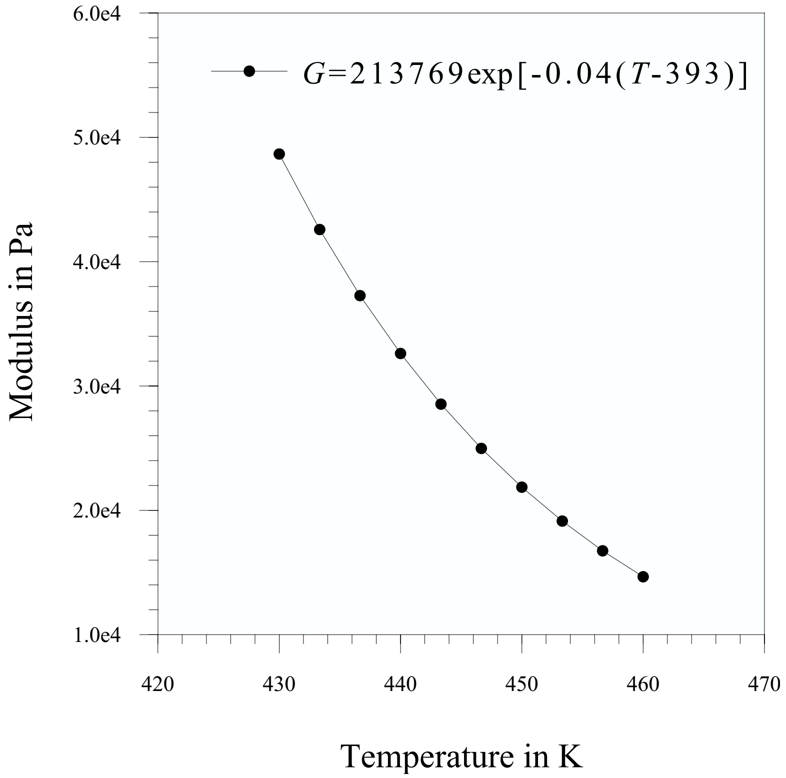

FIG. 17. Modulus of the polymer as a function of temperature. Data is fitted using an exponential model.

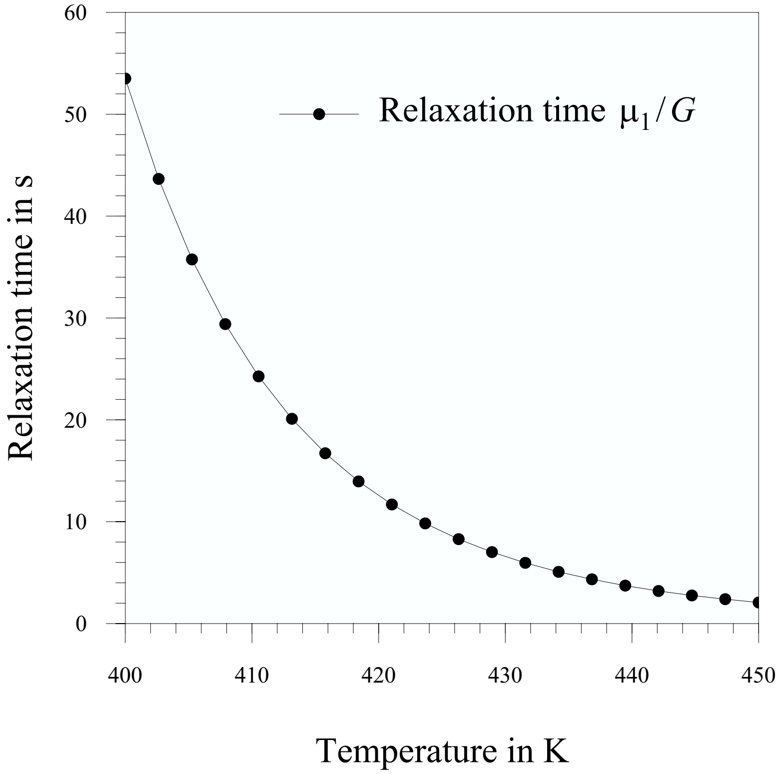

FIG. 18. Relaxation time as a function of temperature.

Figure 18 shows the relaxation time as a function of temperature. The retardation time, which is the ratio of Oldroyd viscosity and modulus follows the same trend.

Table III lists the data used by the phase change model. Role of these parameters on crystallization kinetics is addressed in the section on parametric studies. The crystallization kinetics model implemented for semi–crystalline polymers is used with suitable modifications to model the phase change of amorphous polymers. These changes are: a) modulus tensor of the solidified polymer is specified as isotropic and b) flow induced crystallization factor is turned off. Table IV lists the remaining process data used in the analysis.

TABLE III. Crystallization kinetics data used in the analysis.

Data	Value
Latent heat of solidification	1000 J/kg
Rate of phase change	0.011/s
Power-law exponent	3.0
Flow induced change factor	0.0

2. Estimating Heat Transfer Coefficient

In Gupta's experiments heat transfer from the bubble is achieved via natural convection and radiation heat transfer. Natural convection heat transfer coefficient for such flow configurations will be in the order of $1 - 10\ Wm^{-2}K^{-1}$. In order to gain a better understanding of the distribution of the heat transfer coefficient, natural convection heat transfer is solved using finite element method using a commercially available solver. Figure 19 shows the distribution of heat transfer coefficient along the machine direction. In the analysis, this coefficient is specified as a constant value along the machine direction, hence, an average value is used.

3. Comparison with Gupta's data

Following figures compare the results of the analysis with the experimental data. Since the model developed is transient, in order to attain steady state results, solution is allowed to evolve over time. In the next chapter, details pertaining to transient analysis are presented. In this chapter, for all the cases presented – solution evolved to stable steady state. Figure 20 compares the radius of the bubble computed by the model developed with experimental data.

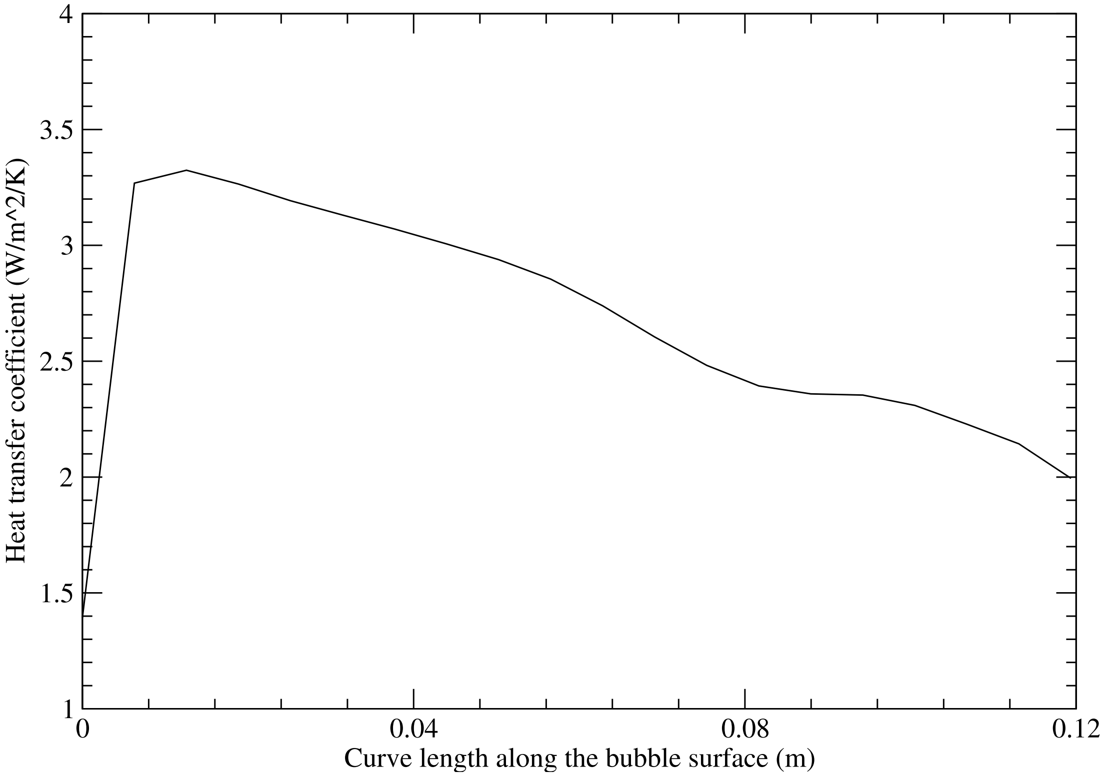

FIG. 19. Heat transfer coefficient along the axis computed using a commercial software.

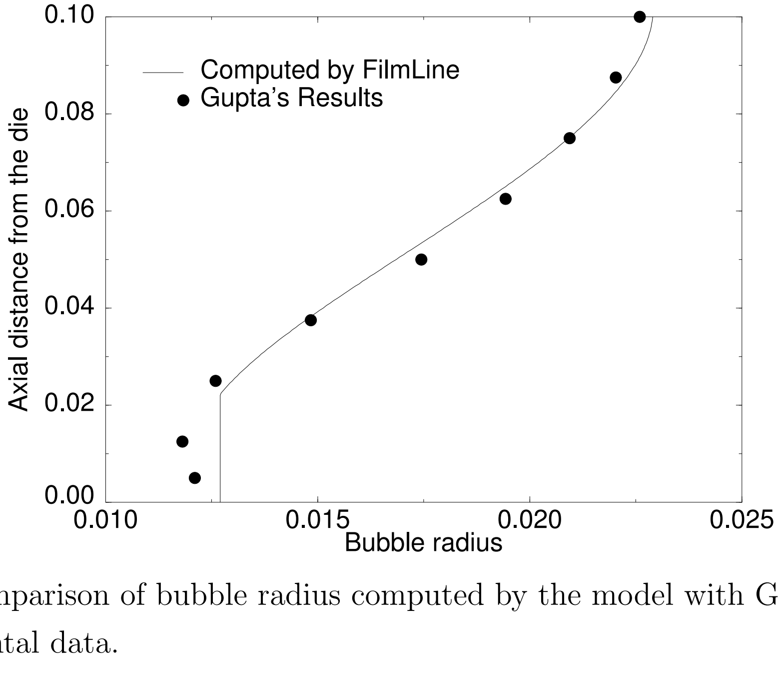

FIG. 20. Comparison of bubble radius computed by the model with Gupta's experimental data.

TABLE IV. Other process conditions used in the analysis.

Data	Value
Convection heat transfer coefficient	5.4 $W/m^2/K$
Temperature of the cooling air	300 K
Emissivity of the bubble surface	0.2
Temperature of the surrounding walls	300 K
Acceleration due to Gravity	0 m/s^2
Material type	*Amorphous*
PTT model slip factor	0.1
PTT model stretch factor	0.01

Unlike most numerical studies available in the literature, which use shooting method, the model used here solves the problem as a two point boundary value problem. Hence, it allows specification of boundary conditions at both nip and die ends. If the radius of the bubble is not constrained at the nip end, then the results diverge from the experimental data. This is seen in Figure 21. Experimental data shows a slight dip near the die exit. In order to capture this dip some special strategies such as, process data varying along the MD has to be used. As shown in Appendix C, it is possible to force the bubble to conform to this dip. However, such an approach will make the model dependent on experimental results. It is shown in Section 3, under some conditions, this dip naturally forms in the numerical analysis as well.

Figure 22 shows the temperature distribution along the axis of the bubble. Even though the energy equation includes conduction terms in modeling heat transfer, this process is strongly advection dominated and condition specified at the nip end for temperature does not play any significant role. For all practical purposes, heat

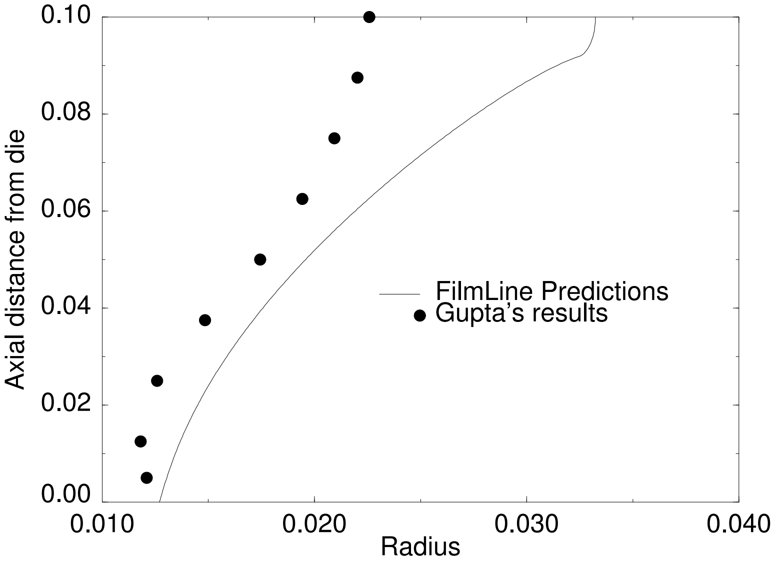

FIG. 21. Radius of the bubble with Neumann condition imposed at the nip end.

conduction terms in the equation can be ignored.

In order to get a better comparison for velocity data, value of the retardation viscosity has to be set to a very low value. Otherwise, velocity will show an exponential trend, unlike the near linear distribution seen in Figure 23. Effect of the retardation viscosity on the solution is further explored in Section D-2.

C. Comparison with Exxon's Data

Exxon's experimental data is significantly different from Gupta's laboratory scale data. It uses forced convection heat transfer by cooling the bubble with turbulent air jets. Depending on the jet velocity, under standard conditions, heat transfer coefficient could vary by an order of magnitude. Figure 24 shows variation of heat transfer coefficient for different air velocities. This result was computed using finite element analysis of forced convection heat transfer using a commercial solver with RNG $k - \epsilon$ model. Table V lists some of the important process data used in the analysis.

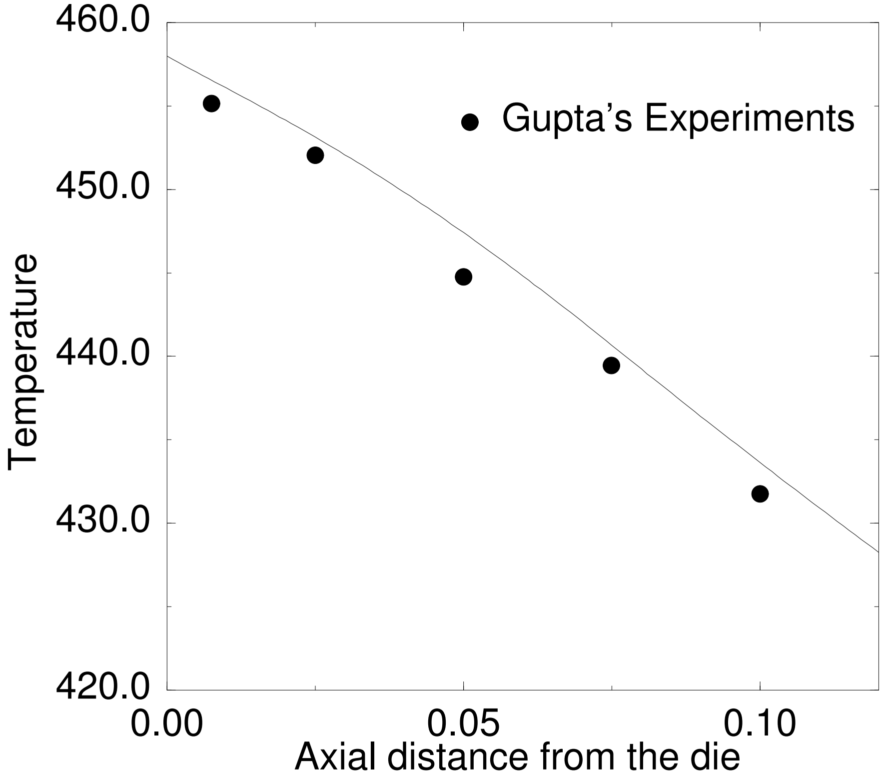

FIG. 22. Temperature of the bubble along the machine direction. Heat transfer is effected by natural convection and thermal radiation.

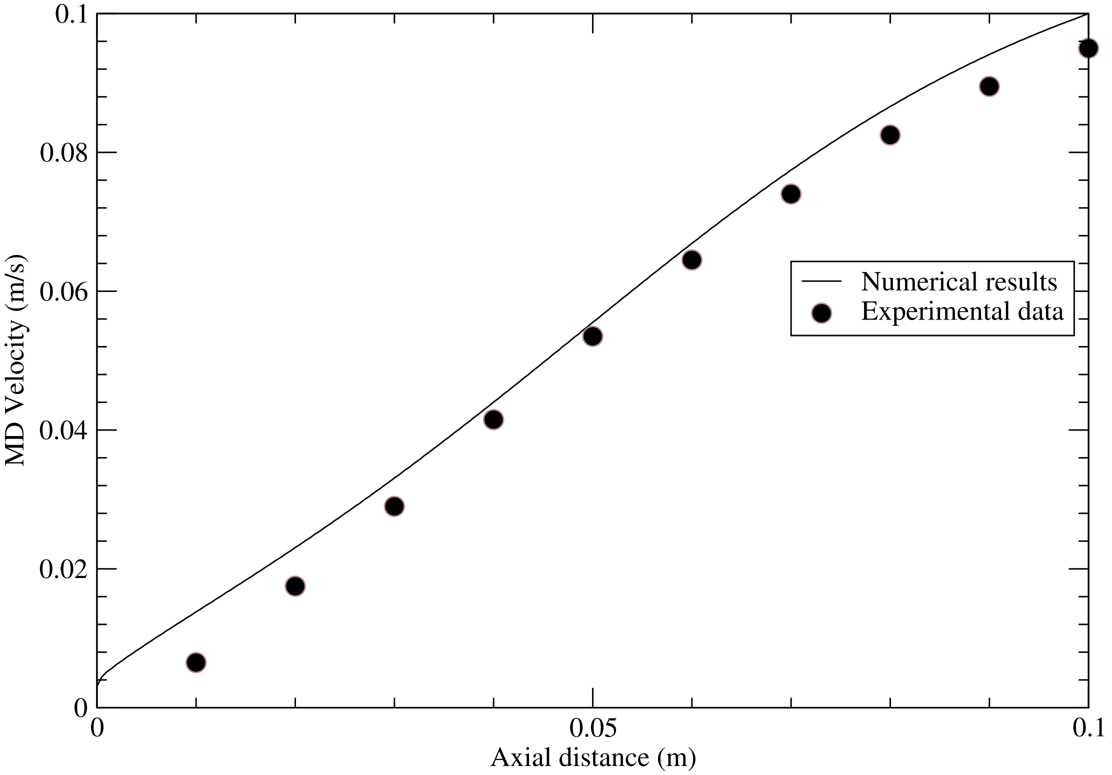

FIG. 23. Velocity of the polymer along the machine direction is compared with Gupta's experimental data.

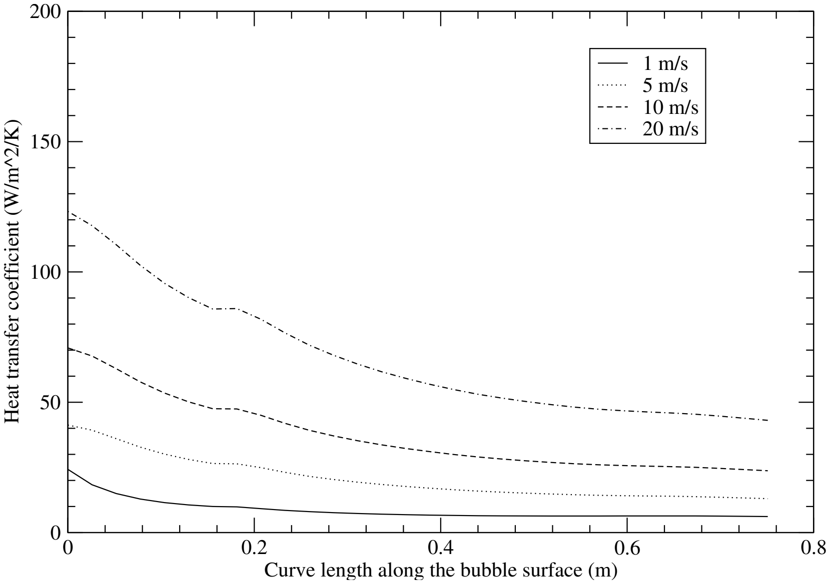

FIG. 24. Heat transfer coefficient along the axis computed using a commercial solver.

TABLE V. Process conditions used for the analysis of Exxon data.

Data	Value
Mass flow rate	$2.90 \times 10^{-4}\ kg/s$
Diameter of the die	$7.62 \times 10^{-2}\ m$
Annular die gap	$1.524 \times 10^{-3}\ m$
Velocity at the die exit	$3.2 \times 10^{-2}\ m/s$
Velocity at the nip end	$0.1\ m/s$
Temperature at the die exit	$489.0\ K$
Freeze line height	$0.8\ m$
Excess pressure inside the bubble	$40.0\ Pa$
Convection heat transfer coefficient	$50\ W/m^2$
Temperature of the cooling air	$290\ K$
Emissivity of the bubble surface	0.2
Temperature of the surrounding walls	$290\ K$
Acceleration due to Gravity	$0\ m/s^2$
Material type	$Crystalline$
PTT model slip factor	0.3
PTT model stretch factor	0.01

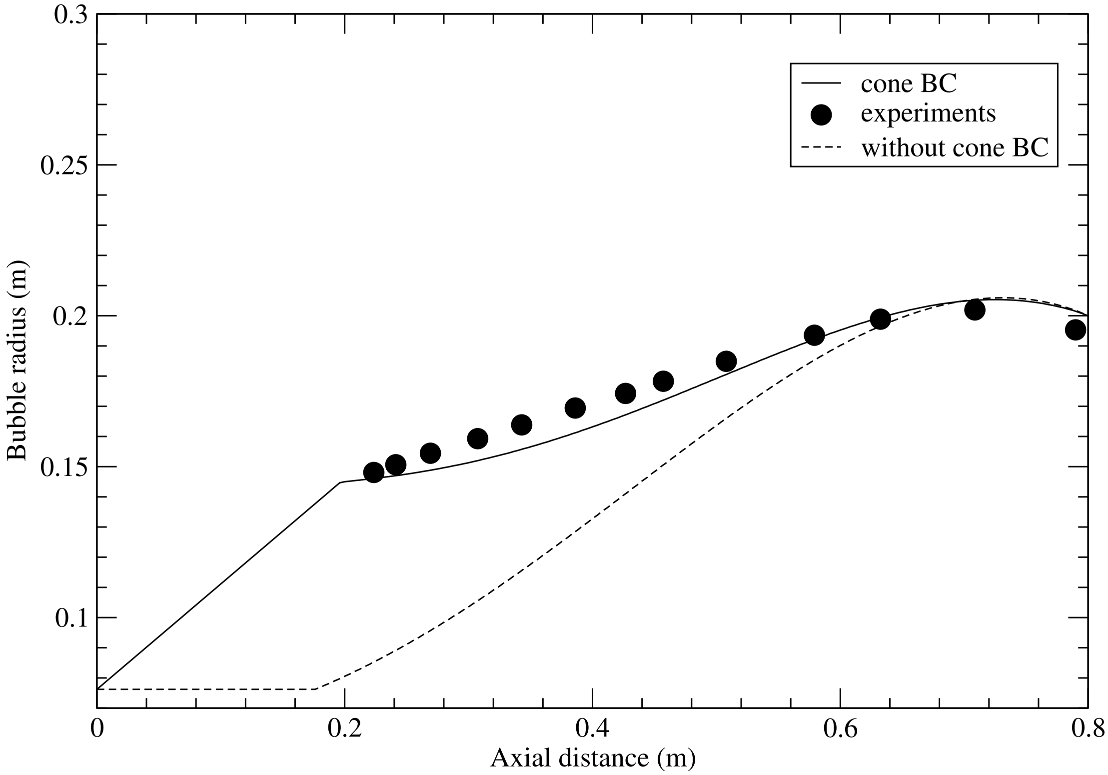

FIG. 25. Comparison of bubble radius with Exxon experimental data. Results with and without cone condition is shown in the figure.

One of the special features of the Exxon process is, it uses a conical ring near the die exit, which forces the material to flow over the surface cone. This leads to a smoother expansion of the air bubble. In order to simulate this, a cone boundary condition was implemented. Using this condition forces the radius of the bubble to conform to the cone as shown in figure 25. The same cone condition is used to force the data in some of the other runs to extend the flow past the extrudate swell region, by specifying a constant diameter.

D. Parametric Studies

1. PTT vs Oldroyd-B

This issue arises largely due the way the equations are solved. In the case of Navier-Stokes equation, diffusion terms are accounted for directly in the momentum equation and their contribution during formulation goes to the operator matrix as well as the forcing function (through boundary conditions). On the other hand, when solving the momentum equation using standard PTT model, viscous effects do not directly enter the operator and they occur only in the forcing function. This makes the equation inherently unstable and has to be smoothed. This can be accomplished by more than one way. Figure 26 shows the velocity distribution along axial distance. The model is subjected to boundary condition on both ends, die and nip rollers. It is clear from the plot that without SUPG correction to the momentum equation, model shows oscillation and it also has difficulty adapting to the condition on the nip rollers end. Even though SUPG correction smoothes it out, it is still not adequate to produce stable results and the model will crash by going out of bounds in few time steps. The most stable approach for this issue is to use a modified constitutive model, $\boldsymbol{\tau} = 2\mu_2\mathbf{D} + \boldsymbol{\tau}_{PTT}$. This is similar to the Oldroyd-B model. This model is denoted as the modified PTT model. The second viscosity μ_2 is denoted as Oldroyd viscosity.

2. Sensitivity to Oldroyd Viscosity

Sensitivity of the results to retardation viscosity depends on the other model parameters. In the typical case, given the high viscosity of thermoplastic polymers, the effect of this is felt only when the viscosity ratio is over ten thousand (see Figure 27). Value used for this parameter should be as low as possible to obtain more accurate results. Higher values result in excessive smoothing of the velocity distribution.

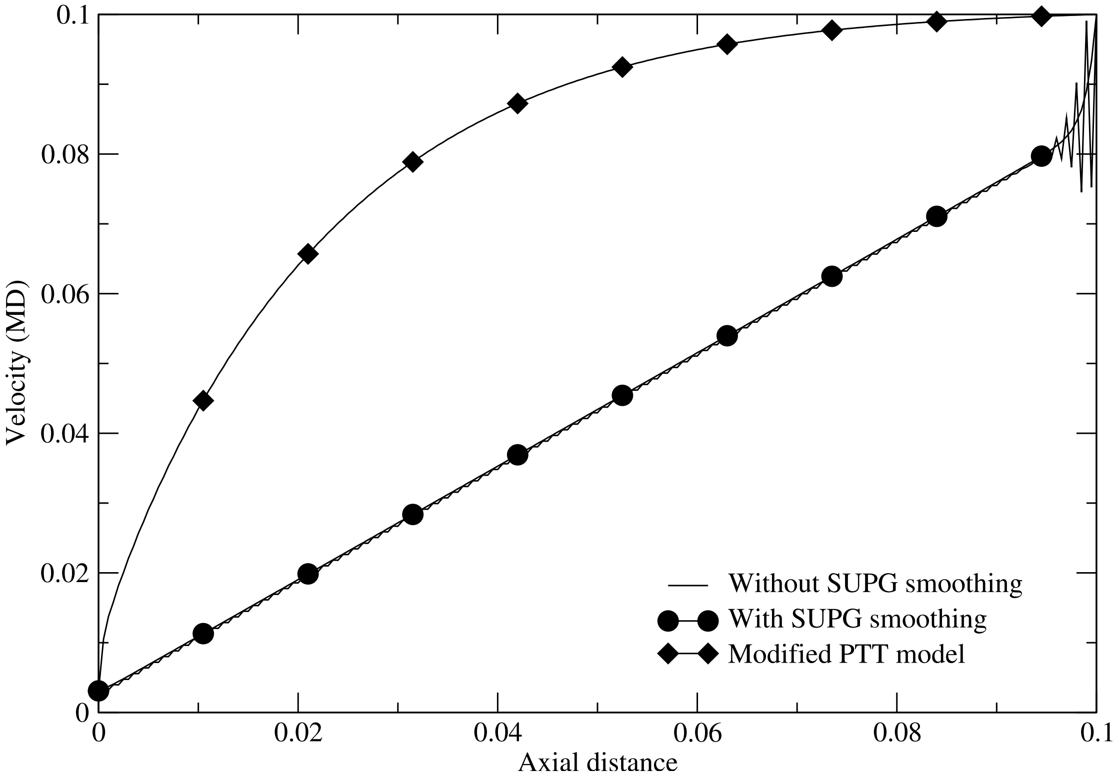

FIG. 26. Velocity distribution along the axial distance under different smoothing conditions. The most stable of these approaches is the Modified PTT model, which presents the constitutive model like Oldroyd-B model.

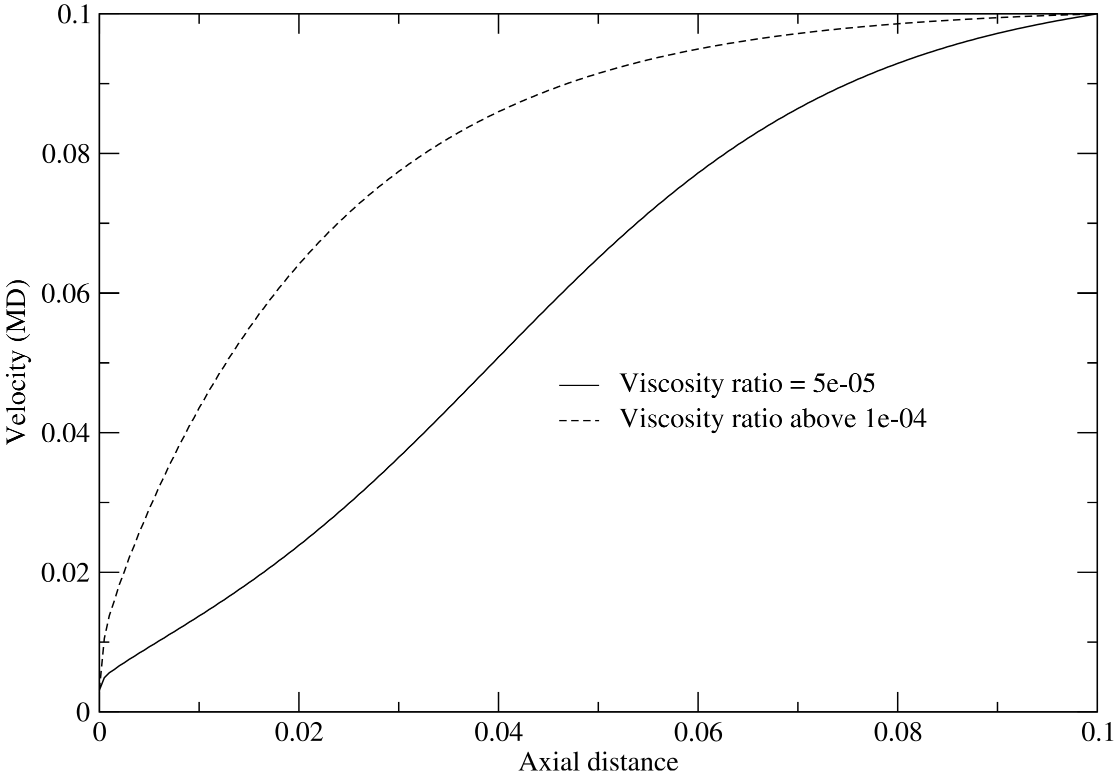

FIG. 27. Velocity distribution along the axial distance for different values of Oldroyd viscosity.

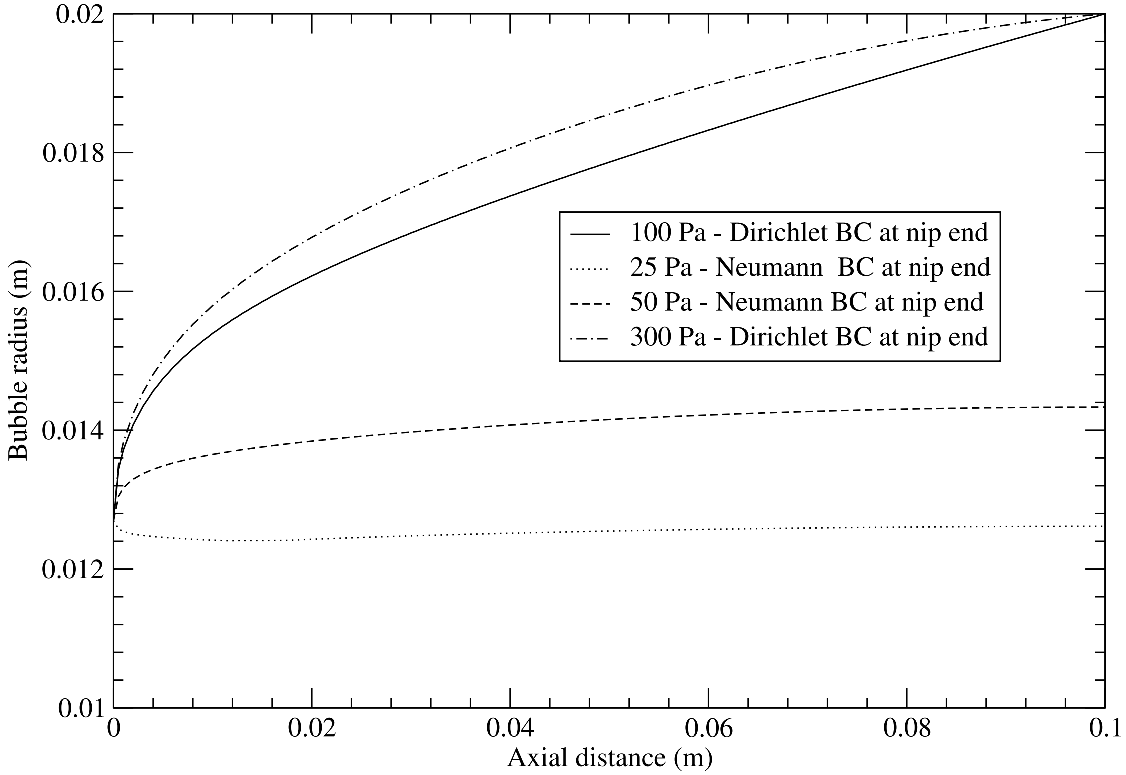

FIG. 28. Excess pressure in the bubble controls the stretch in azimuthal direction.

3. Excess Pressure

Excess pressure in the bubble controls the stretch in the circumferential direction. The value used is in the order of 100 Pa gauge pressure. Actual shape of the bubble depends on the combination of excess pressure and other parameters such as, velocity at the nip and die, and temperature (see Figure 28).

The dip caused near the die is observed in experiments. This can be reproduced by many combination of parameters. One of the key requirements to reproduce the dip noted in Gupta' experimental data is to vary the process conditions such as, heat transfer rate and excess pressure along MD.

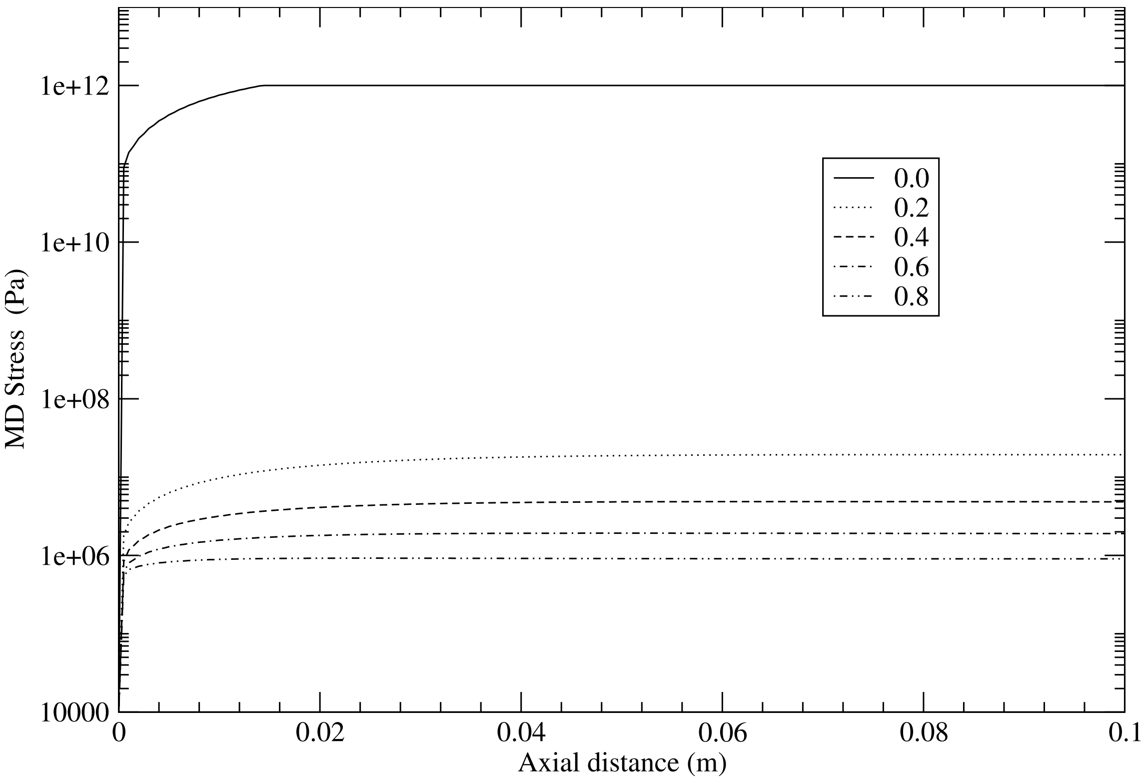

FIG. 29. The effect of PTT slip factor on MD stress.

4. The Effect of Slip Factor

Slip factor is a term specific to models such as PTT, it signifies non-affine motion. In this context, non-affine motion is understood as follows. If the continuum suffers a velocity gradient $\mathbf{L}$ then the individual polymer chains need not adhere to this motion and they can experience a slip. The actual value of this factor depends on the material under consideration and has to be calibrated using experimental data. Based on the available literature, a value in the range 0.2–0.3 is recommended. In this particular example, model fails when the slip factor is over 0.80. Following figures (29, 30, 31) show the effect of slip factor on the stresses and the radius of the bubble.

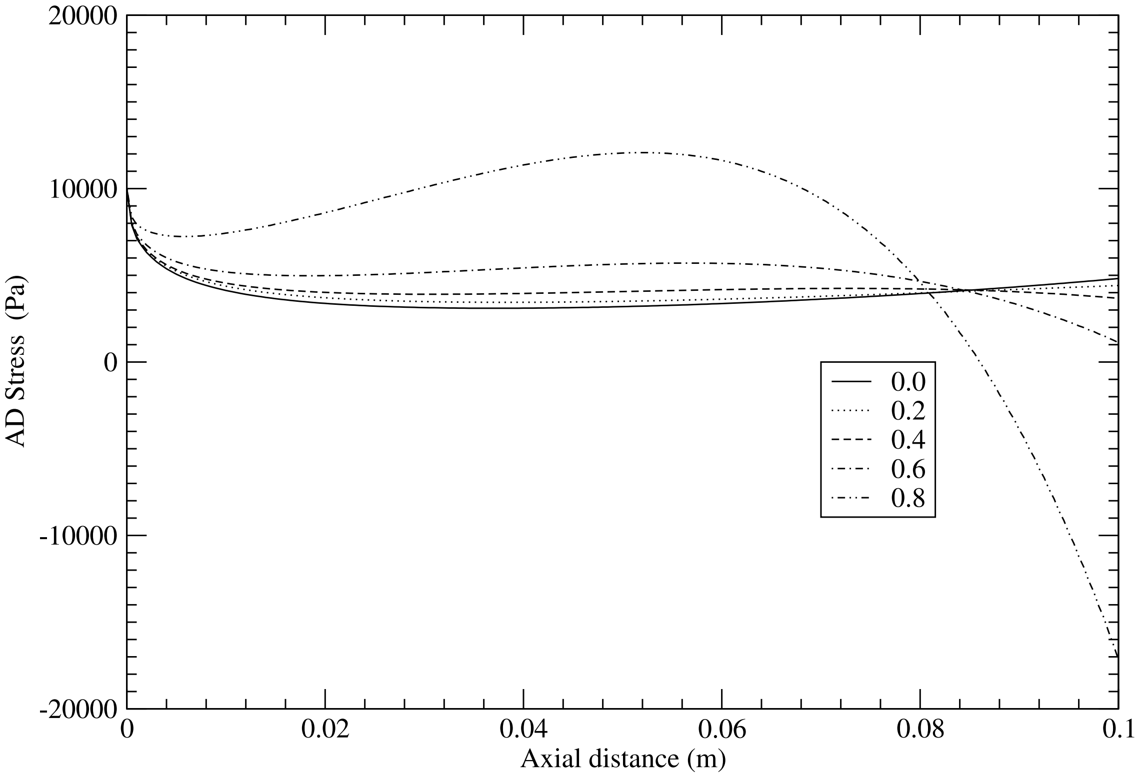

FIG. 30. The effect of PTT slip factor on AD stress.

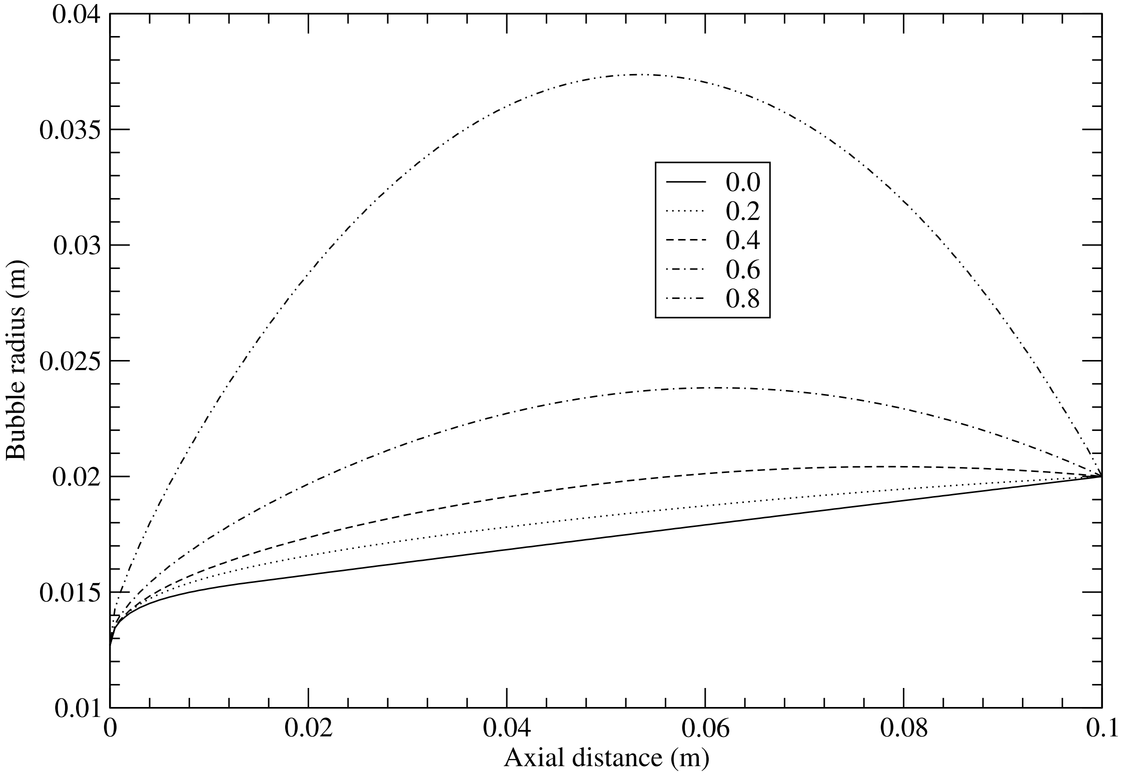

FIG. 31. The effect of PTT slip factor on the radius of the bubble.

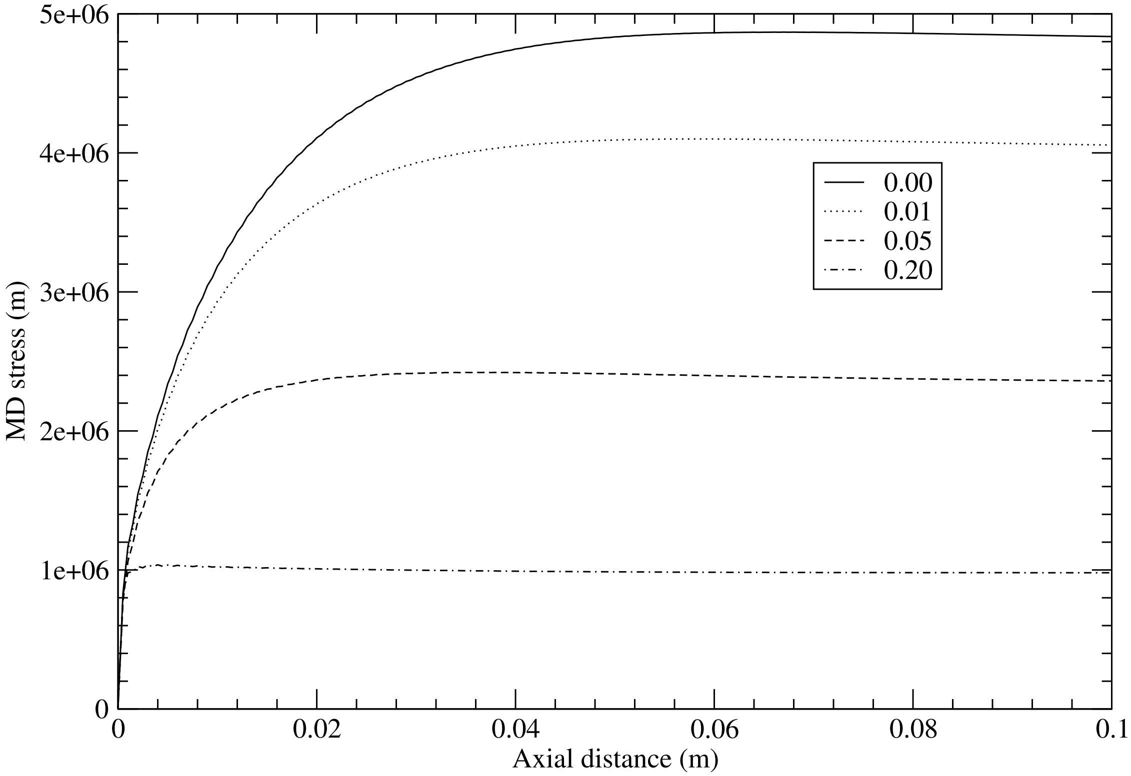

FIG. 32. The effect of PTT stretch factor on MD stress.

5. The Effect of Stretch Factor

Stretch factor is a term specific to models such as PTT. It brings in the extensional effect. Higher values of this factor, makes the model unstable. for most of the analysis, value less than 0.1 is used. Following figures (32, 33, 34) show the effect of stretch factor on the stresses and the radius of the bubble.

6. The Effect of Heat Transfer

Of all the parameters that affect the stability of the process, the rate of heat transfer from the bubble is the most important parameter. In the plot shown below (Figures 35 and 36), bubble collapsed for rates higher than $25W/m^2$. As it will be shown in chapter VII, the only way heat transfer rate can be increased is by increasing the

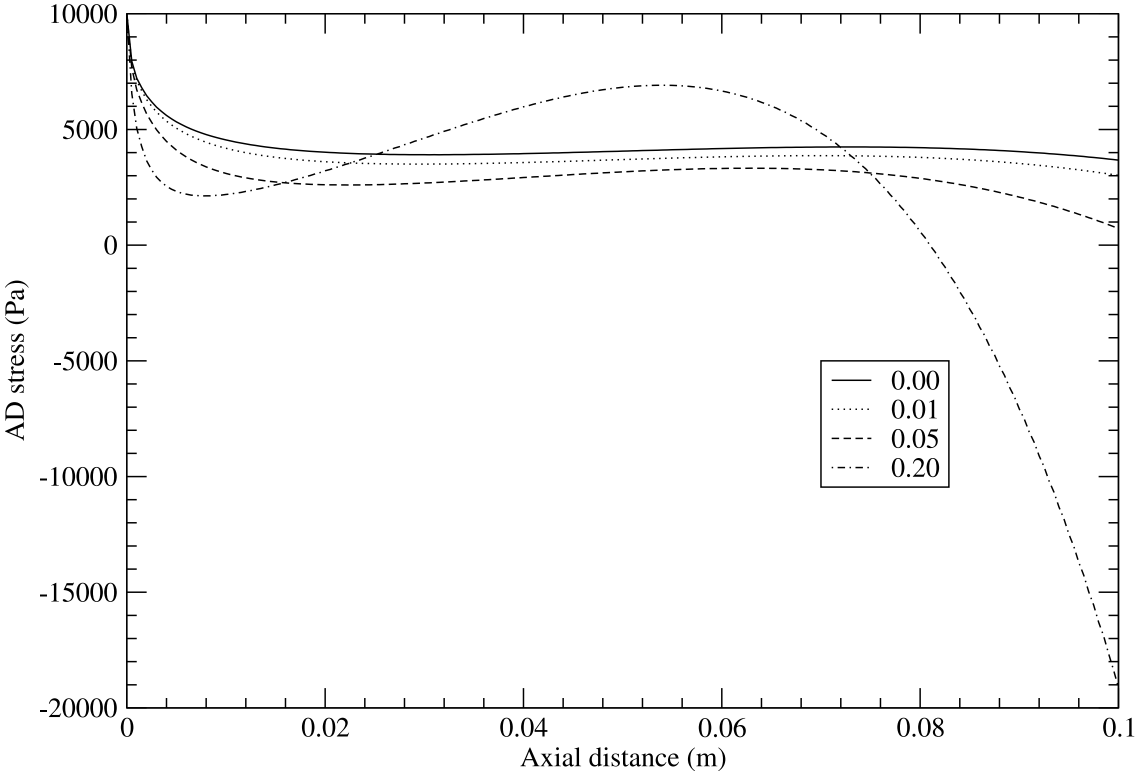

FIG. 33. The effect of PTT stretch factor on AD stress.

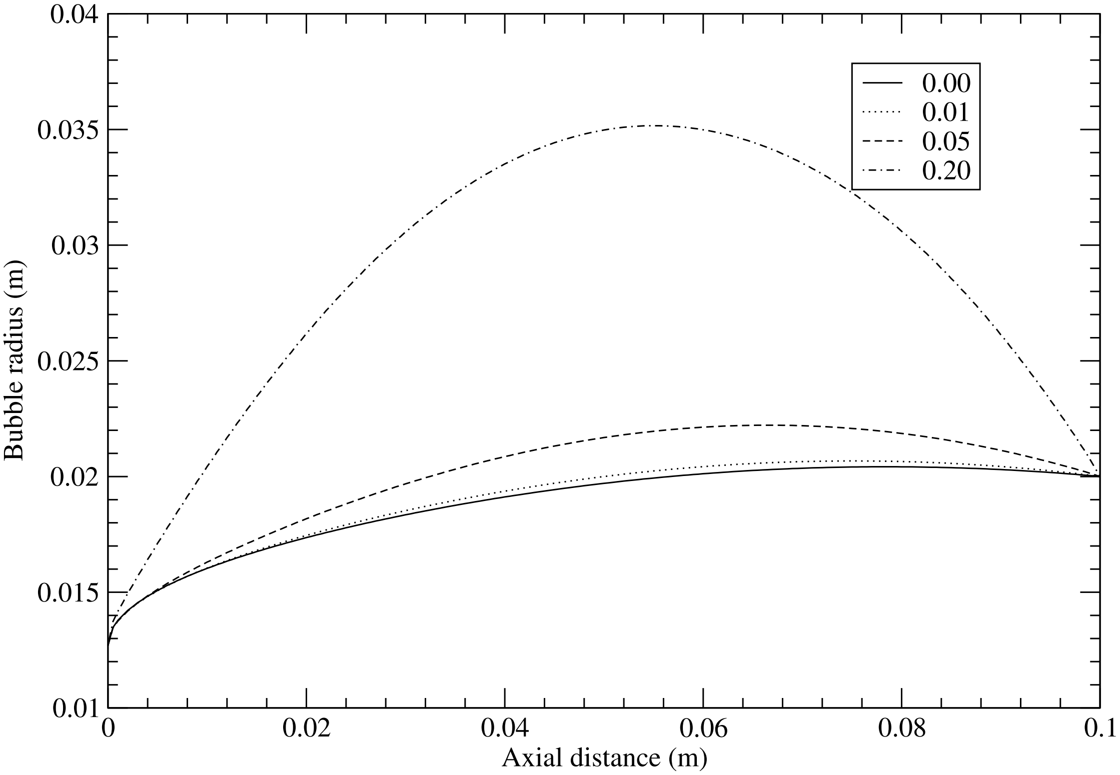

FIG. 34. The effect of PTT stretch factor on the radius of the bubble.

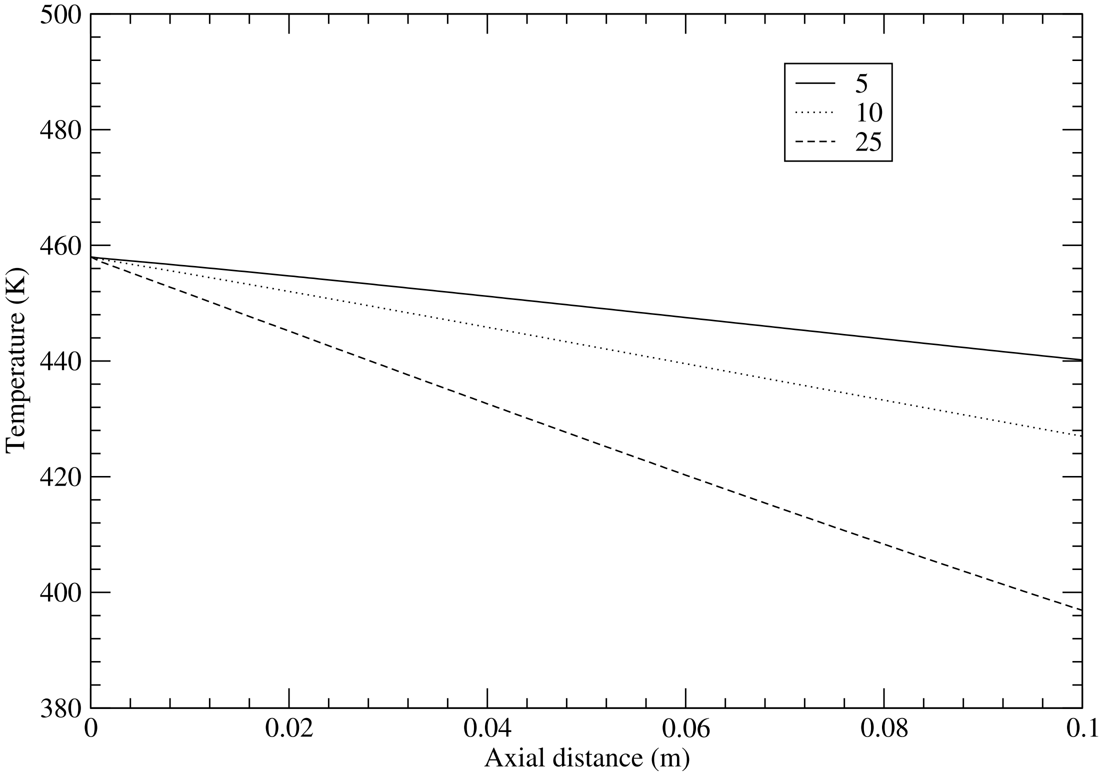

FIG. 35. The effect of convection heat transfer coefficient on the process. Plot shows the temperature distribution for three values of convection coefficients.

die/nip velocity. This can be directly related to particle residence time in the process window. The reason why heat transfer plays a critical role is because of the strong dependence of material properties on temperature of the melt.

Effect of radiation heat transfer is comparable to natural convection heat transfer. If external mechanisms such as, cooling rings are used, then radiation heat transfer is negligible and can be ignored.

7. The Effect of Dirichlet vs Neumann BC

Figure 37 shows the effect of Dirichlet vs Neumann condition for bubble radius at the die exit. When the Neumann condition is imposed, radius of the bubble aligns to most natural state possible for that set of process conditions. On the other hand, Dirichlet

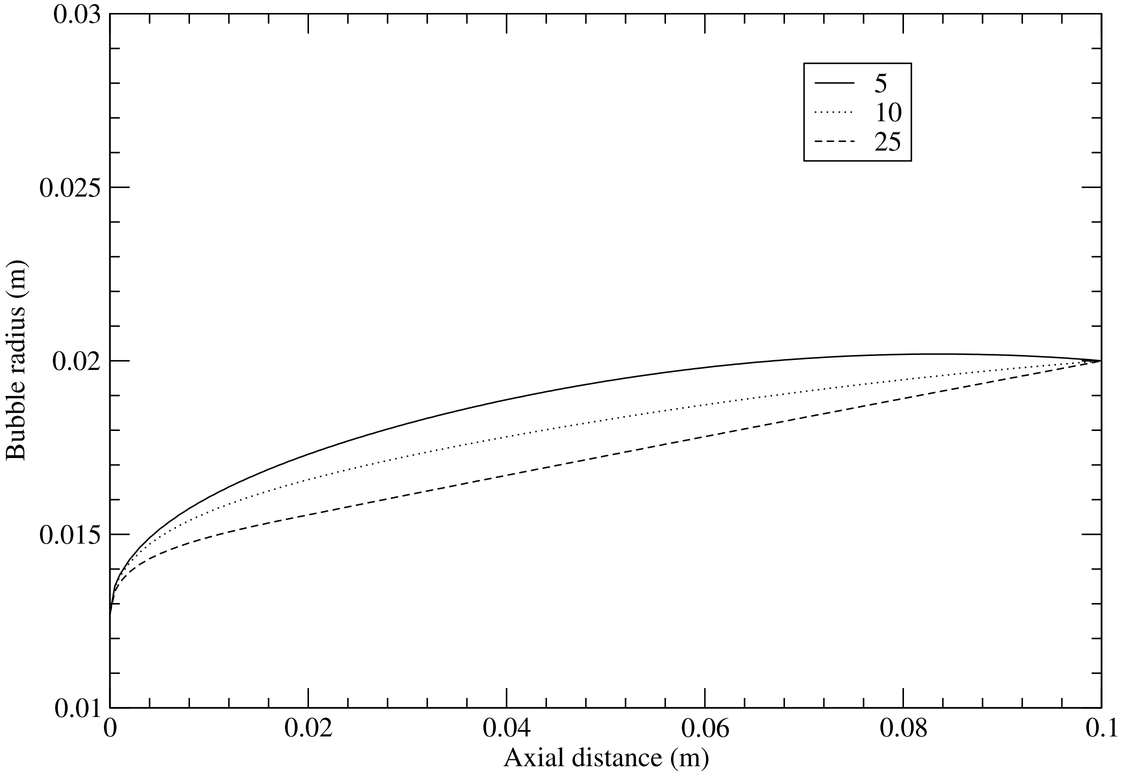

FIG. 36. The effect of convection heat transfer coefficient on the process. Plot shows the bubble shape for three values of convection coefficients.

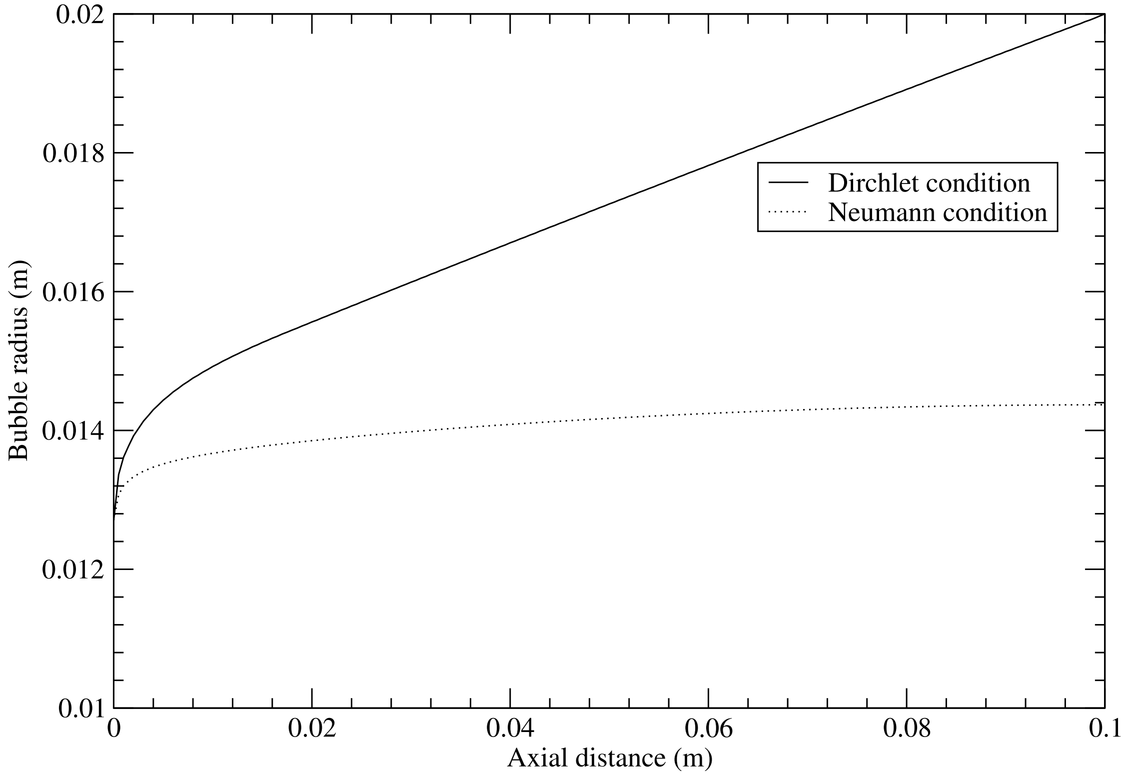

FIG. 37. Difference in the bubble shape due to nip side boundary condition. Analysis used a high heat transfer coefficient of $25W/m^2$.

condition forces the value of the radius at the nip end. From a practical standpoint, it is will not be possible to say what is correct. This is because, in reality, the bubble is constrained at the nip end. However, it is not constrained to the freeze line radius. Ideal approach to this problem is to solve the system of equation with both types of boundary conditions and judge whether the process conditions are optimal for that desired freeze line radius.

E. Closure

Model developed compares well with the available experimental data. Parametric studies conducted highlight different aspects of the model. This model is solved using

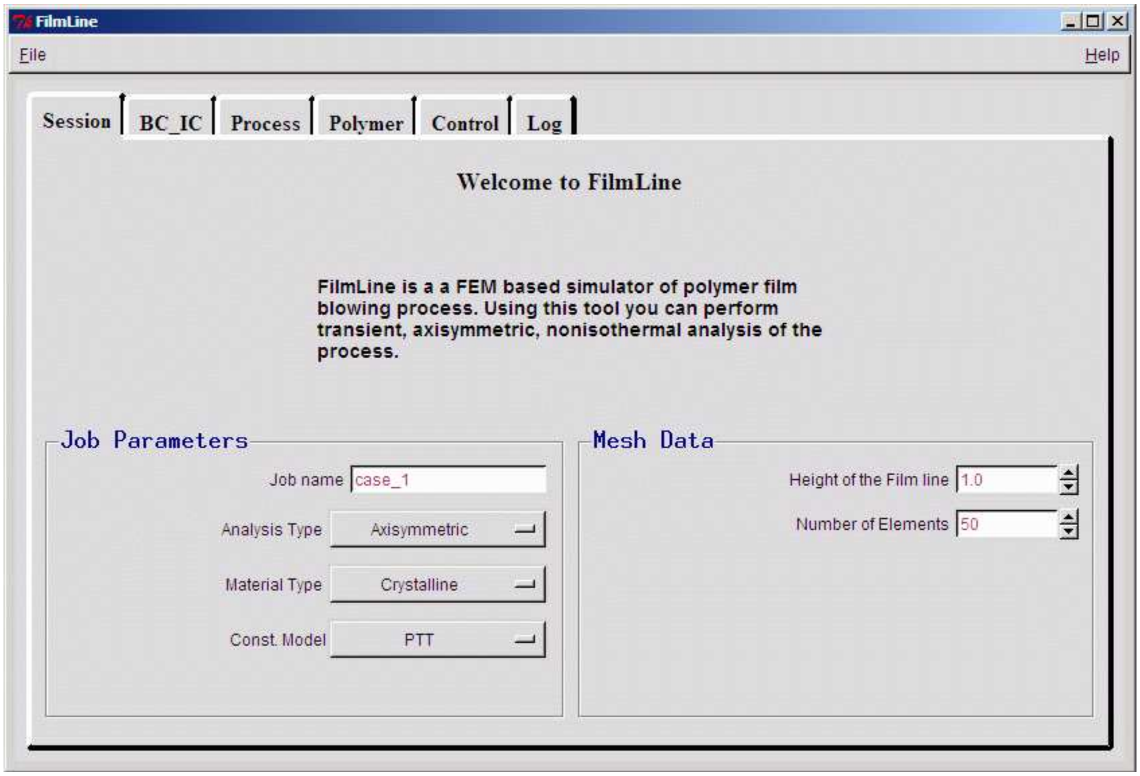

Welcome to FilmLine

FilmLine is a a FEM based simulator of polymer film blowing process. Using this tool you can perform transient, axisymmetric, nonisothermal analysis of the process.

Job Parameters

Job name: case_1

Analysis Type: Axisymmetric

Material Type: Crystalline

Const. Model: PTT

Mesh Data

Height of the Film line: 1.0

Number of Elements: 50

FIG. 38. Pre–processor for the software developed. Together with the software developed, it is called FilmLine.

finite element method and the software is written in C++ using object–oriented methodology. This enables ease of extension and provides ability to add different constitutive models to the existing code with few modifications. Software developed comes with pre and post–processing interfaces shown in figures 38 and 39.

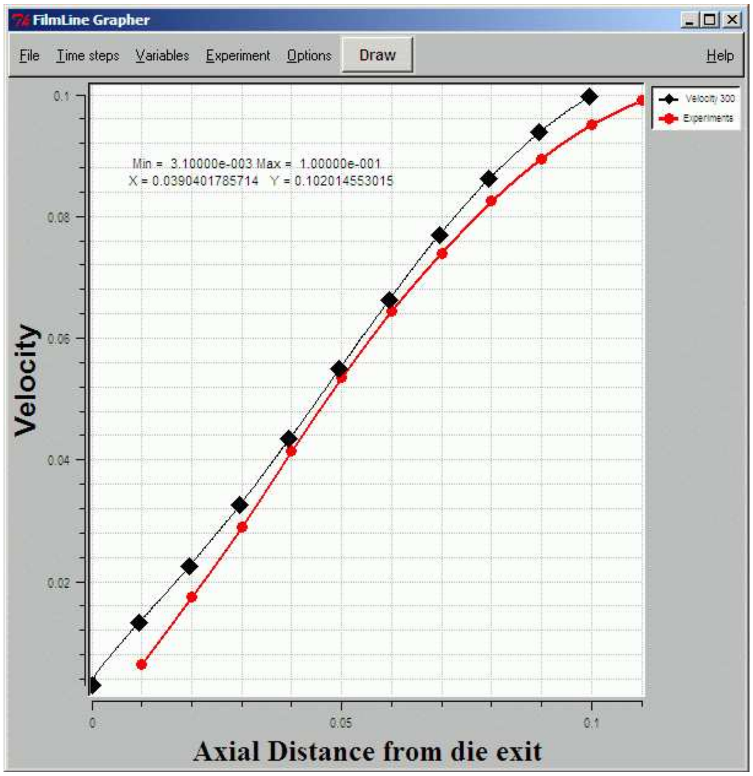

```
Min =  3.10000e-003 Max =  1.00000e-001
X = 0.0390401785714   Y = 0.102014553015
```

FIG. 39. Post–processor for the software developed. If experimental data is available it can compare the results with it.

CHAPTER VII

TRANSIENT ANALYSIS

A. Introduction

Goal of this chapter is to bring out some of the significant aspects of film blowing process using the transient model described in Chapter IV. It is important to analyze the temporal behavior of the process to produce uniform quality films. Results in this chapter show that even if the process data is not time dependent, solution does show transient behavior with fluctuation the radius and thickness of the bubble.

Model equations are discretized in time direction using fully implicit Crank–Nicholson scheme. Due to presence of transient terms, RHS of some of the equations have terms with time derivatives. These terms are computed using a three-point cubic curve fit with values of at t_{n-1}, t_n, and t_{n+1}. Time derivative at t_n is computed based on this curve. At $t = 0$, a simple linear approach is used. Figures 40 − 42 show how the solution evolves to steady state. If the process conditions lead to a stable steady state, then model typically reaches steady state solution in the matter of few seconds. The default time step size used by the model 0.01s.

In this chapter three issues pertaining to transient dynamics of the film blowing process are studied. They are a) sensitivity to perturbations initial conditions, b) radius instability, and c) melt tension instability. In addition, effect of the size of time step on the solution is also discussed.

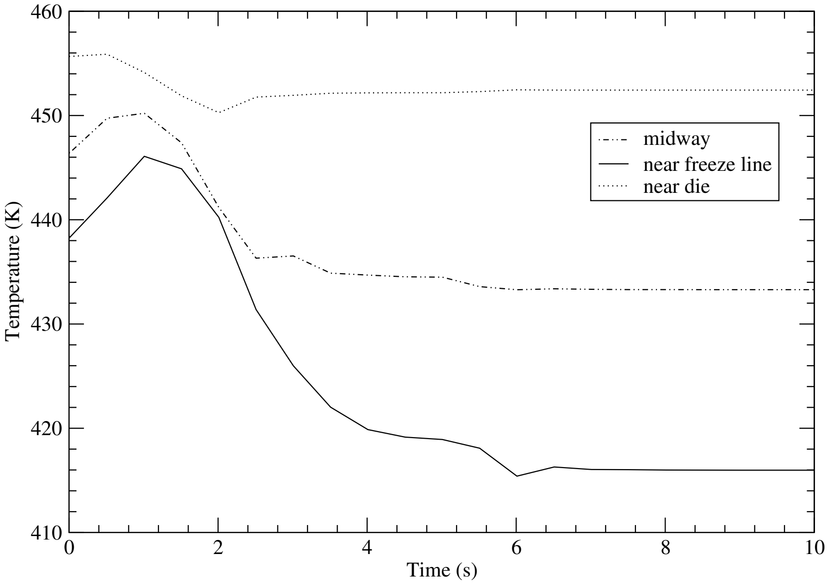

FIG. 40. Evolution to steady state – plot shows temperature as a function of time at three different locations.

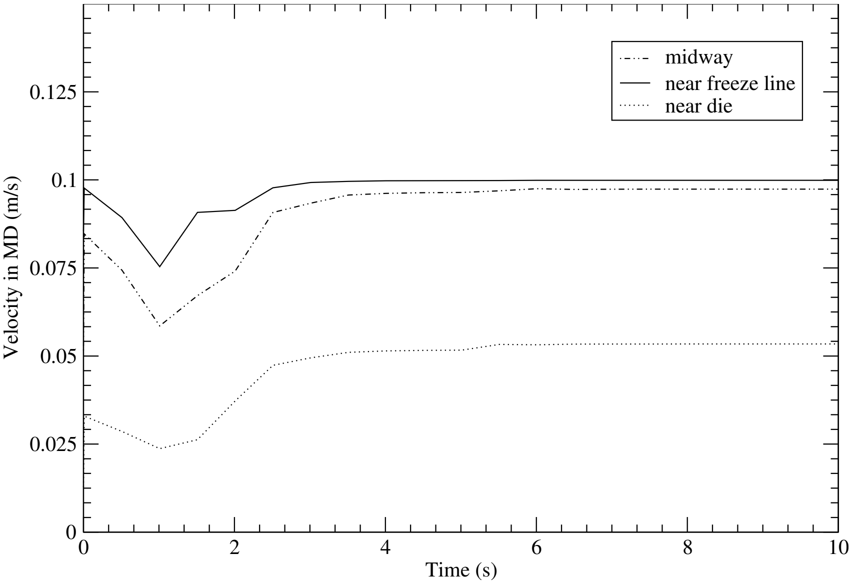

FIG. 41. Evolution to steady state – plot shows velocity as a function of time at three different locations.

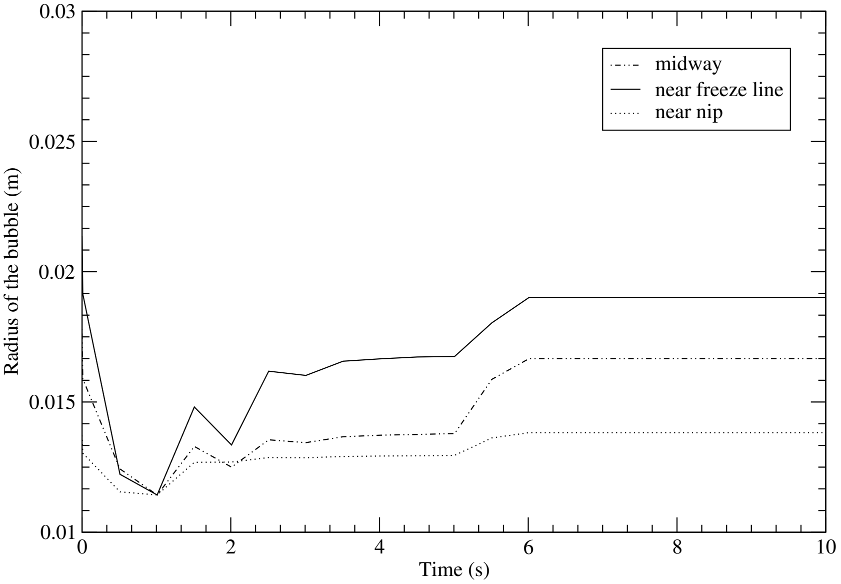

FIG. 42. Evolution to steady state – plot shows velocity as a function of time at three different locations.

B. Size of Time Step

Fully implicit Crank-Nicholson scheme is used for time discretization. This makes the system not sensitive to the time step size. The size of time step used, however, is critical if the boundary data is time dependent. Following example shows the role of time step in an analysis with temperature of the polymer melt has a sinusoidal disturbance at with 1% magnitude and 2s cycle time. Three values of steps: 0.01, 0.1, and 1s is used. It is clear from the figures (43 – 45) that for this problem, optimal value of time step is 0.1s. It provides the best balance between computational time and accuracy. One interesting feature of the model is revealed in the anomaly in Figure 45. This is due to the fact that the radius equation is not an explicitly time dependent equation. Its time dependence derives from the stress terms in the equations, which occur as a ratio and hence, at higher time steps one does see any improved accuracy.

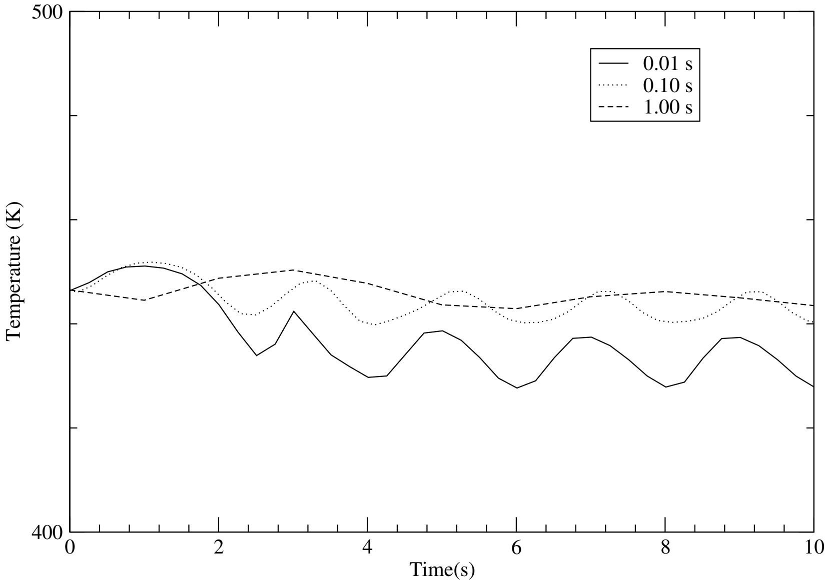

FIG. 43. Sensitivity to time step size. Plot shows temperature at $z = 0.05$ as function of time.

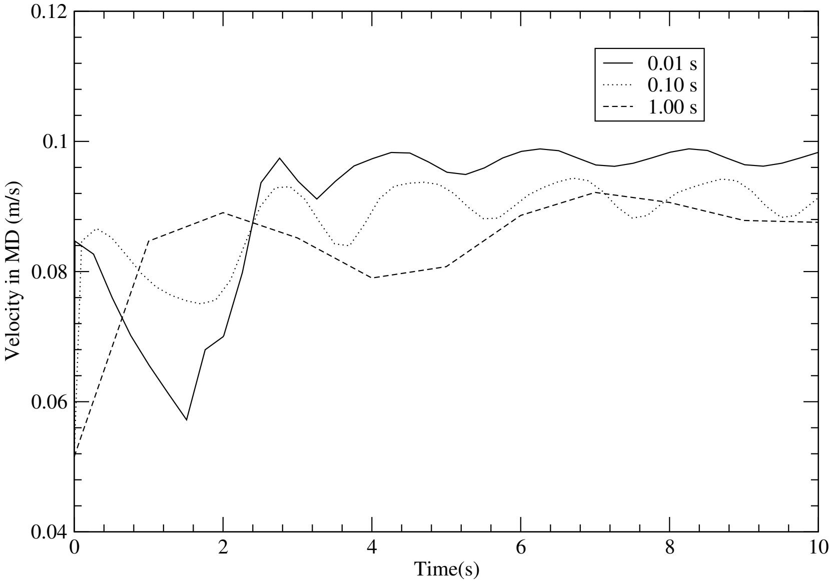

FIG. 44. Sensitivity to time step size. Plot shows velocity at $z = 0.05$ as function of time.

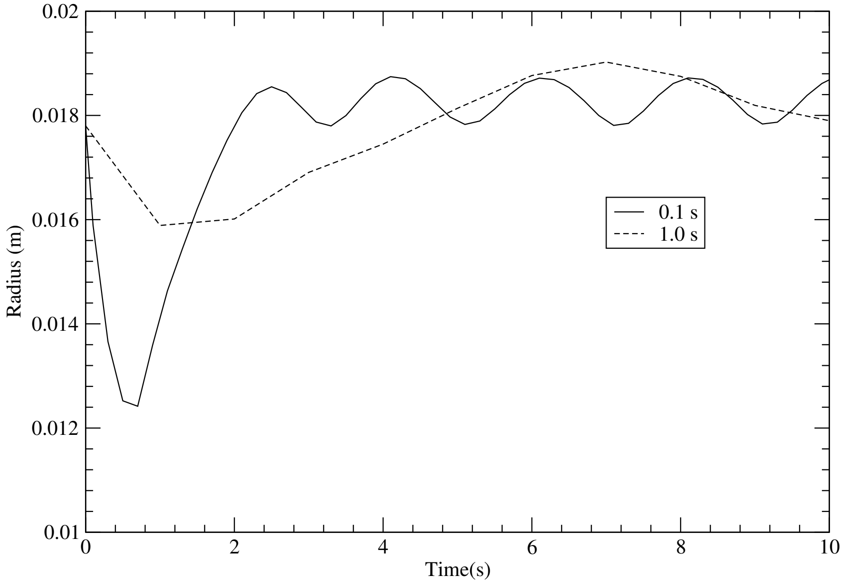

FIG. 45. Sensitivity to time step size. Plot shows radius at $z = 0.05$ as function of time.

C. Sensitivity to Initial Condition

Some of the process conditions can vary as a function of time. These are the velocity of the melt and the temperature at the die exit. In addition to this, there may slight variation in the polymer itself due to the differences in the batch, and mixing stages of extruder. In this section, sensitivity to sinusoidal oscillations in the velocity and temperature data is first considered separately and also together.

Velocity at the die is described used a mean component V_{die} and the sinusoidal oscillation added to it as shown in Figure 46. The oscillation is controlled by a scale factor V_{sf}, which varies from 0 to 0.2 (20%) and the frequency of oscillation, f (1/s). Both these are varied to see the sensitivity of the process to this data. Sensitivity is tested for factors 0.1, 0.15, and 0.20. And factor 0.10 is analyzed at different frequencies, 0.5, 1.0, and 2.0, which in cycles/s would be 2, 1, and 0.5 (see figures 47 - 48)

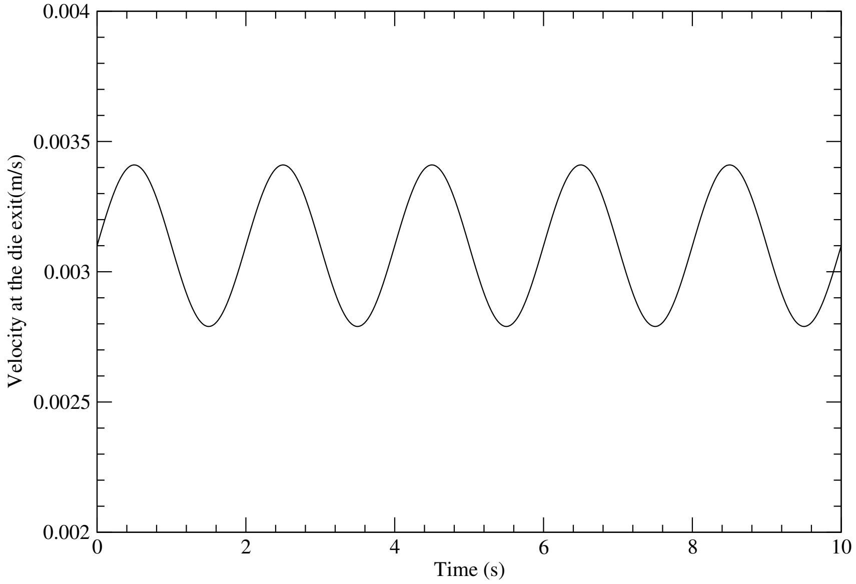

FIG. 46. Velocity boundary condition at the die end. Velocity is made of a mean component and sinusoidally varying component.

$$V_{die}(t) = V_{die}(1 + V_{sf} \sin(2\pi \ f \ t) \tag{64}$$

Sensitivity to temperature of the melt is studied under similar conditions. Results indicate that any irregularities in the temperature at the die has greater effect on the system stability than the velocity. Since temperature affects the melt properties drastically, it is the single important entity that needs to be controlled in the analysis. In this example presented (see figures 49 - 50), bubble collapse occurs for disturbances greater than 5%. Failure is dependent on both the magnitude and the frequency of the disturbance. For instance, the bubble collapse occurred when the frequency was 1 and for the magnitude 5%, however, it fails for frequencies less than 0.5. Plot list the frequency in terms of cycle time (1/frequency).

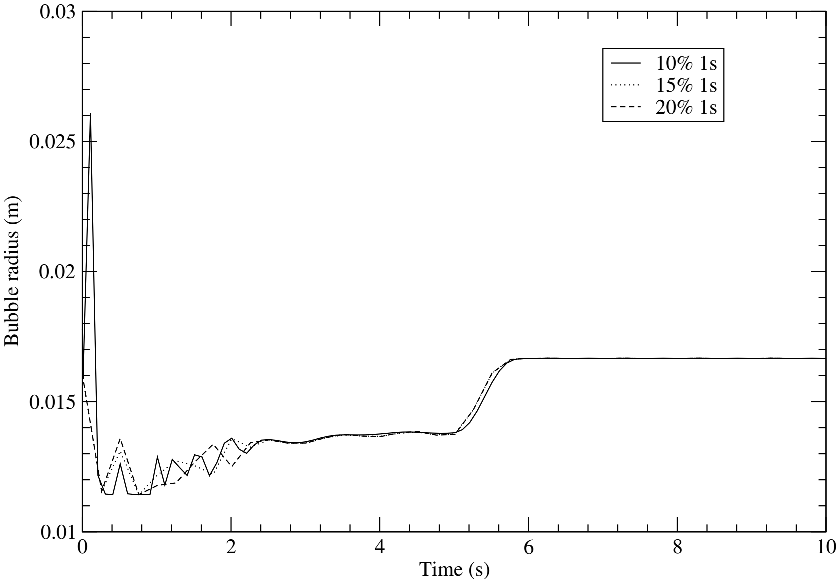

FIG. 47. Behavior of the system to velocity disturbances of different magnitude. System stabilizes itself for disturbances with amplitude less than 20%. Plot shows the radius distribution at 0.05m from the die exit.

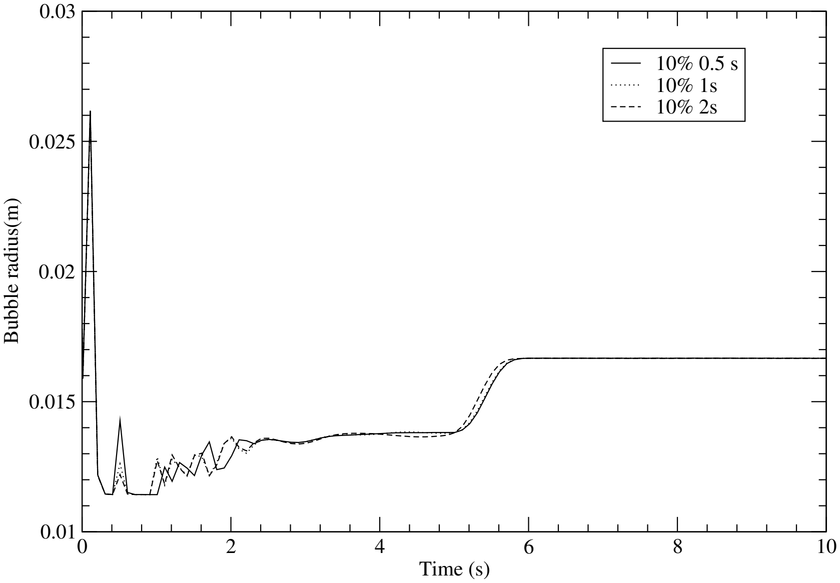

FIG. 48. Behavior of the system to velocity disturbances of different frequencies. Plot shows the radius distribution at 0.05m from the die exit.

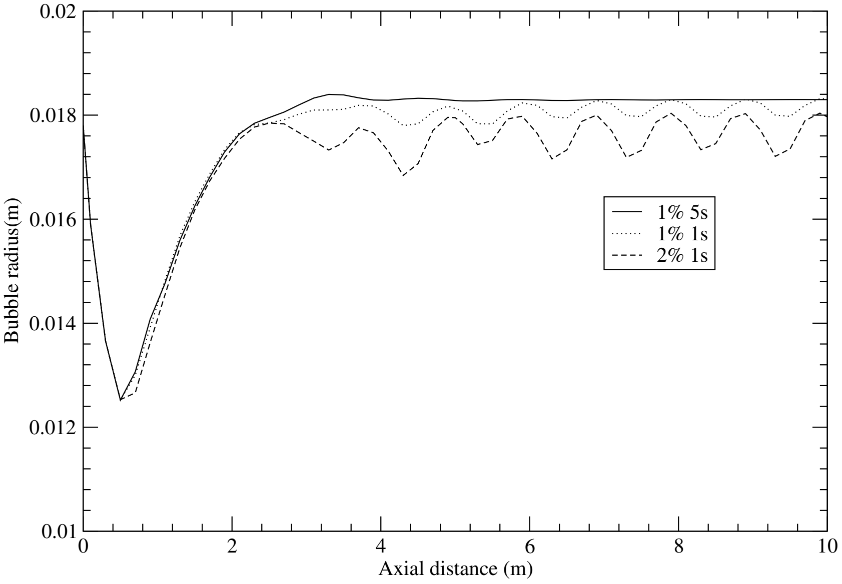

FIG. 49. Behavior of the system to temperature disturbances of different magnitude/frequencies. Plot shows the radius distribution at 0.05m from the die exit.

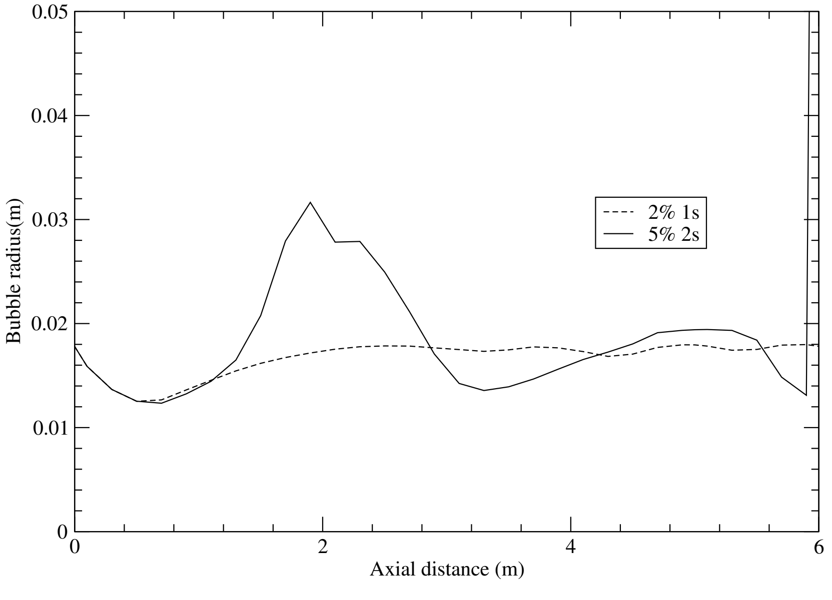

FIG. 50. Behavior of the system to temperature disturbances of different magnitude/cycle times. Bubbles oscillates wildly and collapses for the disturbance of 5% magnitude and 2s cycle time. Plot shows the radius distribution at 0.05m from the die exit.

D. Radius Instability

Under certain process conditions, radius of the bubble starts oscillating and this phenomenon, which is observed in experiments, is known as the radius instability. This instability could arise simply because of fluctuations at the die exit, which is often the most probable cause. This is seen in figures 49 and 50.

These type of disturbance can arise, even if the process conditions are the die exit is steady. One of the possible causes for this type of instability, based on the current numerical investigation, is the combination of high extrudate velocity at the die and higher rate of heat transfer from the bubble. This initially reduces the radius of the bubble and with a corresponding increase in the thickness of the bubble. Latter lowers the rate of heat transfer, which in turn leads to a larger radius and smaller thickness. One such instance is shown in figures 51 – 53. In this example, radius is not constrained at the nip roller end and it is subjected to Neumann condition. Even though some of the oscillations are wild, it never lead to the collapse of the bubble. A correction to this problem will call for fine tuning of the extrudate velocity and largely by slowing it down.

E. Melt Tension Instability

Under certain process conditions, the bubble tends to lift itself up and begins to oscillate between a wine cup like shape and normal bubble. Reason for a wine glass like shape in a steady bubble is due to the high melt strength and deformation begins after some thinning of the tube by a simple uniaxial deformation. With model developed this instability could not be reproduced using Gupta's data. However, the results in the previous section did show an tendency to a oscillation that had elements of melt tension instability.

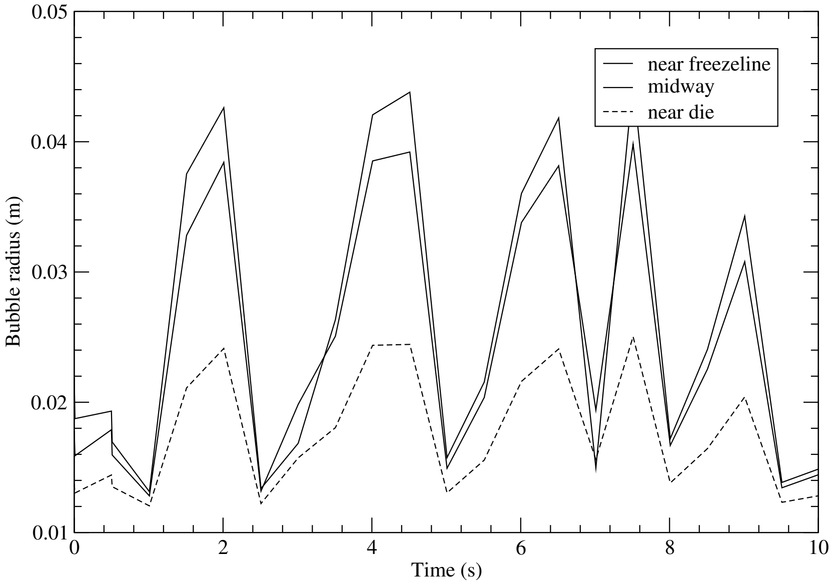

FIG. 51. Radius instability due to high die exit velocity and higher heat transfer rates – plot shows radius of the bubble at three different locations.

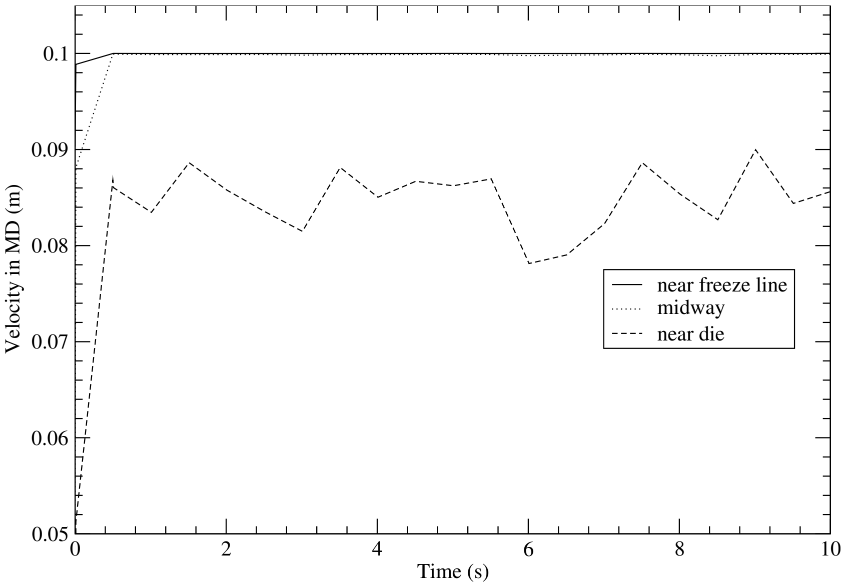

FIG. 52. Radius instability due to high die exit velocity and higher heat transfer rates – plot shows velocity of the bubble at three different locations. Velocity at the nip end is specified using Dirichlet boundary condition, hence the oscillations are less near the nip end.

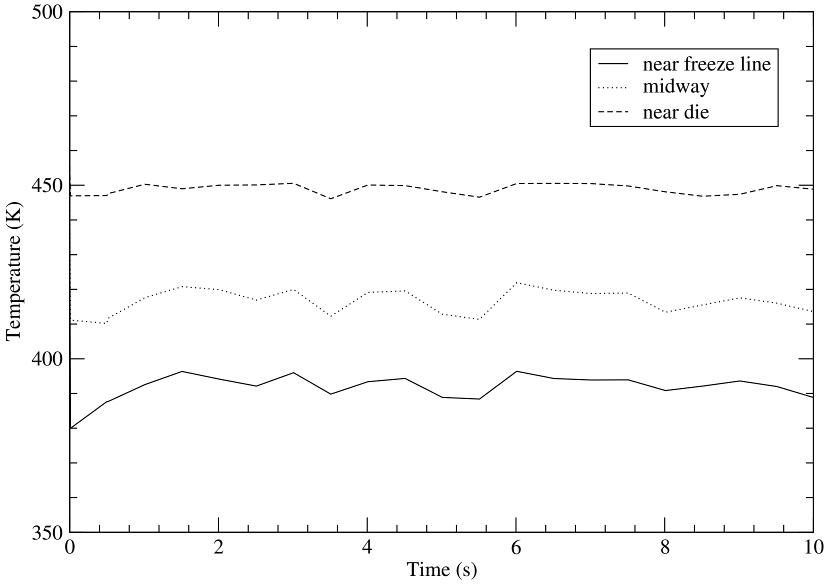

FIG. 53. Radius instability due to high die exit velocity and higher heat transfer rates – plot shows temperature of the bubble at three different locations.

F. Summary

Results presented in this section highlight the value of transient analysis. One of the key parameter that largely causes instability or the lack of it is the rate of heat transfer. This is due to the fact that melt strength is a strong function of temperature and change in the melt properties influence the product quality significantly. Another aspect of bubble stability is the right combination of residence time and heat removal rate. Higher cooling should always accompany higher die velocity. Otherwise the bubble will collapse. Since film blowing process is a highly nonlinear process sensitive to many parameters, especially the constitutive model, it is not possible to develop universal correlations on these stability aspects. Hence, the best approach is to use the software developed under specific circumstances and evaluate the process settings and possible variations in the process parameters.

CHAPTER VIII

CONCLUSIONS

A mathematical model to simulate film blowing process as a transient, axisymmetric, nonisothermal, viscoelastic two-point boundary value problem is developed in this dissertation. Based on the research conducted using this model following conclusions are presented:

1. Model developed compares well with the available experimental data. All the analyses presented in Chapter VI are done using the transient model and solution evolved in all those cases to a stable steady state.
2. Effect of process conditions at the nip roller end, such as the line speed, is a critical process parameter and it controls the solution through a nonlinear equation. Hence, this problem has to be modeled as a two point boundary value problem. Modeling it using shooting method will not capture the complex balance of nip roller speed and die exit velocity. Stability of the process is achieved using such a balance.
3. Heat transfer plays a vital role in the process. Controlling the heat transfer rate alone can bring stability to the process. Heat transfer rate from the process and the residence time of the particles should be in balance. Hence, higher line speeds need higher heat transfer rates.
4. Disturbances in the melt velocity as it exits the die is not very critical if it is less than 10% of the mean value. Typically the bubble stabilizes as it moves towards freeze–line.

5. Disturbances in the melt temperature is quite critical to the process. Since the melt data is a strong function of temperature, any fluctuation in this value is critical.

6. For cyclic disturbances, which will often be the case, cycle times become critical if it is less than 0.5 seconds – that is – if the disturbances are rapid.

7. Time step used in the analysis plays a role in the solution accuracy. This is due to the presence of transient terms in the RHS. This particular aspect of the model needs further investigation and improvement.

8. With the constitutive model implemented, a low value for retardation viscosity must be used to compare well with experimental data. It should be just enough to provide stability to the momentum equation. Increasing this value will smoothen the velocity distribution and will also make the solution more robust.

9. Model developed is able to capture radius instability quite easily. One of the possible causes for this instability is higher heat transfer rates in conjunction with higher nip roller velocity.

10. The melt tension instability instead of manifesting as a separate category, it manifest along with the radius instability.

11. Model developed can be extended easily to use other constitutive models and include different solution techniques. Software developed based on this model is also easily extendable and comes with a GUI.

A. Suggestions for Future Work

Following suggestions offer a logical development path to the current work:

1. Since the focus of the current work is transient dynamics of the process, a basic model is used for crystallization kinetics. This model should be replaced with a more comprehensive model. And there are models available in the literature, which are more comprehensive and accurate. They can be implemented in the current framework. In addition, in the current work it is assumed that the newly crystallized material crystallizes with orientation aligned with the local MD and AD. This assumption can also be relaxed and actual orientation can be computed using the evolution equation for orientation tensor.

2. Analysis of heat transfer through thickness of the film will be useful to study the effects of variable internal and external cooling. This technique is employed in commercial scale film blowing process.

3. Model developed can be extended to analyze non-axisymmetric instabilities. In order to do this, Radius, R in the parametrization should be a function of both MD and AD. This explicit dependence of the AD, ϕ will lead to non-zero diagonals and additional non–zero terms in Christoffel symbols. Using a non–axisymmetric analysis, helical instability and other modes of bubble collapse can be studied.

4. Software using the model developed can be used in conjunction with optimization software such as, Altair® HyperStudy® to do both DOE and optimization studies. Such studies can help to control the process parameters automatically. Prelimnary optimization studies using the software developed showed promising

results and the ability to identify stable process parameters. These results are not included in this dissertation as it digress from the main focus.

5. Some of the model parameters may not be constant along MD. Varying these parameters, such as, excess pressure, heat transfer, coefficient, etc. will make the analysis of more complex situations possible.

REFERENCES

Ainsworth, M. and J. T. Oden, *A Posteriori Error Estimation in Finite Element Analysis* (John Wiley & Sons, New York, 2000).

Aris, R., *Vectors, Tensors, and the Basic Equations of Fluid Mechanics* (Dover Publications, New York, 1962).

Avrami, M., "Kinetics of Phase Change. I," Journal of Chemical Physics **7**, 1103–1112 (1939).

Baldoni, F. and K. R. Rajagopal, "A Continuum Theory for the Thermomechanics of Solidification," International Journal of Nonlinear Mechanics **32**, 3–20 (1997).

Baranov, A. V., N. V. Tyabin, V. A. Gersimenkoi and L. G. Raiz, "Mathematical Description of the Rheodynamics and Heat Transfer Associated with the Blown Film Process," Journal of Engineering Physics **54**, 639–645 (1992).

Bowen, R. M., *Introduction to Continuum Mechanics for Engineers* (Plenum Press, New York, 1989).

Brenner, S. C. and L. R. Scott, *The Mathematical Theory of Finite Element Methods* (Springer-Verlag, New York, 1994).

Brooks, A. N. and T. J. R. Hughes, "Streamline Upwind/Petrov-Galerkin Formulations for Convection Dominated Flows with Particular Emphasis on the Incommpressibe Navier-Stokes Equations," Computer Methods in Applied Mechanics and Engineering **32**, 199–259 (1982).

Cain, J. J. and M. M. Denn, "Multiplicities and Instabilities in Film Blowing," Polymer Engineering and Science **28**, 1527–1541 (1988).

Campbell, G. A. and B. Cao, “Modeling the Blown Film Process from Die to Frost Line,” Technical Association of the Pulp and Paper Industry Journal **70**, 41–44 (1987).

Campbell, G. A., N. T. Obot and B. Cao, “Aerodynamics in the Blown Film Process,” Polymer Engineering and Science **32**, 751–759 (1992).

Cao, B. and G. A. Campbell, “Viscoelastic–Elastic Modeling of Tubular Blown Film Processing,” AIChe Journal **360**, 420–430 (1990).

do Carmo, M. P., *Differential Geometry of Curves and Surfaces* (Prentice–Hall, EngleWoods, NJ, 1976).

Doi, M. and S. F. Edwards, *Theory of Polymer Dynamics* (Oxford University Press, Oxford, 1988).

Dunn, J. E. and K. R. Rajagopal, “Fluids of Differential Type: Critical Review and Thermodynamic Analysis,” International Journal of Engineering and Science **33**, 689–729 (1995).

Eder, G., H. Janeschitz-Kriegel and S. Liedauer, “Crystallization Process in Quiescent and Moving Polymer Melts under Heat Transfer Conditions,” Progress in Polymer Science **15**, 629–714 (1990).

Findley, W. N., J. S. Lai and K. Onaran, *Creep and Relaxation in Nonlinear Viscoelastic Materials* (Dover Publications, New York, 1976).

Gupta, R. K., *A New Non-Isothermal Rheological Constitutive Equation and Its Application to Industrial Film Blowing Process*, Ph.D. Dissertation, Department of Chemical Engineering, University of Delaware, Newark (1980).

Han, C. D. and J. Y. Park, “Studies on Blown Film Extrusion II. Analysis of Deformation and Heat Transfer Processes,” Journal of Applied Polymer Science **19**, 3277–3290 (1975).

Hughes, T. J. R. and M. Mallet, “A New Finite Element Formulation for Computational Fluid Dynamics: III The Generalized Streamline Operator for Multidimensional Advective-Diffusive Systems,” CMAME **58**, 305–328 (1986a).

Hughes, T. J. R. and M. Mallet, “A New Finite Element Formulation for Computational Fluid Dynamics: IV The Discontinuity Capturing Operator for Multidimensional Advective-Diffusive Systems,” CMAME **58**, 329–336 (1986b).

Hughes, T. J. R., M. Mallet and A. Mizukami, “A New Finite Element Formulation for Computational Fluid Dynamics: II Beyond SUPG,” CMAME **54**, 341–355 (1986).

Issacson, E. and H. B. Keller, *Analysis of Numerical Methods*, second edition (Dover Publications, New York, 1994).

Jinan, C., “Studies on the Mechanism of Draw Resonance in Melt Spinning,” JAPS **42**, 143–151 (1991).

Kanai, T. and J. L. White, “Dynamics, Heat Transfer and Structure Development in Tubular Extrusion of Polymer Melts: A Mathematical Model and Predictions,” Journal of Polymer Engineering **2**, 135–157 (1985).

Keller, H. B., *Numerical Solution of Two Point Boundary Value Problems* (SIAM, Bristol, U.K., 1976).

Khan, S. A. and R. G. Larson, “Comparison of Simple Constitutive Equations for Polymer Melts in Shear and Biaxial and Uniaxial Extensions,” Journal of Rheology **31**, 207–234 (1987).

Kulkarni, J. A. and A. N. Beris, “A Model for the Necking Phenomenon in High-Speed Fiber Spinning Based on Flow-Induced Crystallization,” Journal of Rheology **42**, 4–24 (1998).

Kurtz, S. J., “Some Key Challenges in Polymer Processing Technology,” in *Proceedings of the 1992 Winter Annual Meeting of ASME: Recent Advances in Non-Newtonian Flows*, edited by D. A. Siginer (American Society of Mechanical Engineers, New York, 1992), pp. 1–13.

Lambrigger, M., “Non-isothermal Polymer Crystallization Kinetics and Avrami Master Curves,” Polymer Engineering and Science **38**, 610–615 (1998).

Larson, R. G., “Instabilities in Viscoelastic Flows,” Rheologica Acta **31**, 213–263 (1992).

Marsden, J. E. and T. J. R. Hughes, *Mathematical Foundations of Elasticity* (Dover Publications, New York, 1994).

Mayavaram, R. S. and J. N. Reddy, “Numerical Simulation of Film Blowing Process: A Critique of Shooting Method,” Unpublished Technical Report, Computational Mechanics Laboratory, Department of Mechanical Engineering, Texas A&M University, College Station, Texas 77843 (1996).

Minoshima, W. and J. L. White, “Instability Phenomena in Tubular Film, and Melt Spinning of Rheologically Characterized High Density, Low Density and Linear Low Density Polyethylenes,” Journal of Non-Newtonian Fluid Mechanics **19**, 275–302 (1986).

Oden, J. T. and J. N. Reddy, *Variational Methods in Theoretical Mechanics*, second edition (Springer-Verlag, Berlin, Germany, 1983).

Pearson, J. R. A. and C. J. S. Petrie, “The Flow of a Tubular-Film Interpretation of the Model and Disccussion of the Solutions,” Journal of Fluid Mechanics **42**, 1–19 (1970a).

Pearson, J. R. A. and C. J. S. Petrie, “The Flow of Tubular Film: Part 1 Formal Mathematical Representation,” Journal of Fluid Mechanics **40**, 1–19 (1970b).

Peters, G. W. M. and F. P. T. Baajens, “Modelling of Non-Isothermal Viscoelastic Flows,” Journal of Non-Newtonian Fluid Mechanics **68**, 205–224 (1997).

Petrie, C. J. S., “Comparison of Theoretical Predictions with Published Experimental Measurements on the Blown Film Process,” AIChE Journal **21**, 275–xxx (1975).

Petrie, C. J. S., *Elongational Flows* (Pitman Publishing Limited, London, 1979).

Rao, A., *Study of Molecular Orientation and Phase Transition in Polymers During the Film Blowing Process*, Ph.D. Dissertation, Department of Mechanical Engineering, Texas A&M University, College Station (1998).

Rao, J., *Modeling of Crystallization in Polymers*, Ph.D. Dissertation, Department of Mechanical Engineering, Texas A&M University, College Station (1999).

Reddy, J. N., *An Introduction to the Finite Element Method*, second edition (McGraw Hill, New York, 1993).

Reddy, J. N. and D. K. Gartling, *Finite Element Method in Heat Transfer and Fluid Dynamics* (CRC Press, Boca Raton, FL., 1994).

Simpson, D. M. and I. R. Harrison, “The Use of Deformation Rates in the Scale-Up of Polyethylene Film,” in *Proceedings of 49th Annual Technical Conference of the Society of Plastics Engineers* (The Society of Plastics Engineers, Brookfield, CT, 1991), pp. 203–205.

Veque, R. J. L., *Numerical Methods for Conservation Laws* (Brikhauser Verlag, Berlin, Germany, 1992).

Yeow, Y. L., “Stability of Tubular Film Flow: A Model of the Film-Blowing Process,” Journal of Fluid Mechanics **75**, 577–591 (1976).

APPENDIX A
GEOMETRY CALCULATIONS

Calculation of the metric tensor, radii of curvature, Christoffel symbols, and the rate of deformation tensor are presented in this appendix. The details of these calculations and the conditions in which they are applicable can be found in do Carmo (1976). The axisymmetric assumption leads to orthogonal parametrization. Hence, the metric tensor is diagonal and the Christoffel symbols are greatly simplified. These calculations can be used to arrive the model equations from the general setting in curvilinear coordinates by imposing the restrictions pertaining to the bubble surface under consideration.

The mathematical formalism used for these calculations are described in the following paragraph.

Cartesian Framework

The coordinates and the basis vectors are denoted by (x_1, x_2, x_3) and $(\mathbf{i}_1, \mathbf{i}_2, \mathbf{i}_3)$. In this space, the basis and its reciprocal are identical. When there is no ambiguity, the conventional notation (x,y,z) for the coordinates and $(\mathbf{i}, \mathbf{j}, \mathbf{k})$ for the unit vectors will be used.

Surface Coordinates

The curvilinear coordinates on the bubble are indicated by (ξ_1, ξ_2, ξ_3), these are associated with the contravariant vectors defined on the surface $(\mathbf{u}_1, \mathbf{u}_1, \mathbf{u}_3)$. The coordinate ξ_2 is identical to the azimuthal angle ϕ and co-ordinate ξ_3 is identical to the thickness parameter h. The parametrization associated with the surface is denoted $(\beta^1, \beta^2, \beta^3)$

and where there is no ambiguity, (z, ϕ, h) is used. Similarly the covariant vectors will be denoted as $(\mathbf{u}_z, \mathbf{u}_\phi, \mathbf{u}_h)$ wherever it improves readability.

First Fundamental Form and Metric

Let $\mathbf{X}$ be a vector valued function defining the position vector of points on the polymer film. This function depends on the axial coordinate z, the azimuthal coordinate ϕ and the normal coordinate h.

$$\mathbf{X}(z, \phi, h) = (R\cos\phi + Hh\cos\theta cos\phi)\mathbf{i} + (R\sin\phi + Hh\cos\theta\sin\phi)\mathbf{j} + (z - Hhsin\theta)\mathbf{k} \tag{65}$$

In the above equation, R denotes the radius of the bubble and H denotes the thickness of the bubble. The axial coordinate z is measured from die exit and the thickness coordinate h is measured from the outer surface of the bubble to inner surface. Even though we are interested in the equations restricted to the bubble surface, the parametrization is written for the three-dimensional bubble in order to capture all the terms. This will become evident as we proceed further with the calculations.

From this definition all the other details can be derived using the standard tools of differential geometry. The radius R and the thickness H do not depend on ϕ due to axisymmetry. The Partial derivatives of $\mathbf{X}$ with respect to the parameters give the basis vectors. Of these, the vectors $\mathbf{u}_z$ and $\mathbf{u}_\phi$ span the tangent plane at this point. These vectors are covariant vectors and they transform like a function. The surface coordinates are denoted by ξ_1 and ξ_2. The coordinate ξ_1 runs along the machine direction and ξ_2 coincides with the azimuthal coordinate.

$$\begin{aligned}\mathbf{u}_z = \frac{\partial \mathbf{X}}{\partial z} &= \left(\frac{\partial R}{\partial z}\cos\phi + \frac{\partial H}{\partial z}h\cos\theta cos\phi - Hh\sin\theta\cos\phi\frac{\partial\theta}{\partial z}\right)\mathbf{i} \\ &+ \left(\frac{\partial R}{\partial z}\sin\phi + \frac{\partial H}{\partial z}h\cos\theta\sin\phi - Hh\sin\theta\sin\phi\frac{\partial\theta}{\partial z}\right)\mathbf{j} \\ &+ \left(1 - h\frac{\partial H}{\partial z}\sin\theta - hH\cos\theta\right)\mathbf{k}\end{aligned}$$

This equations simplified to the following form when the thin membrane approximation is invoked.

$$\mathbf{u}_z = \frac{\partial R}{\partial z}\cos\phi\,\mathbf{i} + \frac{\partial R}{\partial z}\sin\phi\,\mathbf{j} + \mathbf{k}$$

The complete details of the derivation with terms involving h will not be presented here. However, the computations retain these terms and only in the end the restriction $h = 0$ is imposed.

$$\mathbf{u}_\phi = \frac{\partial \mathbf{X}}{\partial \phi} = -R\sin\phi\,\mathbf{i} + R\cos\phi\,\mathbf{j}$$

$$\mathbf{u}_h = \frac{\partial \mathbf{X}}{\partial h} = H\cos\theta\,\cos\phi\,\mathbf{i} + H\cos\theta\,\sin\phi\,\mathbf{j} - H\sin\theta\,\mathbf{k}$$

The vectors ($\mathbf{u}_z$, $\mathbf{u}_\phi$, $\mathbf{u}_h$) are contravariant and it can be proved easily from the definition. Any vector on the tangent plane can be represented as a combination of $\mathbf{u}_z$ and $\mathbf{u}_\phi$ and the inner product of these vectors form the components of the metric tensor which is used in measuring the distances on the surface. Let P be a point of the surface, from the first fundamental form, the inner product $< . >_p$ on the tangent plane T_p is defined. For the sake of simplicity, suffix p is omitted.

$$g_{11} = E =< \mathbf{u}_z, \mathbf{u}_z >= (1 + \frac{\partial R}{\partial z}^2)$$

$$g_{12} = g_{21} = F =< \mathbf{u}_z, \mathbf{u}_\phi >= 0$$

$$g_{22} = G =< \mathbf{u}_\phi, \mathbf{u}_\phi >= (R)^2$$

It can also be shown that $g_{33} = H^2$ and $g_{13} = g_{23} = 0$.

$$\mathbf{g} = g_{ij}\mathbf{u}^i \otimes \mathbf{u}^j \tag{66}$$

The metric tensor is time dependent as the bubble radius R and the thickness H are functions of time. We assume that the changes with respect to time are smooth and regular. This assumption is in agreement with the experimental observation of the process.

Second Fundamental Form and Radii of Curvature

The principal radii of curvature, the mean and Gauss curvature, and other interesting details like the type of the bubble surface can be calculated from the second fundamental form. The bubble surface under consideration has all the nice properties like orientability, smoothness, etc. At a point P on the surface of the film, a tangent plane with a basis $\mathbf{u}_z$ and $\mathbf{u}_\phi$ was defined.

The rate of change of tangent in the case of a curve embedded in a $\mathbb{R}^3$ will give the curvature. This information in the case of a surface can be computed from the rate of change of the normal to the tangent plane. The second fundamental form and the related theorems provide the machinery to do these calculations. Details of the these theorems is be found in the reference cited in the prelude of this appendix. The principal radii of curvature can be calculated as follows.

$$
\begin{aligned}
\frac{\partial \mathbf{u}_z}{\partial z} &= \mathbf{X}_{zz} = \frac{\partial^2 R}{\partial z^2}\cos\phi\,\mathbf{i} + \frac{\partial^2 R}{\partial z^2}\sin\phi\,\mathbf{j} \\
\frac{\partial \mathbf{u}_z}{\partial \phi} &= \mathbf{X}_{z\phi} = \mathbf{X}_{\phi z} = -\frac{\partial R}{\partial z}\sin\phi\,\mathbf{i} + \frac{\partial R}{\partial z}\cos\phi\,\mathbf{j} \\
\frac{\partial \mathbf{u}_z}{\partial h} &= \mathbf{X}_{z\phi} = \left(\frac{\partial H}{\partial z}\cos\theta\,\cos\phi - H\sin\theta\,\cos\phi\frac{\partial theta}{\partial z}\right)\,\mathbf{i} \\
&+ \left(\frac{\partial H}{\partial z}\cos\theta\,\sin\phi - H\sin\theta\,\sin\phi\frac{\partial theta}{\partial z}\right)\,\mathbf{j} \\
&+ \left(\frac{\partial H}{\partial z}\sin\theta\, - H\cos\theta\,\frac{\partial theta}{\partial z}\right)\,\mathbf{k} \\
\frac{\partial \mathbf{u}_\phi}{\partial \phi} &= \mathbf{X}_{\phi\phi} = -R\cos\phi\,\mathbf{i} - R\sin\phi\,\mathbf{j} \\
\frac{\partial \mathbf{u}_\phi}{\partial h} &= \mathbf{X}_{\phi h} = \mathbf{X}_{h\phi} = -H\cos\theta\,\sin\phi\,\mathbf{i} + H\cos\theta\,\cos\phi\,\mathbf{j} \\
\frac{\partial \mathbf{u}_h}{\partial h} &= \mathbf{X}_{hh} = 0
\end{aligned}
$$

From the above second derivatives and the normal, using the second fundamental form, one can compute the radii of curvature.

$$
\begin{aligned}
e =< \mathbf{N}, \mathbf{X}_{zz} > &= \frac{\frac{\partial^2 R}{\partial z^2}}{\sqrt{1 + \frac{\partial R}{\partial z}^2}} \\
f =< \mathbf{N}, \mathbf{X}_{z\phi} > &= 0 \\
g =< \mathbf{N}, \mathbf{X}_{\phi\phi} > &= \frac{R}{\sqrt{1 + \frac{\partial R}{\partial z}^2}}
\end{aligned}
$$

In the above equations, $\mathbf{N}$ is the normalized $\mathbf{u}_h$. Since the parametrization is orthogonal, f is zero. From the values of the e, f, g, and E, F, G we can compute the radii of curvature. It is important to observe here that the curvature information is buried in the rate of change, $d\mathbf{N}$ and it is extracted via e,f, and g (note that $\mathbf{N}_z, \mathbf{X}_z >=< \mathbf{N}, \mathbf{X}_{zz} >$, likewise for the other two derivatives). The Gaussian curvature K and the mean curvature H are given by the following equations. These relationships can be arrived at from the direct computation of the matrix representation of $d\mathbf{N}$ in the natural basis of the tangent plane,$\{\mathbf{u}_z$ and $\mathbf{u}_\phi\}$.

$$\text{Gaussian Curvature, } C_g = \frac{eg - f^2}{EG - F^2} = -\frac{\frac{\partial^2 R}{\partial z^2}}{(1 + \frac{\partial R}{\partial z})^2 R}$$

$$\text{Mean Curvature, } C_m = \frac{1}{2}\frac{eG + Ge + Ff}{EG - F^2} = \frac{1}{2}\left[\frac{1}{R\sqrt{1 + \frac{\partial R}{\partial z}^2}} - \frac{\frac{\partial^2 R}{\partial z^2}}{(1 + \frac{\partial R}{\partial z}^2)^{\frac{3}{2}})}\right]$$

From the Gaussian and the mean curvatures, the principal curvatures can be obtained by solving the characteristic equation. The roots of the characteristic equation can be guessed in this case from the expressions of C_g and C_m.

$$k_1 = -\frac{\frac{\partial^2 R}{\partial z^2}}{(1 + \frac{\partial R}{\partial z}^2)^{\frac{3}{2}})} \tag{67}$$

$$k_2 = \frac{1}{R\sqrt{1 + \frac{\partial R}{\partial z}^2}} \tag{68}$$

And the radii of curvature are the reciprocal of the curvatures given by the above expressions.

$$\mathcal{R}_1 = -\frac{(1 + \frac{\partial R}{\partial z}^2)^{\frac{3}{2}})}{\frac{\partial^2 R}{\partial z^2}} \tag{69}$$

$$\mathcal{R}_2 = R\sqrt{1 + \frac{\partial R}{\partial z}^2} \tag{70}$$

The bubble surface curves in two principal directions, first along the machine direction and it is in the direction of $\mathbf{X}_z$ and other along the azimuthal direction (along X_ϕ). The curvatures along these directions are k_1 and k_2 respectively. Sign of the Gaussian curvature indicates the nature of the surface. In this case it depends on the sign of the second derivative of the radius R. Beyond the freeze-line R can be assumed constant, even if it varies slightly (increasing) it is linear. Hence, the surface is parabolic beyond the freeze line. Above the die and below the freeze-line, the behavior of the surface is complex. Radius of the bubble increases continuously from the die to the freeze-line when the process is successful, however, this does not help in determining the sign of the second derivative of the radius. In a typical case, points on the surface along the machine direction changes in the followng sequence: parabolic, elliptic, parabolic, hyperbolic and then finally to parabolic.

Christoffel Symbols

The basis vectors $\mathbf{u}_z$ and $\mathbf{u}_\phi$ are not constants. Hence, unlike the cartesian framework, computing the derivatives involve differentiating the basis vectors themselves. For instance, consider the vector $\mathbf{a}$:

$$\mathbf{a} = a^i \mathbf{u}_i$$

$$\frac{\partial \mathbf{a}}{\partial \beta^j} = \frac{\partial a^i}{\partial \beta^j} \mathbf{u}_i + a^i \frac{\partial \mathbf{u}_i}{\partial \beta^j}$$

and,

$$\frac{\partial \mathbf{u}_i}{\partial \beta^j} = \Gamma^k_{ij} \mathbf{u}_k$$

hence,

$$\frac{\partial \mathbf{a}}{\partial \beta^j} = \frac{\partial a^i}{\partial \beta^j} \mathbf{u}_i + a^i \Gamma^k_{ij} \mathbf{u}_k$$

The coefficients Γ^k_{ij} are called the Christoffel symbols. The notation used here follows Aris (1962), even though it is compact, it is not as elegant as the one used by do Carmo (1976). For the given surface these coefficients can be computed easily. The axisyymetry assumption, which leads to the orthogonal parametrization, reduces the number of non-zero Christoffel symbols. It should be noted that the Christoffel sybols, even though written like a tensor, is not a tensor. The following equation is used to compute the Christoffel symbols.

$$\Gamma^i_{jk} = \frac{1}{2} g^{ip} \left(\frac{\partial g_{pj}}{\partial \beta^k} + \frac{\partial g_{pk}}{\partial \beta^j} - \frac{\partial g_{jk}}{\partial \beta^p} \right) \tag{71}$$

The summation convention is used in the above equation. Due to the orthogonality of the parametrization, $g_{ij} = 0$ if $i \neq j$. This simplifies the computations to a great extent. Another important point that should be borne in mind is the simplification $h = 0$ should be invoked only after computing the derivative of g_{ij}. This calculation can be made simple in the following way.

$$\frac{\partial g_{jk}}{\partial \beta^p} = \frac{\partial}{\partial \beta^p} (< \mathbf{u}_j, \mathbf{u}_k >) =< \frac{\partial \mathbf{u}_j}{\partial \beta^p}, Bu_k > + < \mathbf{u}_j, \frac{\partial \mathbf{u}_k}{\partial \beta^p} >$$

and for instance,

$$\frac{\partial g_{11}}{\partial h} = 2 < \mathbf{u}_1, \frac{\partial \mathbf{u}_1}{\partial h} >$$

and in this case we can simplify it by restricting both $\mathbf{u}_1$ and its derivative $\frac{\partial \mathbf{u}_1}{\partial h}$ to the surface at $h = 0$. If the derivative of $\mathbf{u}_1$ with respect to h is computed after restricting to the surface imposing $h = 0$, then the derivative will vanish. Hence is it is important to carry out the calculations in full three-dimensional form till the last step. The following set of equations give the Christoffel symbols for the axisymmetric bubble surface.

$$
\begin{aligned}
\Gamma^1_{11} &= \frac{\frac{\partial^2 R}{\partial z^2}\frac{\partial R}{\partial z}}{1+\frac{\partial R}{\partial z}^2} = \tan\theta\frac{\partial\theta}{\partial z} \qquad (72)\\
\Gamma^2_{11} &= 0 \qquad (73)\\
\Gamma^3_{11} &= -\frac{1}{H}\frac{\frac{\partial^2 R}{\partial z^2}}{\sqrt{1+\frac{\partial R}{\partial z}^2}} = -\frac{1}{H}\sec\theta\frac{\partial\theta}{\partial z} \qquad (74)\\
\Gamma^1_{12} &= 0 \qquad (75)\\
\Gamma^2_{12} &= \frac{\partial R}{\partial z}\frac{1}{R} = \frac{\tan\theta}{R} \qquad (76)\\
\Gamma^3_{12} &= 0 \qquad (77)\\
\Gamma^1_{13} &= H\cos\theta\frac{\partial\theta}{\partial z} \qquad (78)\\
\Gamma^2_{13} &= 0 \qquad (79)\\
\Gamma^3_{13} &= \frac{1}{H}\frac{\partial H}{\partial z} \qquad (80)
\end{aligned}
$$

$$
\begin{aligned}
\Gamma^1_{21} &= \Gamma^1_{12} = 0 \qquad (81)\\
\Gamma^2_{21} &= \Gamma^2_{12} = \frac{\tan\theta}{R} \qquad (82)\\
\Gamma^3_{21} &= \Gamma^3_{12} = 0 \qquad (83)\\
\Gamma^1_{22} &= \frac{-R\frac{\partial R}{\partial z}}{1+\frac{\partial R}{\partial z}^2} = \frac{-R\tan\theta}{\sec^2\theta} \qquad (84)\\
\Gamma^2_{22} &= 0 \qquad (85)\\
\Gamma^3_{22} &= \frac{R}{H}\cos\theta \qquad (86)\\
\Gamma^1_{23} &= 0 \qquad (87)\\
\Gamma^2_{23} &= -\frac{H}{R}\cos\theta \qquad (88)\\
\Gamma^3_{23} &= 0 \qquad (89)
\end{aligned}
$$

$$\begin{aligned}
\Gamma^1_{31} &= \Gamma^1_{13} = H\cos\theta\frac{\partial\theta}{\partial z} && (90)\\
\Gamma^2_{31} &= \Gamma^2_{13} = 0 && (91)\\
\Gamma^3_{31} &= \Gamma^3_{13} = \frac{1}{H}\frac{\partial H}{\partial z} && (92)\\
\Gamma^1_{32} &= \Gamma^1_{23} = 0 && (93)\\
\Gamma^2_{32} &= \Gamma^2_{23} = -\frac{H}{R}\cos\theta && (94)\\
\Gamma^3_{32} &= \Gamma^3_{23} = 0 && (95)\\
\Gamma^1_{33} &= -\frac{H}{\sec^2\theta}\frac{\partial H}{\partial z} && (96)\\
\Gamma^2_{33} &= 0 && (97)\\
\Gamma^3_{33} &= 0 && (98)
\end{aligned}$$

Using the above equations, the covariant derivative on the bubble surface can be computed. It should noted that of the 27 components, there are only 13 non-zero terms. The reasons for this simplification are , the problem under consideration is on a surface instead of a generic curvilinear setting, and the orthogonal parametrization.

APPENDIX B

SUMMARY OF THE MODEL

Important equations in the transient axisymmetric model developed in this work are summarized in this appendix. These equations are presented along with the relevant boundary conditions in physical coordinates. The equations presented are:

1. Rate of deformation tensor ($\mathbf{D}$)
2. Conservation of mass (to compute H)
3. Conservation of momentum in machine direction (to compute V)
4. Conservation of momentum in transverse direction (to compute P)
5. Conservation of momentum in normal direction (to compute R)
6. Constitutive model (to compute $\boldsymbol{\tau}$)
7. Conservation of energy (to compute T)
8. Crystallinity Model (to compute χ)

Directions

1. Principal direction 1: Machine direction z or β^1.
2. Principal direction 2: Transverse direction ϕ or β^2
3. Principal direction 3: Normal direction h

Rate of Deformation Tensor

$$D_{\underline{11}} = \frac{1}{\sec\theta}\frac{\partial \sec\theta}{\partial t} + cos\theta\frac{\partial V_{\underline{1}}}{\partial z} \tag{99}$$

$$D_{\underline{22}} = \frac{1}{R}\frac{\partial R}{\partial t} + \frac{V_{\underline{1}}\cos\theta}{R}\frac{\partial R}{\partial z} \tag{100}$$

$$D_{\underline{33}} = \frac{1}{H}\frac{\partial H}{\partial t} + \frac{V_{\underline{1}}\cos\theta}{H}\frac{\partial H}{\partial z} \tag{101}$$

Radii of Curvature

$$\mathcal{R}_1 = -\frac{\sec^3\theta}{\partial\theta/\partial z} \tag{102}$$

$$\mathcal{R}_2 = R\sec\theta \tag{103}$$

Equation for H – Conservation of mass

$$\frac{1}{\sec\theta}\frac{\partial \sec\theta}{\partial t} + \frac{1}{R}\frac{\partial R}{\partial t} + \frac{1}{H}\frac{\partial H}{\partial t} + \cos\theta\frac{\partial V_{\underline{1}}}{\partial z} + \frac{V_{\underline{1}}\cos\theta}{R}\frac{\partial R}{\partial z} + \frac{V_{\underline{1}}\cos\theta}{H}\frac{\partial H}{\partial z} = 0 \tag{104}$$

Conservation of Momentum in MD

$$\rho\left[\frac{\partial V_{\underline{1}}}{\partial t} + V_{\underline{1}}\cos\theta\frac{\partial V_{\underline{1}}}{\partial z}\right] = -\rho g cos\theta + \frac{1}{RH}\frac{\partial}{\partial z}\left(RH\cos\theta\sigma_{\underline{11}}\right) + \sin\theta\frac{\partial\theta}{\partial z}\sigma_{\underline{11}} \tag{105}$$

Equation for P – Conservation of Momentum in CD

$$P = \tau_{\underline{22}} + P_{drag} \tag{106}$$

Equation for R – Conservation of Momentum in ND

$$\frac{\Delta P_{excess}}{H} + \rho\frac{V_{\underline{1}}^2}{\mathcal{R}_1} = -\rho g sin\theta + \frac{\sigma_{\underline{\underline{11}}}}{\mathcal{R}_1} + \frac{\sigma_{\underline{\underline{22}}}}{\mathcal{R}_2} \tag{107}$$

Conservation of Energy

$$\rho C_p\frac{\partial T}{\partial t} + \rho C_p V_{\underline{1}}\cos\theta\frac{\partial T}{\partial z} + \frac{h_c}{H}(T - T_c) + \frac{C_{SB}\epsilon}{H}(T^4 - T_w^4) = \frac{\cos\theta}{RH}\frac{\partial}{\partial z}\left(kRH\frac{\partial T}{\partial z}\right) \tag{108}$$

Crystallization Kinetics

$$\frac{\partial\chi}{\partial t} + \rho C_p V_{\underline{1}}\cos\theta\frac{\partial\chi}{\partial z} = nK(T)(1-\chi)\left(-log_e(1-\chi)\right)^{\frac{n-1}{n}}\exp(c_\chi II_D) \tag{109}$$

Phan–Thien–Tanner Model

$$\frac{\partial\tau_{\underline{\underline{11}}}}{\partial t} \quad + \quad V_{\underline{1}}\cos\theta\frac{\partial\tau_{\underline{\underline{11}}}}{\partial z} \quad + \quad 2\mathcal{L}_{\underline{\underline{11}}}\tau_{\underline{\underline{11}}} \quad - \quad 2\tau_{\underline{\underline{11}}}\cos\theta\sin\theta\frac{\partial\theta}{\partial t} \quad + \quad \frac{Y}{\lambda}\tau_{\underline{\underline{11}}} \quad = \quad 2GD_{\underline{\underline{11}}} \tag{110}$$

$$\frac{\partial\tau_{\underline{\underline{22}}}}{\partial t} \quad + \quad V_{\underline{1}}\cos\theta\frac{\partial\tau_{\underline{\underline{22}}}}{\partial z} \quad + \quad 2\mathcal{L}_{\underline{\underline{22}}}\tau_{\underline{\underline{22}}} \quad - \quad 2\frac{\tau_{\underline{\underline{22}}}}{R}\frac{\partial R}{\partial t} \quad + \quad \frac{Y}{\lambda}\tau_{\underline{\underline{22}}} \quad = \quad 2GD_{\underline{\underline{22}}} \tag{111}$$

$$\frac{\partial\tau_{\underline{\underline{33}}}}{\partial t} \quad + \quad V_{\underline{1}}\cos\theta\frac{\partial\tau_{\underline{\underline{33}}}}{\partial z} \quad + \quad 2\mathcal{L}_{\underline{\underline{33}}}\tau_{\underline{\underline{33}}} \quad - \quad 2\frac{\tau_{\underline{\underline{33}}}}{H}\frac{\partial H}{\partial t} \quad + \quad \frac{Y}{\lambda}\tau_{\underline{\underline{33}}} \quad = \quad 2GD_{\underline{\underline{33}}} \tag{112}$$

Kelvin-Voight Model

$$\tau_{\underline{\underline{11}}} = E_{11}\varepsilon_{\underline{\underline{11}}} + \eta_e D_{\underline{\underline{11}}} \tag{113}$$

$$\tau_{\underline{\underline{22}}} = E_{22}\varepsilon_{\underline{\underline{22}}} + \eta_e D_{\underline{\underline{22}}} \tag{114}$$

$$\tau_{\underline{\underline{33}}} = E_{33}\varepsilon_{\underline{\underline{33}}} + \eta_e D_{\underline{\underline{33}}} \tag{115}$$

APPENDIX C
A CRITIQUE OF SHOOTING METHOD

Introduction

Numerical simulation of film blowing process using the shooting method is inadequate to capture the essential dynamics of proces. This appendix discusses the drawback that plagues this approach. The analysis presented in this appendix is based on the recent works using shooting method for simulating film blowing process (Cao and Campbell, 1990). The main drawback of shooting method is its inability to include the effect of the boundary conditions from the nip roller side. Hence, it is not possible to specify the nip roller velocity, which is the most important process condition as it directly affects the productivity. The Plastic–Elastic–Transition (PET) model developed by Cao and Campbell (1990) is used to describe the constitutive behavior. Even though the idea behind this approach is physically reasonable, the model in its present form is far from satisfactory as the assumptions beyond the PET line force the solution to behave in the desired manner.

Modeling Assumptions

1. Bubble is axisymmetric. The analysis domain begins just after the extrudate swell and stops just before the guide rolls. At the guide rolls geometry changes from axisymmetric to plane symmetry, hence modeling cannot be carried out till the nip rolls with the present model.

2. Field constitutive equations are averaged over the thickness leading to a thin membrane approximation. This assumption is based on the observation that

the thickness is much smaller than the bubble radius and both the radii of curvature.

3. Inertia effects are ignored. In a typical process it can be shown that Reynolds number is very small.
4. Process is assumed to be steady.
5. Polymer considered in the analysis is amorphous.
6. Deborah number is of the order of one, hence, the polymer melt is treated as a viscoelastic material. Constitutive model developed by Cao and Campbell (1990) is used.
7. Fourier number is very small, hence the temperature variation across the thickness are neglected.
8. The effects of surface tension and gravity are neglected in the present model.

Kinematics

Velocity gradients are calculated using local coordinates shown in Figure 54. Detailed description of the calculations can be found in Pearson and Petrie (1970a & 1970b). The local cartesian coordinates (ξ_1, ξ_2, ξ_3) are defined such that origin is in the inner surface of the film and at the die exit. Let (v_1, v_2, v_3) be the components of velocity in this coordinate system. At $\xi_2 = 0$, velocity $v_2 = 0$ and at $\xi_2 = h$, $v_2 = dh/dt$ and it represents the thinning down of the film. The velocity gradients are given by

$$\frac{\partial v_2}{\partial \xi_2} = \frac{\frac{dh}{dt} - 0}{h - 0} = \frac{1}{h}\frac{dh}{dt}$$

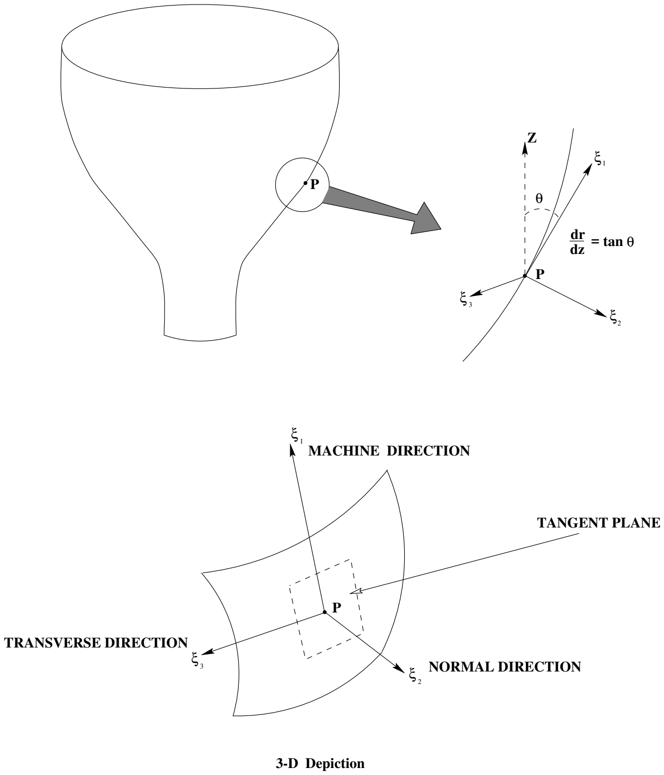

FIG. 54. Coordinate system used in the analysis.

$$\frac{\partial v_3}{\partial \xi_3} = \frac{2\pi \frac{dr}{dt}}{2\pi r} = \frac{1}{r}\frac{dr}{dt}$$

and using the continuity equation

$$\frac{\partial v_1}{\partial \xi_1} + \frac{\partial v_2}{\partial \xi_2} + \frac{\partial v_3}{\partial \xi_3} = 0$$

the third velocity gradient can be obtained

$$\frac{\partial v_1}{\partial \xi_1} = -[\frac{1}{r}\frac{dr}{dt} + \frac{1}{h}\frac{dh}{dt}]$$

These relationships can be further simplified as

$$\frac{dh}{dt} = \frac{\partial h}{\partial t} + \frac{\partial h}{\partial \xi_1}\frac{\partial \xi_1}{\partial t} + \frac{\partial h}{\partial \xi_2}\frac{\partial \xi_2}{\partial t} + \frac{\partial h}{\partial \xi_3}\frac{\partial \xi_3}{\partial t} = \frac{dh}{dz}\frac{dz}{d\xi_1}\frac{d\xi_1}{dt} = v_1 \cos\theta \frac{dh}{dz},$$

$$\frac{\partial v_2}{\partial \xi_2} = \frac{v_1 \cos\theta}{h}\frac{dh}{dz}$$

Similarly,

$$\frac{\partial v_3}{\partial \xi_3} = \frac{v_1 \cos\theta}{r}\frac{dr}{dz},$$

$$\frac{\partial v_1}{\partial \xi_1} = \frac{v_1 \cos\theta}{v_1}\frac{dv_1}{dz}$$

Hence, the rate of deformation tensor **D** can be written as

$$\mathbf{D} = v_1 \cos\theta \begin{bmatrix} \frac{1}{v_1}\frac{dv_1}{dz} & 0 & 0 \\ 0 & \frac{1}{h}\frac{dh}{dz} & 0 \\ 0 & 0 & \frac{1}{r}\frac{dr}{dz} \end{bmatrix} \tag{116}$$

Force Balance

Since inertia terms and the transient terms in the momentum equations are neglected, they reduce to simple force balance equations. Balance of the axial forces between a section at z and the freeze line height, z_f (or above) will give

$$2\pi r h \sigma_{11} \cos\theta - \pi r^2 \Delta p = F_z - \pi r_f^2 \Delta p.$$

Differentiating the above equation with respect to z will result in

$$\frac{d\sigma_{11}}{dz} = -\sigma_{11}\frac{1}{r}\frac{dr}{dz} - \sigma_{11}\frac{1}{h}\frac{dh}{dz} - \sigma_{11}\frac{dr}{dz}\frac{d\theta}{dz} - \frac{\Delta p}{h\cos\theta}\frac{dr}{dz}.$$

The normal force balance can be written as

$$\frac{h\sigma_{11}}{R_1} + \frac{h\sigma_{33}}{R_2} = \Delta p$$

and substituting for the radii of curvature, R_1 and R_2 (see appendix B) we get

$$-h\sigma_{11}\frac{d\theta}{dz} + \frac{\sigma_{33}h}{r} = \Delta p \sec\theta.$$

Rearranging the above equation, an expression to compute the angle θ can be obtained as

$$\frac{d\theta}{dz} = \frac{\sigma_{33}}{r\sigma_{11}} - \frac{\Delta p \sec\theta}{h\sigma_{11}} \tag{117}$$

This equation can be used to eliminate the excess pressure, Δp from the axial force balance equation, and we obtain

$$\frac{d\sigma_{11}}{dz} = \frac{-\sigma_{11}}{h}\frac{dh}{dz} + \frac{\sigma_{33} - \sigma_{11}}{r}\frac{dr}{dz}$$

It can be further rearranged to obtain an equation for the thickness h

$$\frac{dh}{dz} = \frac{h}{\sigma_{11}}\frac{d\sigma_{11}}{dz} - \frac{h(\sigma_{33} - \sigma_{11})}{r\sigma_{11}}\frac{dr}{dz} \tag{118}$$

Constitutive Model

Constitutive model developed by Cao and Campbell (1990) is used in here. This model describes the transition from liquid–like behavior to solid–like behavior based on a rheological constraint rather than the kinematic constraint $dr/dz = 0$. The transition is identified as Plastic–Elastic Transition (PET) and this need not coincide with the freeze line which is based on a kinematic constraint. This model incorporates strain hardening behavior and describes the rheology of the liquid zone through a modified contravariant Maxwell model and the solid zone through a modified Hookean model.

The effect of strain hardening is incorporated into the model through the alignment strength, ψ. Cao and Campbell present a modified definition of alignment strength taking into account of the fact that alignment is strong in uniaxial elongational flows, weak in biaxial elongational flows, and neutral in planar and shear flows. It is given by

$$\psi = |I_1 - I_2|\frac{I_1}{I_2}$$

where I_1 and I_2 are the first and second invariants of the finger tensor C^{-1} and defined by

$$I_1 = \text{Trace of } \mathbf{C}^{-1}(t, t')$$

$$I_2 = \text{Trace of } \mathbf{C}(t, t')$$

A structure memory function ζ is defined to quantify the effects of alignment strength and elongation rate on yield strength, modulus, and viscosity:

$$\zeta = C_h \int_{-\infty}^{t} \sqrt{\Pi_D}\psi \exp\left[-(t-t')/\lambda_{eff}\right] dt'$$

where Π_D is the second invariant of $\mathbf{D}$. Effective modulus, viscosity, relaxation and yield stress are defined by following equations.

$$G_{eff} = G(1+\zeta)$$

$$\lambda_{eff} = \eta_{eff}/G_{eff}$$

$$\eta_{eff} = \frac{\eta}{1 - \frac{Y_{eff}/\sqrt{3}}{\sqrt{\Pi_\tau}}}$$

$$Y_{eff} = Y\zeta$$

where Π_τ is the second invariant of τ. Using the above definitions constitutive model is developed along these lines.

$$\sigma_{11} = -p + \tau_{11}$$

$$\sigma_{22} = -p + \tau_{22} = 0 \Rightarrow p = \tau_{22}$$

$$\sigma_{33} = -p + \tau_{33}$$

If $\sqrt{\Pi_\tau} > Y_{eff}/\sqrt{3}$ then modified Maxwell's model is used to describe the material otherwise modified Hookean model is used. This condition marks the Plastic-Elastic Transition (PET) line. Hence, below the PET line the constitutive equation is of the form

$$\lambda_{eff} \overset{\triangledown}{\tau} + \tau = 2\eta_{eff}\mathbf{D} \tag{119}$$

which can be written down as,

$$\frac{d\tau_{11}}{dz} = \frac{2}{v}\frac{dv}{dz}\tau_{11} + \frac{2\eta_{eff}}{\lambda_{eff}}\frac{1}{v}\frac{dv}{dz} - \frac{\tau_{11}}{\lambda_{eff} v\cos\theta} \tag{120}$$

$$\frac{d\tau_{22}}{dz} = \frac{2}{h}\frac{dh}{dz}\tau_{22} + \frac{2\eta_{eff}}{\lambda_{eff}}\frac{1}{h}\frac{dh}{dz} - \frac{\tau_{22}}{\lambda_{eff} v\cos\theta} \tag{121}$$

$$\frac{d\tau_{33}}{dz} = \frac{2}{r}\frac{dr}{dz}\tau_{33} + \frac{2\eta_{eff}}{\lambda_{eff}}\frac{1}{r}\frac{dr}{dz} - \frac{\tau_{33}}{\lambda_{eff} v\cos\theta} \tag{122}$$

and below PET line modified Hookean model as described below is used.

$$\begin{aligned} \tau_{11} &= 2G_{eff}\varepsilon_{11} \\ \tau_{22} &= 2G_{eff}\varepsilon_{22} \\ \tau_{33} &= 2G_{eff}\varepsilon_{33} \end{aligned}$$

where ε_{11}, ε_{22} and ε_{33} are defined based the deformation at the PET line. Continuity of r, h and v are ensured through the boundary conditions.

$$\varepsilon_{11} = \left(\frac{\tau_{11}}{2G_{eff}}\right)_{PET} + \ln\left(\frac{v}{v_{PET}}\right)$$

$$\varepsilon_{22} = \left(\frac{\tau_{22}}{2G_{eff}}\right)_{PET} + \ln\left(\frac{h}{h_{PET}}\right)$$

$$\varepsilon_{33} = \left(\frac{\tau_{33}}{2G_{eff}}\right)_{PET} + \ln\left(\frac{r}{r_{PET}}\right)$$

Heat Transfer

The equation that describes the temperature distribution can be obtained through energy balance on an element of the film. Heat transfer to the cooling air via convection heat transfer and to the surrounding walls via radiation heat transfer are considered. In the equation presented the latent heat contribution due to crystallization is not included as the first model concerns itself with amorphous polymers. In the present model viscous dissipation terms are ignored The present model assumes the absence of internal cooling. Under these assumptions the energy equation is given by

$$\frac{dT}{dz} = \frac{-U(T-T_a)}{\rho C_p h v \cos\theta} - \frac{-\Lambda\epsilon}{\rho C_p h v \cos\theta}(T^4 - T_a^4) \qquad (123)$$

Numerical Scheme

The mathematical model described in the previous section results in a two–point boundary value problem with a system of coupled nonlinear ordinary differential equations (summarized in appendix C). In principle, the equations for velocity v and the pressure p can be eliminated in the given model resulting in a set of 7 equations. However, when some of the assumptions used in the model development are removed such a reduction is not possible. Hence, the complete set of 9 equations is solved without further simplification.

The given two–point boundary value problem is posed as an initial value problem and solved using the shooting method. A detailed discussion on various approaches to solve two point boundary value problem can be found in Keller (1976).

In film blowing process, beyond the freezeline it is reasonable to assume that the deformation of film ceases beyond the freezeline. Hence, the radius of the film does not change significantly beyond the freezeline (dr/dz=0). Boundary condition at the nip roll end can be specified either as the take–up force or as the velocity of the film. Cain and Denn (1988) report that specification of velocity often leads to a stable solution. In the present model, the problem is not solved as a two–point boundary value problem, but as an initial value problem. All the boundary conditions are specified only at the die exit. The force balance equation in the principal direction 1 is integrated to bring in the effect of take–up force F_z and modified suitably to specify the initial condition for σ_{11}

$$\sigma_{11} = \frac{F_z + \pi \Delta p (r_o^2 - r_f^2)}{2\pi r_0 h_0 \cos\theta_0} \tag{124}$$

In the above equation, the presence of the unknown freeze line radius r_f leads to an iterative approach. Hence, to solve the problem, freezeline radius has to be assumed. Solution to the problem is obtained by marching from the die exit to the freezeline using a fourth order Runge-Kutta scheme. Often, the freezeline is determined by the condition $dr/dz = 0$. The predicted value of the freezeline radius is used to restart the solution process at the die exit, and the iterations are continued till $||r_f^{new} - r_f^{old}|| < tolerance$. In the model developed by Cao and Campbell, beyond the PET line, $d\theta/dz$ is assumed to be zero and θ is forced to be a small positive number (close to zero). These assumptions, force the radius behave linearly with axial distance with slope $dr/dz = \tan\theta$. Hence, in the present model the PET line and the freeze line coincides. However, if these assumptions are removed, the standard condition could be used.

Process Data

Initial Conditions

At the die exit, $z = 0$, the following initial conditions are applied to solve the problem: the suffix 0 denotes the value at $z = 0$ and the suffix f denotes the value at freezeline height.

$$\begin{aligned} h &= h_0 \\ r &= r_0 \\ v &= v_0 = \frac{\dot{m}}{2\pi r_0 h_0 \cos\theta_0} \\ \theta &= \theta_0 \\ \sigma_{11} &= \frac{F_z + \pi \Delta p (r_o^2 - r_f^2)}{2\pi r_0 h_0 \cos\theta_0} \\ \sigma_{33} &= \sigma_{33}|_0 \\ p &= 0 \\ T &= T_0 \end{aligned}$$

At the die exit, the finger tensor is assumed to be the unit tensor. This in effect ignores all deformation history prior to that point. From the above equation, it can be seen that radius at the freezeline height is required to specify one of the initial condition. Hence it calls for an iterative approach to obtain the solution. The values θ_0 and $\sigma_{33}|_0$ are unknown and they are treated as parameters. Other parameters in the problem:

- Excess pressure inside the bubble, Δp
- Axial force at the nip rolls, F_z
- Mass flow rate, $\dot{m}$

- Heat transfer coefficient, U
- Cooling air temperature, T_a
- Emissivity, λ
- Surrounding wall temperature, T_w
- Hardening coefficient, C_h
- Modulus coefficient, C_G
- Step size, Δz

The modulus coefficient is introduced in the expression for modulus by Cao and Campbell (1990) to adjust its value in order to match the experimental results. This modification has no physical basis. The value of material properties depend on the polymer resin under consideration. In the present appendix, properties of amorphous polystyrene is used to compare the results with the experimental results (Gupta, 1981).

Material Properties

The following material properties are used in the study:

- Modulus $= (8 \times 10^4 + (393 - T) \times 10^3) Pa$
- Viscosity $= 8.8 \times 10^4 \exp[18904(1/T - 1/443)] Pa.s$
- Yield stress $= 1 \times 10^{-15} \exp[20000/T] Pa$
- Density $= 1050 kg/m^3$
- Specific heat $= 1910 J/kg.K$

The format of the data file used for the simulation is presented in appendix D.

Results and Discussions

Performance of the model developed is evaluated by comparing the results of the simulations with the experimental results of Gupta(1981). The experiments reported by Gupta (1981) were conducted on a laboratory scale film blowing equipment. A one inch die was used ($r_0 = 0.0127$m) in the experiments to blow films using amorphous polystyrene under both isothermal and non-isothermal conditions. The process did not rely on forced convection heat transfer for cooling the film and it was achieved via natural convection and radiation heat transfer. Of the various experimental runs, only the runs #18, #19, and #20, had a blow–up ratio greater than one. For the purpose of comparison results of run #18 were considered.

Figure 55 shows the comparison of the radius profile with experimental results. Excellent agreement between the simulation and the experiment is partly due to the *apriori* knowledge of the experimental results. Figure 56 shows the distribution of the slope angle θ. From these figures and the information available in the work of Cao and Campbell (1990), following inferences can be made.

The initial condition for θ is chosen in order to get a better match with the experimental results. This value changes for different experimental runs. In a steady state model it is not possible to estimate the value θ through theoretical analysis of the problem. On the other hand, a transient finite element analysis need not address this question and the simulation can be started with a more realistic initial condition.

In the Cao and Campbell's work, at the PET line, not only the constitutive model switches from upper convected Maxwell to modified Hookean model, governing equations are also altered and few additional assumptions are made. The value of θ is chosen as a constant whose value is assumed to be a small positive number. Arbitrariness of this assumption is clearly seen in Figure 56. Hence the variation of

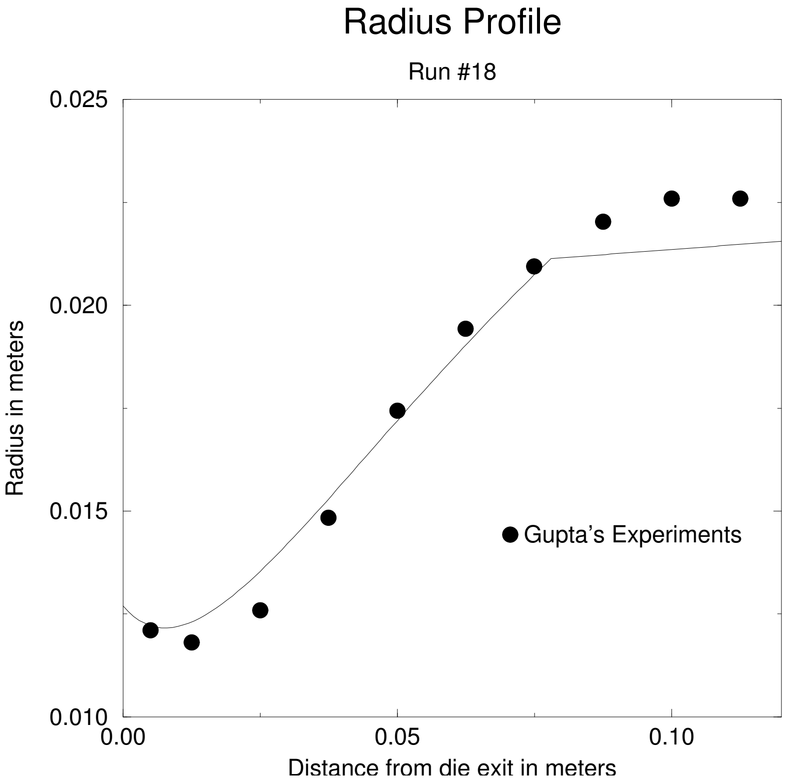

FIG. 55. Comparison of the radius profile obtained using the numerical simulation with the experimental results of Gupta (1981)

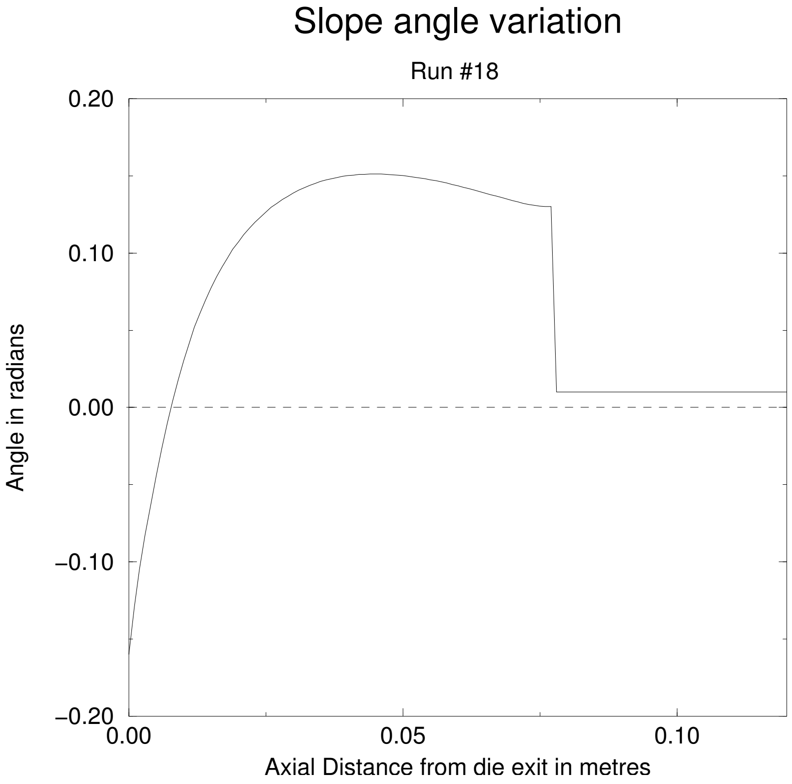

FIG. 56. Variation of slope angle θ along the bubble surface

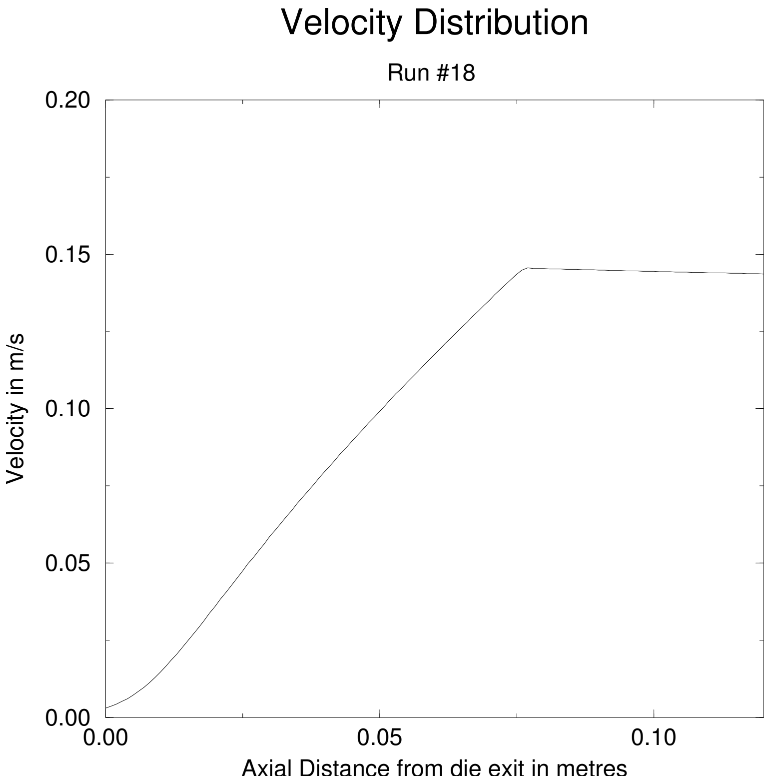

FIG. 57. Variation of the velocity along the bubble surface

the radius beyond the PET line is predetermined to behave like a straight line with a small slope ($\tan\theta$). Hence, the condition $dr/dz = 0$ will never be achieved and the freezeline will have to coincide with the PET line. These assumptions greatly modify the solution behavior beyond the freeze line. Hence, the claim that the PET model extends the solution beyond the freezeline (Cao and Campbell, 1990) is incorrect. From Figure 56, it clear that for the value of θ at the freeze line solution behavior is much higher than zero and the film will tend diverge. Without the assumptions that are made beyond the freezeline, convergence is difficult to obtain. The variation of velocity and thickness is shown in figures 57 and 58. The assumptions beyond PET line affect the nature of these variations.

Figure 59 compares the performance of three different constitutive model. When

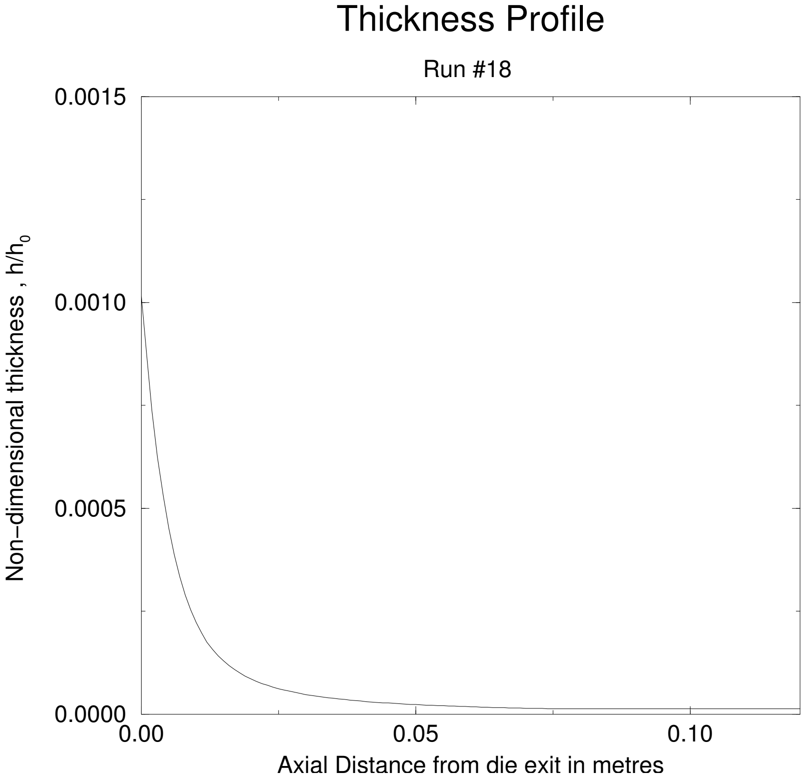

FIG. 58. Variation of film thickness along the bubble surface

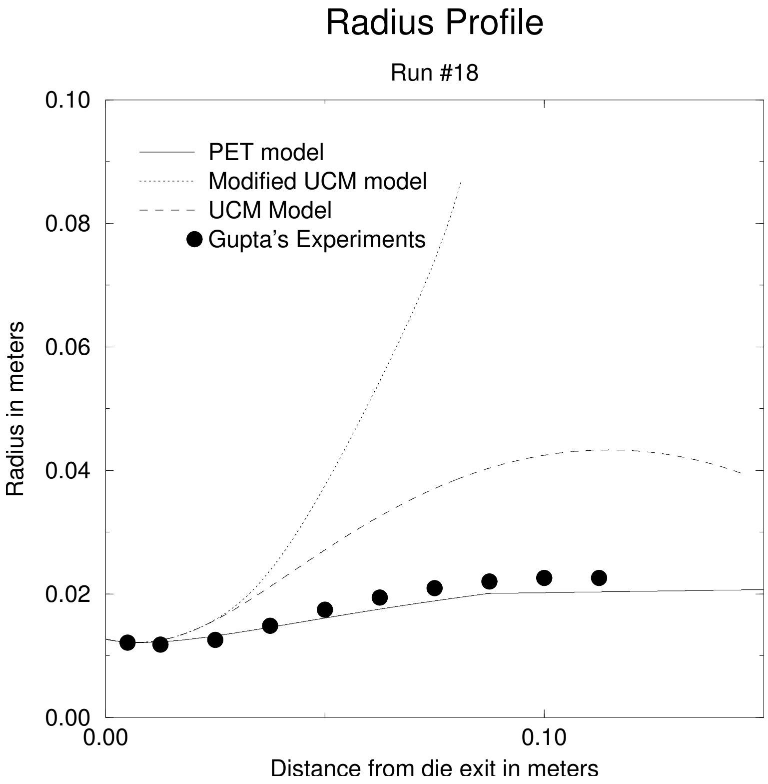

FIG. 59. Comparison of the radius profiles predicted by different constitutive models

the simple upper convected Maxwell model extended beyond the freezeline the film collapses and the property values has to be changed even to obtain an agreement with the existing experimental result. In some case the instead of collapsing, the solution can also diverge. Even in the case of modified upper convected model, the performance is not satisfactory. As it was discussed in the previous paragraph, the better performance of the PET model is purely due the assumptions beyond the PET line and not its ability to model the process better.

Figure 60 shows the distribution of the temperature of the polymer film. Heat transfer analysis includes the heat loss due to convection and radiation. In the experiments conducted by Gupta, cooling was purely due to natural convection as no external air cooling was used. Hence, the contribution of radiation heat transfer in the analysis is significant. However, the value of emissivity of the polymer film is difficult to measure and exact specification of its value is necessary to eliminate the source of errors in the analysis. Since the value was not mentioned in Cao and Campbell (1990), analysis was carried out for different values of emissivity and the table VI clearly indicates the importance of this issue. Figure 61 shows the radius distribution when the heat loss due to radiation is neglected. Since the heat loss from the film to surrounding air is via natural convection, the role of radiation heat transfer is very important. Since the material property descriptions depend on the temperature of the film, by altering the heat transfer rates, the plastic–elastic transition can be delayed. Due to the reduced heat loss, plastic–elastic transition is delayed. The bubble tends to collapse before the PET line under these conditions and the abrupt change in the behavior of the bubble after PET line is clearly indicates the incorrectness of the assumptions used at the PET line.

The film heat transfer coefficient is often assumed to be uniform along the bubble surface and it is value is changed by 50–100% to match the experimental results (Cao and Campbell, 1990).

Shooting method fails to simulate film blowing process accurately due to its inability in enforcing the conditions like $dr/dz = 0$ beyond the freezeline in a natural manner. It is also not possible to prescribe the velocity boundary condition at the nip roller end using the present model. This is a very critical parameter and it is a direct measure of the productivity of the system. Attempting to simulate film blowing using the shooting method is like attempting to the blow the bubble and achieve a stable film blowing process by only controlling the conditions at the die end in an experimental facility, which is not possible. The accuracy of the simulation indeed depends on the constitutive model and the material property descriptions. However, the inaccuracies due to the numerical method used should not go unnoticed.

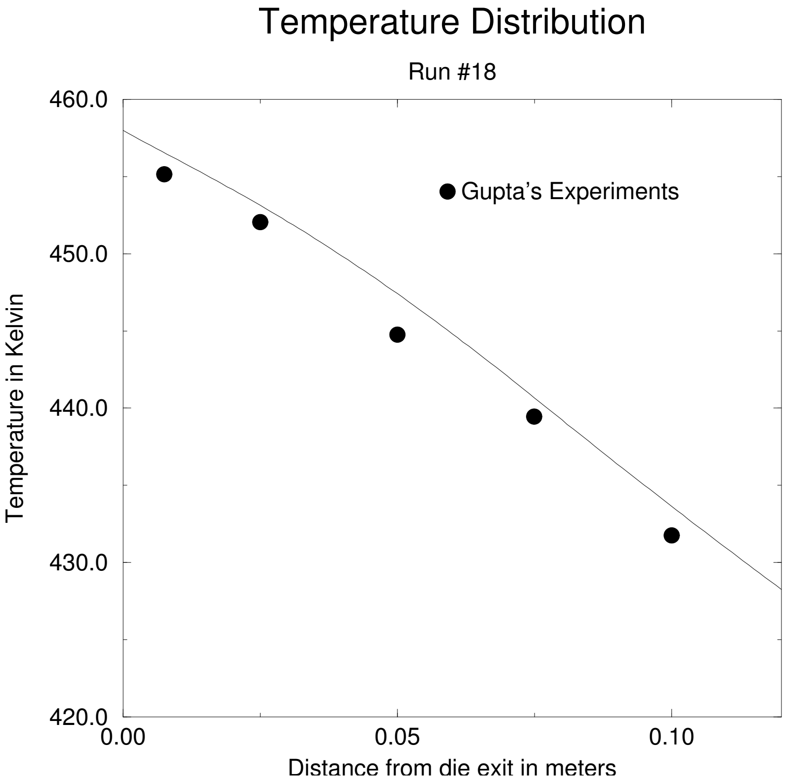

FIG. 60. Comparison of the temperature profile obtained using the numerical simulation with the experimental results of Gupta (1980)

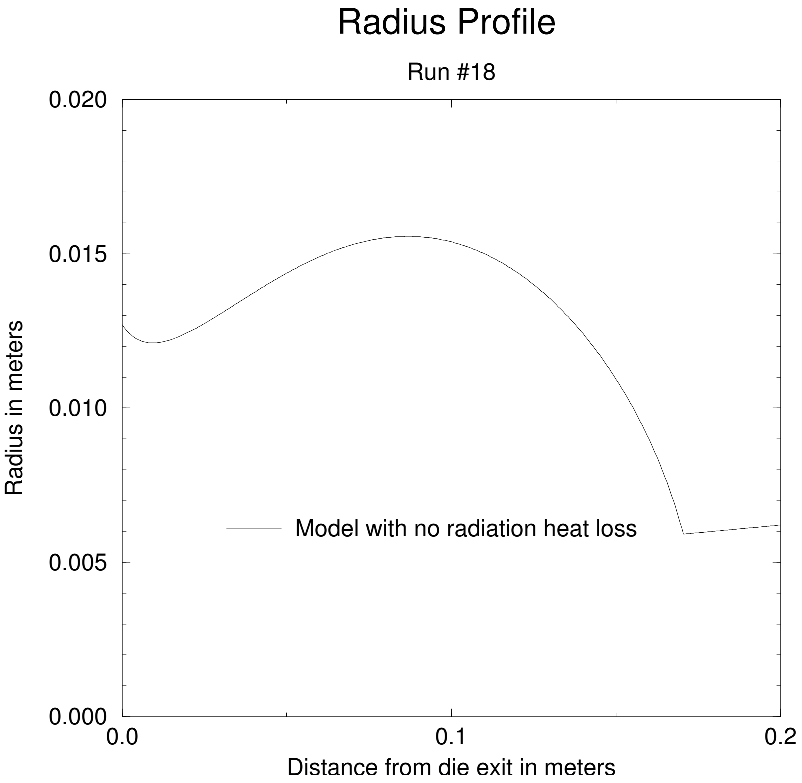

FIG. 61. Variation of bubble radius in the absence of radiation heat transfer

TABLE VI. The influence of radiation heat transfer on the process.

Emissivity	z_{PET} in cm	r_{PET} in cm	T_{PET} in K
0.0	17.0	0.591	435
0.1	12.3	1.859	434
0.2	7.8	2.103	440
0.3	7.4	1.971	439
0.4	5.9	1.953	441
0.5	5.3	1.887	440
0.6	4.4	1.827	440
0.7	4.2	1.805	440
0.8	4.4	1.770	440
0.9	4.2	1.743	440
1.0	4.2	1.725	440

Summary

Simulation of polymer film blowing process using a steady state model was presented. The shooting method used pose the two point boundary value problem derived from the model into an initial value problem is one of the sources of error, this method not only fails to naturally extend itself beyond the freezeline it is incapable of simulating the process below the freezeline accurately. The PET model used to describe the constitutive behavior of the polymer, in its present form uses unreasonable assumptions to force the desired behavior on the solution. The nature of the assumptions beyond the PET line, like θ is a small non-zero constant forces dr/dz to be non-zero, would naturally result in the identification of PET line with the freeze line which may not be incorrect. The sensitivity of the solution to process data like emissivity and initial condition of the slope angle, which are not known accurately reduces the reliability of the simulation as a design tool. However, as mentioned in the previous section, many of the disadvantages associated with the present model can be removed by properly posing the problem.

VITA

Ravisankar S. Mayavaram was born in Chennai, India in 1967. He graduated with BSME from Bharatiyar University (1984), MSME from ITT Madras (1992) and Ph.D. in mechanical engineering from Texas A&M University (2005). Dr. Mayavaram is currently working in Altair Engineering, Inc. and his residential address is 15517, Fisher Island Dr, Austin, TX 78717. He can be reached by sending e-mail to ravi@ambaa.org or msr@altair.com.

This document was typeset in LaTeX by Ravisankar S. Mayavaram.